Examining the Role of Lysyl Oxidase Enzymes in Atrial Fibrillation Induced by Volume Overload

Dana Evelyn Sherrard

A Thesis submitted to the Faculty of Graduate Studies in Partial Fulfillment of the Requirements for the Degree of Master of Science

Department of Biology
York University
Toronto, Ontario

August 2024

Abstract

Atrial fibrillation (AF), the most prevalent cardiac arrhythmia, is characterized by significant atrial electrical and structural remodelling. We previously showed that endurance exercise in mice promotes AF associated with atrial hypertrophy, immune cell infiltration, and fibrosis. Notably, collagen transcription remains unchanged, suggesting fibrosis results from collagen stabilization by the Lysyl Oxidases (LOX) family of enzymes, which facilitate collagen crosslinking.

To explore the interplay of fibrosis, and AF vulnerability, we established a murine model of aortic regurgitation (AR), which causes elevated filling pressures leading to atrial stretch.

Compared to sham mice, AR mice exhibited markedly increased ($P<0.0001$) susceptibility to AF (71% versus 0%), accompanied by a decrease ($P=0.0243$) in atrial refractoriness (AERP), elevated fibrosis in the left atria (LA) (~11.2% versus ~5.4%, $P<0.0001$), a 2-fold increase ($P=0.0008$) in macrophage infiltration and a 6% increase ($P=0.0609$) in macrophages expressing LOXL2. Treatment with the LOXL2 inhibitor, PXS-5382, reduced ($P<0.0001$) AF inducibility by 61%, shortened ($P=0.0117$) AF duration (from 14.3±8.4s to 4.1±5.7s), and attenuated ($P=0.0002$) fibrosis (to 5.5%) without affecting ($P=0.4299$) AERP. The effects of treatment with a LOX inhibitor, PXS-5505, blocking all LOX isozymes, had varied and complex effects. PXS-5505 prevented ($P=0.0150$) fibrosis without reducing ($P=0.6382$) AF inducibility in AR mice while also promoting ($P=0.0119$) inducibility in sham mice by 22% and fibrosis ($P=0.0088$) by 4.2%. Neither pan-LOX nor LOXL2 inhibition mitigated AF susceptibility in endurance swim training.

These findings demonstrate that LOXL2 plays a pivotal role in atrial structural remodelling and AR-induced AF susceptibility; supporting the conclusion that targeting LOXL2 may be a useful therapeutic target in AF.

Keywords: atrial fibrillation, fibrosis, lysyl oxidase, aortic regurgitation, endurance training, arrhythmias.

Acknowledgments

First and foremost, I would like to thank my supervisor, Dr. Peter Backx, for his invaluable guidance, personal and scientific, over the last couple of years throughout my Masters degree. He has instilled in me confidence and motivation to strive for excellence and to be a more rigorous critical thinker; skills I know will be utilized throughout my life. I am beyond grateful to have learned from such a distinguished scholar.

I would also like to thank my committee members, Dr. Chris Perry and Dr. Ali Abdul-Sater, for their guidance and support throughout my research. They made me feel secure in my ability to ask questions, and their students openly welcomed assisting me in troubleshooting and learning new techniques.

I would be remiss not to extend great thanks to Dr. Rob Lakin, soon-to-be Dr. Renée Gorman, and Dr. Mihir Parikh for their patience and willingness to teach me many of the experimental techniques utilized and for their intellectual contributions to the project. They not only acted as imperative elements to my academic success but also comprised part of my personal support system, and for this, I am extremely grateful.

I would also like to thank the present and past members of Dr. Backx's laboratory for their assistance and support. In particular, I would like to thank Ryan Debi for his role in supporting the lab as a whole and as a guide when designing this study. Moreover, thank you to my volunteer – Hasti Tajdari – for your immense help with the swims.

Lastly, I extend my sincerest and utmost gratitude to my close friends and family for their unconditional love and support. Thank you for uplifting me through the more difficult phases and always reminding me of my capabilities. You are my rocks.

Copyright

Table of Contents

Abbreviations

AF	Atrial Fibrillation
AGEs	Advanced Glycation End Products
AP	Action Potential
APD	Action Potential Duration
AR	Aortic Regurgitation
BAPN	Beta-Aminopropionitrile
BMP	Bone Morphogenic Protein
CO	Cardiac Output
CRP	C Reactive Protein
CVD	Cardiovascular Disease
DAD	Delayed Afterdepolarization
EAD	Early Afterdepolarization
ECC	Excitation - Contraction Coupling
ECM	Extracellular Matrix
EF	Ejection Fraction
ERP	Effective Refractory Period
HR	Heart Rate
ICANS	Intrinsic Intracardiac Autonomic Nervous System
IHC	Immunohistochemical
LA	Left Atria
LV	Left Ventricle
LOX	Lysyl Oxidase
LOXL#	Lysyl Oxidase Like 1/2/3/4
MMP	Matrix Metalloproteinase
PBS	Phosphate Buffer Saline
PDGF	Platelet-Derived Growth Factor
PFA	Paraformaldehyde
PWth	Posterior Wall Thickness
RV	Right Ventricle
SA	Sinoatrial
SMAD	Mothers Against Decapentaplegic
SPARC	Secreted protein Acidic and Cysteine Rich
SR	Sinus Rhythm
SRCR	Scavenger Receptor Cysteine Rich
SV	Stroke Volume
TG	Transglutaminase
TGF-β	Transforming Growth Factor - Beta
THBS	Thrombospondin
TIMP	Tissue Inhibitor of Metalloproteinase
TNF	Tumour Necrosis Factor
VO	Volume Overload

Figures and Tables List

Chapter 1: Introduction

1.1 Atrial Fibrillation

Atrial fibrillation (AF) is the most prevalent supraventricular arrhythmia in humans, projected to affect over 16 million US residents by the year 2050 [1,2]. AF is characterized by both structural and electrical changes in atrial tissues, known as remodelling (i.e., changes in size, shape, structure, and function in response to a chronic stimulus), and presents as fibrillations or irregular quivering of the atrial cardiac muscles [3]. AF disrupts synchronous atrial contractions, thereby compromising ventricular pumping and impairing cardiac output. AF also elevates the risks of heart failure and stroke 2-fold due to the pooling of blood in the atria, promoting thromboembolisms, inefficient systemic blood transportation, and weakened diastolic function [4–6]. AF can manifest as paroxysmal, where episodes occur intermittently and spontaneously revert to normal sinus rhythm (SR); persistent if lasting more than 7 days necessitating intervention; or permanent if lasting beyond a year without response to treatment [5,7].

1.1.2 Epidemiology: Symptoms, Diagnosis & Treatment

Awareness of AF has markedly advanced over the past half-century, contributing to a threefold increase in diagnoses [8]. The rise, however, stems primarily from improved surveillance rather than an escalation in prevalence. AF manifests with symptoms such as low blood pressure, shortness of breath, chest pains, dizziness, fainting or heart palpitations, which are common in various other cardiovascular diseases (CVD). Moreover, many cases are asymptomatic, complicating diagnosis and underscoring the necessity for deeper insight into underlying mechanisms of AF.

AF is primarily diagnosed by electrocardiogram but can be accompanied by blood tests, echocardiography, and cardiac magnetic resonance imaging to assess potential underlying causes and alternative side effects [7]. Treatment approaches range from lifestyle adjustments to pharmaceutical interventions such as beta blockers or blood thinners, and in some cases, medical procedures like cardioversion, ablation, or the Maze procedure. Preventive decisions are tailored to address the underlying conditions predisposing individuals to AF, and treatment is decided upon based on the presentation – whether it be paroxysmal, persistent, or permanent.

1.2 Cardiac Physiology

The heart functions as the central organ of the cardiovascular system, serving as a mechanical pump that circulates oxygenated blood throughout the body and transports deoxygenated blood to the lungs [9]. This pumping action is controlled through a process called excitation-contraction coupling (ECC), wherein electrical signals in muscle cells of the heart (i.e., cardiomyocytes), known as the action potential (AP), initiate a rise in intracellular calcium (Ca^{2+}) leading to mechanical contractions. It is important to note cardiomyocytes, do not possess automaticity; they rely on receiving electrical signals propagated from the sinoatrial node (SA node) to initiate contraction. The ECC coordination and organized spread of AP is achieved through the process described next.

The AP begins at the SA node in the right atrium, where specialized cells exhibit automaticity and can spontaneously depolarize to generate their own AP [10]. From the SA node, the electrical impulse travels from cardiomyocyte to cardiomyocyte, spreading through the atria via Bachman's bundle, eventually reaching a specialized region of the heart called the atrioventricular node (AV node). Within the AV node, the electrical signal spreads from cell to cell, eventually arriving at the Bundles of His and subsequently moving to the Purkinje fibres, which deliver the electrical signal to the ventricular muscle cells in an orderly manner, ensuring synchronous ventricular contraction and blood ejection.

The AP process is divided into five distinct phases: Resting (phase 4), Depolarization (phase 0), Peak Voltage (phase 1), Plateau (Phase 2), and Repolarization (Phase 3) (Figure 1.1). During phase 4, the longest period in the cardiac cycle, the resting membrane potential is maintained between -90 and -40mV, allowing for chamber filling during diastole. Depolarization (phase 0) rapidly follows when the membrane potential reaches the -40mV threshold due to a surge of sodium (Na^{+}) ions influx. This triggers contraction as the cardiomyocytes continue to depolarize. Peak Voltage (phase 1) occurs at approximately +30 mV, causing the closure of all channels except voltage-gated potassium (K^{+}) channels, initiating systole, and ejecting approximately 60% of blood from the chambers. Plateau (phase 2) briefly maintains the membrane potential due to balanced Ca^{2+} influx and K^{+} efflux before repolarization (phase 3) ensues as Ca^{2+} channels close and K^{+} channels open further for efflux.

The duration required to complete these five phases of the AP is known as the Action Potential Duration (APD). This duration determines the minimum time required between

generating new APs, termed the Effective Refractory Period (ERP). The ERP serves as a safeguard mechanism for maintaining SR by preventing premature beats from eliciting subsequent contractions until cardiomyocytes have fully recovered [11].

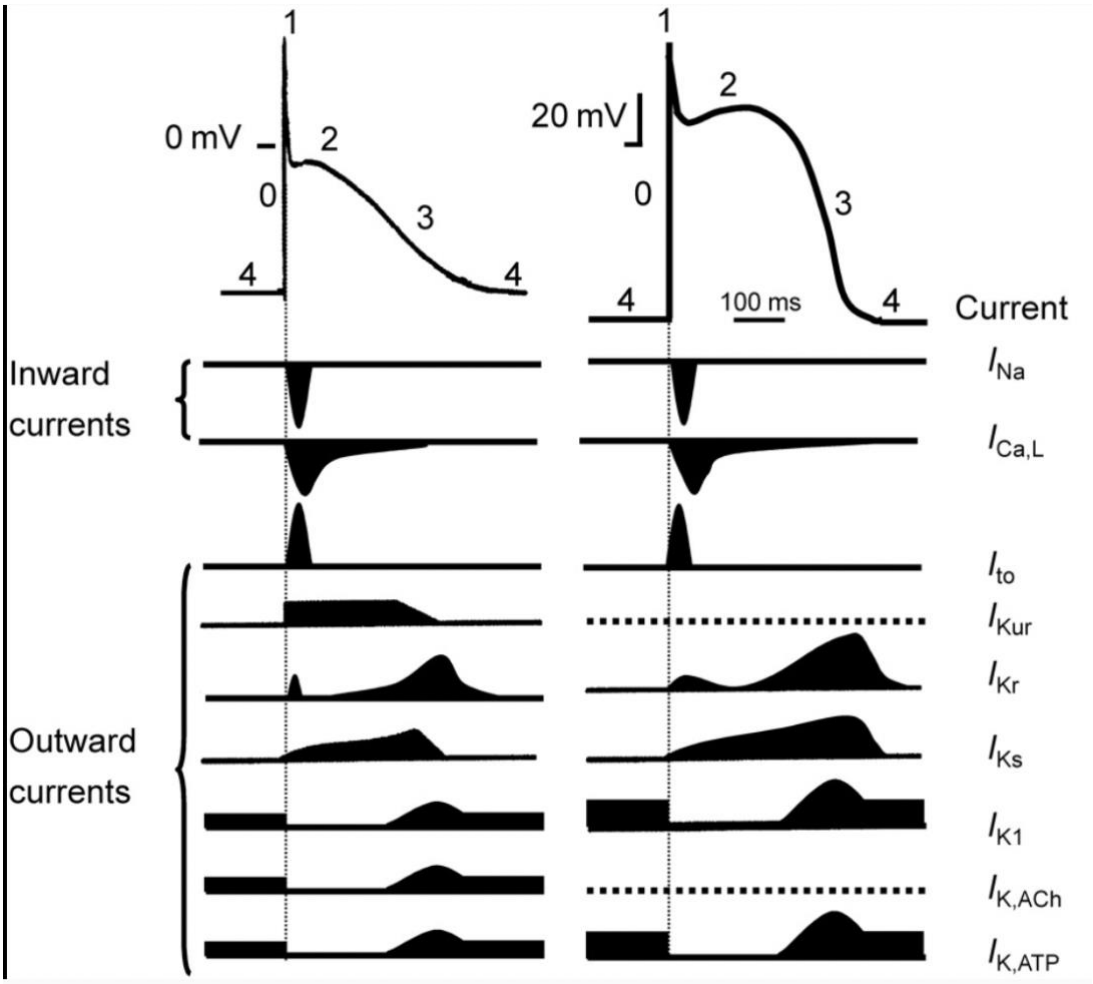

Figure 1.1 Cardiac Action Potential (AP) Waveforms. The upper panels illustrate a typical cardiac AP in the atria (left) and ventricle (right), delineating the five phases. In the lower panels, transmembrane ion currents depict the rate of change of the AP, highlighting inward depolarizing and outward repolarizing currents. The atrial AP exhibits a notably diminished plateau (Phase 2), a shorter APD, and a more positive resting membrane potential (Phase 4) compared to the ventricular AP. Additionally, the ventricular AP lacks I_{kur} 'ultra-rapid outward delayed potassium rectifier current.' Copyright © 2008, European Heart Journal [12].

1.3 The Athletes Heart

Regular exercise is widely acknowledged for its substantial benefits to cardiovascular health, effectively reducing the risk of developing CVD and lowering cardiovascular mortality [13]. This positive impact stems from the heart's ability to remodel (change of form and function) and operate more efficiently in response to physical activity. The nature of this remodelling depends on factors such as type, duration, intensity, frequency, and overall cumulative dose of physical activity or exercise.

Physical activity is a broad term defined by actions that occur in one's daily life, such as occupational, household, sports, or conditioning. A subset of physical activity that is planned, structured, and repetitive and intended to improve or maintain physical fitness is known as exercise [14]. For the purpose of this study, we will focus on 'exercise' when discussing the athlete's heart.

Exercise can be broadly categorized into strength training (isometric static anaerobic), endurance training (isotonic dynamic aerobic) or a combination of both. In this study, the focus will be on endurance activities like running or swimming. Endurance exercise is characterized by sustained increases in cardiac output (CO) and oxygen consumption (VO2), independent of changes in vascular resistance [15]. Each exercise session imposes a volume overload (VO) on the heart, necessitating high physiological and metabolic demands. With chronic endurance exercise, the heart adapts by undergoing eccentric hypertrophy, where the ventricular chambers enlarge without a corresponding increase in myocardium thickness [16]. Specifically, the right ventricle (RV) dilates more than the left ventricle (LV) due to its thinner chamber walls and lower pressure system [17].

During endurance exercise, both ejection fraction (EF) - the percent of blood ejected from the heart with each contraction - and fractional shortening (FS) - a measure of left ventricle (LV) function increase. A common misconception is that EF and FS decrease at rest due to LV dilation and eccentric hypertrophy [18]. However, at rest, there is a reduction in end-diastolic volume (preload), while stroke volume (SV) – the volume of blood ejected from the LV per xsystolic cycle - increases due to the more efficient myocardial remodelling. Since SV directly influences CO, the heart's overall efficiency improves. This enhancement also increases contractile reserves, indicating the heart's ability to utilize a greater proportion of its maximum capacity under stress conditions [15].

1.4 Atrial Fibrillation Pathogenesis

AF is marked by significant electrical and structural remodelling that transforms the cardiac phenotype, increasing susceptibility to arrhythmia. While AF primarily manifests as an electrical disorder, it is associated with structural changes within the heart, allowing AF to be initiated and sustained. As AF advances, abnormal impulse firing becomes more frequent, further promoting structural remodelling. This phenomenon underscores the concept that "AF begets AF," indicating that the progression of AF reinforces its own persistence and severity over time.

1.3.1 Electrical Remodelling: Cardiac Arrhythmogenesis

Arrhythmogenesis requires both triggers and a vulnerable substrate that facilitates the perpetuation of fibrillation [19]. Triggers often originate from ectopic foci, which refer to the generation of spontaneous AP in cells outside the SA node. These ectopic foci are commonly found in the pulmonary veins. Typically, ectopic foci exhibit automaticity at irregular rates, thereby disrupting SR [20]. The resultant abnormal depolarizations can elicit re-entry events, wherein an impulse propagates through a circuit and returns to stimulate tissue that has not yet recovered its excitability (refractory tissue) [21]. This phenomenon of re-entry is a key mechanism in arrhythmias, including AF, where irregular electrical activity perpetuates itself, as will be explained further in the following section.

The circuit wavelength, determined by the impulse conduction velocity multiplied by the effective refractory period (ERP), serves as the best predictor of arrhythmia inducibility with re-entry [22]. Slowed conduction velocities, often due to hypertrophy or increased fibrotic tissue, combined with shortened ERPs (thus reducing APD), promote re-entry by facilitating rapid re-excitation of the tissue. These conditions create a conducive environment for the perpetuation of arrythmias like AF.

Cardiac arrhythmias exhibit significant variability, occurring in different locations (supraventricular or ventricular) and manifesting in various forms such as tachycardia and bradycardia. The underlying disease and specific mechanism dictate the type and location of arrhythmia observed. Despite this variability, re-entry and the presence of ectopic foci are fundamental and overlapping mechanisms in arrhythmogenesis, particularly in the development of AF.

1.3.1.1 Contribution of Re-entry and Conduction Block to AF

Re-entry occurs when an electrical impulse fails to terminate and persists by circulating through a circuit, re-exciting tissue after the refractory period [23,24]. For re-entry to initiate, two conditions must be met: the impulse must return to its origin, and there must be a unidirectional block [25]. If the block is due to a distinct anatomical structure, such as fibrotic tissue, which remains fixed in location, it is termed 'anatomical' re-entry. This form of re-entry creates two distinct paths: one following the usual course and another allowing slow retrograde conduction through the block (Figure 1.2). In contrast, if impulse propagation results from heterogeneity in cell conductivity rates across the tissue, it is termed 'functional' re-entry [19,25]. In regions of considerable cellular variability, like the left atria (LA) - the primary target of AF – functional block will contribute to re-entry [26]. This concept underpins the multiple wavelet theory of AF, which suggests that AF is maintained by multiple electrical wavelets that emanate from various focal sources, randomly propagating across the atria through unique routes [23,27].

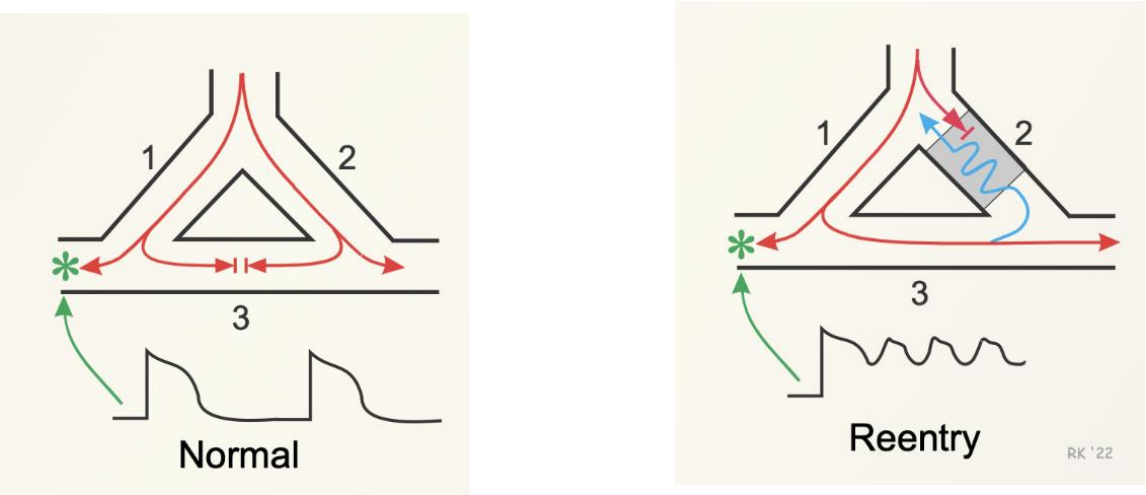

Figure 1.2 A Model of Re-Entry. In normal impulse conduction (left panel), a Purkinje fibre bifurcates (1 and 2) with orthograde impulse propagation along each pathway (3). An electrode (green asterisks) records a single AP conducted down branch 1. Any AP travelling into branch 3 from branch 1 will be nullified by an AP travelling down branch 2 into branch 3. In contrast, re-entry (right panel) involves a scenario with a unidirectional block, allowing retrograde impulse propagation with slowed conduction velocities (blue). Here, an AP travelling down branch 1 flows through branch 3 and excites tissue via branch 2, establishing a circuit for the AP to perpetuate. This tissue must not be within its ERP to be re-excitable; otherwise, it remains unexcitable, and the AP propagation ceases. Copyright © 2021, Cardiovascular Physiology Concepts [28].

1.3.1.2 Triggered Automaticity

Triggered automaticity describes the phenomenon where the preceding AP influences the timing of a subsequent AP. If the subsequent AP occurs before the termination of the prior AP, specifically during phase 2 or 3, it is termed 'Early Afterdepolarization' (EAD) [20]. EADs typically occur when Ca^{2+} channels have recovered from inactivation, allowing them to reopen and generate a positive voltage oscillation [29]. This condition is often associated with prolonged APD, which provides sufficient time for Ca^{2+} channel recovery.

On the other hand, if the subsequent AP occurs after the termination of the preceding AP, specifically during diastole, it is termed 'Delayed Afterdepolarization' (DAD). DADs are driven by the spontaneous release of Ca^{2+} from the sarcoplasmic reticulum in the presence of Ca^{2+}-sensitive currents or under the influence of catecholamines, as commonly observed in hypertrophied hearts [20,30,31]. Unlike EADs, DADs are typically induced at relatively rapid rates and are associated with shortened APD.

These distinct forms of triggered automaticity highlight different mechanisms by which abnormal depolarizations can occur in cardiac cells, contributing to arrhythmogenesis under various physiological and pathological conditions.

1.3.1.3 Autonomic Modulation of Cardiac Rhythm

Autonomic modulation can also influence SR through input from the parasympathetic or sympathetic nervous systems. The parasympathetic nervous system (PNS), which has preganglionic synapses inside the myocardium, primarily acts via the Vagus nerve to decrease the heart rate (HR) [32]. This effect is particularly prevalent during exercise in which elevated levels of acetylcholine (ACh) in the synapse bind to muscarinic receptors, inhibiting the alpha subunit of the G-protein and thereby reducing sympathetic activation [33]. However, excess Ach can also lead to regional heterogeneity of the autonomic activity, potentially inducing arrhythmia. Ach activates the $I_{K,ACh}$ channel, which shortens repolarization time and hyperpolarizes the resting membrane potential, thus preventing the refiring of APs [33].

Conversely, the sympathetic nervous system (SNS), which synapses at the paravertebral ganglion outside the heart, acts to increase one HR. For example, during stress, the SNS releases catecholamines that enhance the inward current (I_{NCX}) flow of Na^+ and Ca^{2+} ions into pacemaker

cells of the SA node. This influx depolarizes the SA nodal cells, initiating AP cycles and interrupting SR [32].

Additionally, the heart possesses an intrinsic intracardiac autonomic nervous system (ICNS) which can independently modulate cardiac electrophysiology by interacting with the efferent nerve supply [34]. ICNS can release specific neurotransmitters to initiate parasympathetic or sympathetic responses, thereby maintaining autonomic balance and adjusting cardiac tone accordingly. This intrinsic regulation contributes significantly to dynamic control of the HR and cardiac function under varying physiological conditions.

1.3.2 Structural Remodeling: Hypertrophy, Inflammation, Fibrosis

Many conditions associated with AF involve elevated atrial pressures and stretch, which act as potent stimuli for inducing atrial hypertrophy, inflammation, and fibrosis [35,36]. These physiological changes form the fundamental basis of structural remodelling in the atria, creating a substrate that promotes and sustains atrial fibrillation. Understanding and addressing these processes are essential for developing effective strategies to manage and treat AF in clinical practice.

1.3.2.1 Hypertrophy

Atrial hypertrophy refers to the enlargement of atrial chambers in response to chronic pressure (PO) or volume overload (VO) and is a key precursor of AF. This adaptation process allows the atria to accommodate increased blood volumes or pressures due to various cardiovascular conditions. Hypertrophy can manifest as either concentric thickening of the myocardium due to PO or eccentric dilation of the chamber with minimal effect on the myocardium due to VO. In contrast to the LV, hypertrophy of the LA is particularly critical in the context of AF initiation.

Under acute mechanical overload, such as during transient stretches, electrophysiological changes associated with atrial stretch are often reversible [37]. For instance, studies on Langendorff-perfused rabbit hearts have shown ERP and the inducibility of AF regressed to baseline levels within three minutes of releasing acute stretch [38]. However, chronic atrial overload leads to prolonged recovery of ERPs and irreversible heterogeneity in impulse conduction, which exacerbates AF [37]. Clinical studies have demonstrated a correlation between

LA size and AF incidence. AF occurrence was rare (3%) when LA dimensions were less than 40mm but common (54%) when exceeding 40mm [39]. Moreover, LA dimensions greater than 45mm reduced the likelihood that cardioversion would sustain SR beyond six months [39]. The Framing Heart Study reported a 39% increase in AF development for every 5mm increase in LA diameter. [40].

Mechanistically, stretch-activated ion channels in cardiomyocytes play a crucial role in mechanoelectrical response to atrial overload. However, the exact response varies. Cation stretch-activated channels trigger acute AF by shortening atrial ERP (AERP) and increasing the heterogeneity of APD, thereby providing a substrate for the re-entry of impulse waves [41]. However, conflicting studies exist regarding the direction of the impact of acute atrial dilation of AERP. Some studies show that LA dilation does not affect AERP but rather contributes to local conduction slowing and blocking in specific atrial regions, such as the free wall along the anterior pectinate muscles. Others indicated increased activation frequency in the pulmonary veins [42]. These discrepancies emphasize the heterogeneous responses to atrial hypertrophy and its complex role in promoting AF pathogenesis.

1.3.2.2 Inflammation

Inflammation is pivotal in AF pathophysiology, initiating oxidative stress, cytokine release, and immune cell infiltration into atrial tissues. Chronic inflammation contributes to both electrical and structural remodelling of the atria, thereby promoting the perpetuation of AF. The exact mechanisms underlying the immune response remain under investigation in our lab and many others. However, it is established that there is a positive feedback loop between inflammatory responses and AF progression. Inflammation induces further remodelling, creating a substrate that is more susceptible to impulse re-entry and sustained arrhythmia.

In both early and late-stage chronic VO models, as well as seen in AF patients, an increase in CD45+ (hematopoietic) and CD68+ (macrophage) cells within the atria is observed, which is absent with patients in SR [43–45]. Furthermore, connections between inflammation and AF have been made. For example, AF and inflammation facilitate hypercoagulable states and present with elevated C-reactive protein (CRP) concentrations [44,46]. CRP levels positively correlate with arrhythmia duration and LA dimension [47]. Other common cytokines such as IL-1β, IL-6, and TNF are released during AF and inflammation, promoting changes in cardiac cell types

and function and contributing to cardiac remodelling, as seen with AF [48]. Inflammation also affects atrial electrical signalling pathways by modulating the distribution and amount of atrial jap junction proteins, connexin 40 and 43, which are crucial for electrical coupling between atrial myocytes [44]. Even more, inflammation-induced activation of NF-κB, a transcription factor, alters Na+ channel expression, thereby modifying atrial impulse conduction [44]. Lastly, inflammation can promote atrial fibrosis - a substrate for conduction block and anatomical re-entry - through the expression of cytokines like transforming growth factor – beta (TGF-β1), platelet-derived growth factor (PDGF) and endothelin 1 (ET-1) derived from immune cells [49]. These cytokines play critical roles in the differentiation of interstitial fibroblasts into myofibroblasts, leading to the upregulation of extracellular matrix (ECM) components – as will be discussed in the following section.

1.3.2.3 Fibrosis

Fibrosis is characterized by excessive deposition of ECM proteins, especially collagen I and III [50]. Fibrosis disrupts normal atrial architecture and functions as a double-edged sword. In the presence of mechanical overload and atrial stretch, fibrogenesis is essential for maintaining chamber integrity [51]. However, excessive fibrotic tissue leads to decreased cardiac mechanical function due to enhanced myocardial stiffness and heterogeneity in electric impulse propagation, both of which promote the development and perpetuation of AF [52].

The ECM is a complex network comprised of fibrillar (collagens) and non-fibrillary (basement membrane, glycoproteins, proteoglycans) components which provide structural and signalling functions throughout the myocardium [53]. The cardiac ECM is primarily comprised of collagens (I, III, IV), non-collagenous glycoproteins (fibronectin and laminin), proteoglycans, glycosaminoglycans, and elastins [54]. Fibrillar collagens, consisting of 80% type I and 10% type III, form fibrils anchored to the basement membrane through collagen type IV and fibronectin to provide structure to the myocardium for transmission of mechanical forces [54,55]. This scaffolding acts as a net for growth factors, cytokines, chemokines, proteases, and many other proteins which can affect ECM growth and degradation [54]. Any disruption of the ECM will thus alter the overall function of the myocardium. The primary focus of this study will surround excessive fibrillar collagen deposition, however, some preliminary investigation into non-fibrillar components will briefly be presented.

Cardiac fibrosis presents in several forms: reparative, reactive, infiltrative or endomyocardial. Reparative fibrosis occurs interstitially in response to a loss of myocardial material, irreversibly diminishing contractile and electrical function in the focal region (Figure 1.3). Reactive fibrosis, found in the perivascular space, responds to changes in mechanical load or inflammation (Figure 1.3). This type of fibrosis increases the interstitial compartment volume with minimal effect on the viability or volume of the myocardium itself [3,56]. Its progression depends on chronic stimuli, yet it can potentially regress if the stimuli are reduced or removed [57]. Infiltrative fibrosis also occurs interstitially but results from the progressive deposition of insoluble proteins or glycosphingolipids [58]. Lastly, endomyocardial fibrosis affects the endocardium of the ventricles in young children. Its etiology is somewhat unclear but is thought to involve an immunological response [57].

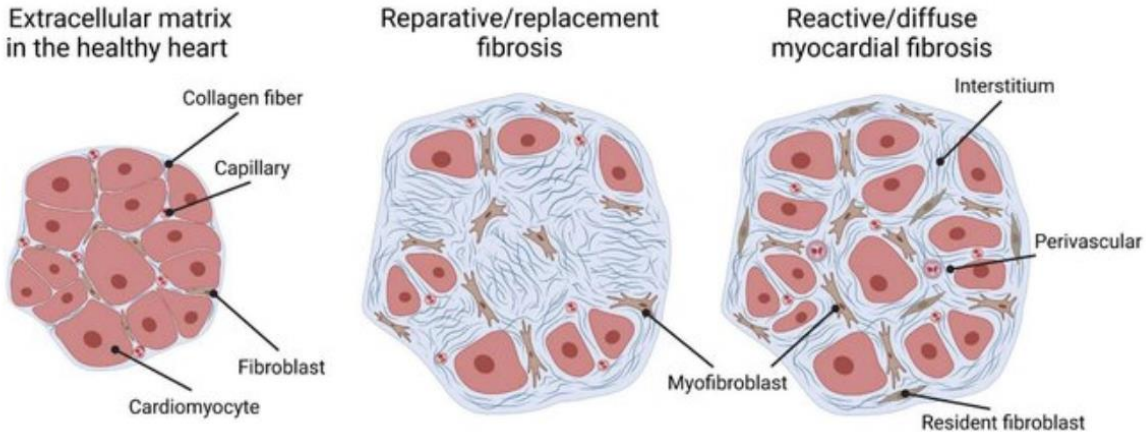

Figure 1.3 Reparative and Reactive Cardiac Fibrosis. Healthy ECM (left) depicts the three-dimensional network of collagen fibres, which act as a network to embed cardiac cells (i.e., fibroblast, cardiomyocytes) and capillaries. Reparative fibrosis (middle) depicts myocardial loss and collagen scarring formed during healing to replace the dying cardiomyocytes. Reactive fibrosis (right) depicts diffused deposition of crosslinked collagen in the interstitial and perivascular regions without loss of myocardium. Copyright © 2022, Frontiers in Cardiovascular Medicine [59].

As briefly discussed in section 1.3.11, fibrotic tissue serves as an anatomical blockade facilitating unidirectional conduction block and slowing conduction by creating areas of non-conductive tissue that impede normal electrical pathways and facilitate the formation of re-entry circuits. This occurs through disruption of the myocardium's anisotropic conductivity (Figure 1.4). Cardiac conduction velocity is directionally dependent on the orientation of the cardiomyocytes [60]. Therefore, in the presence of excess connective tissue, membrane resistance between cells increases causing discontinuous cellular connection. Transverse propagation of impulses is possible only where myocardial tissue has created a bridge across the gaps. Furthermore, these connective tissue deposits disrupt longitudinal linear conduction, forcing an irregular zig-zag pattern of impulse conduction, thereby increasing conduction distances and slowing conduction velocity [60,61]. In such conditions, the wavefront is prolonged, creating an excitable gap conducive to re-entry, promoting the development of AF.

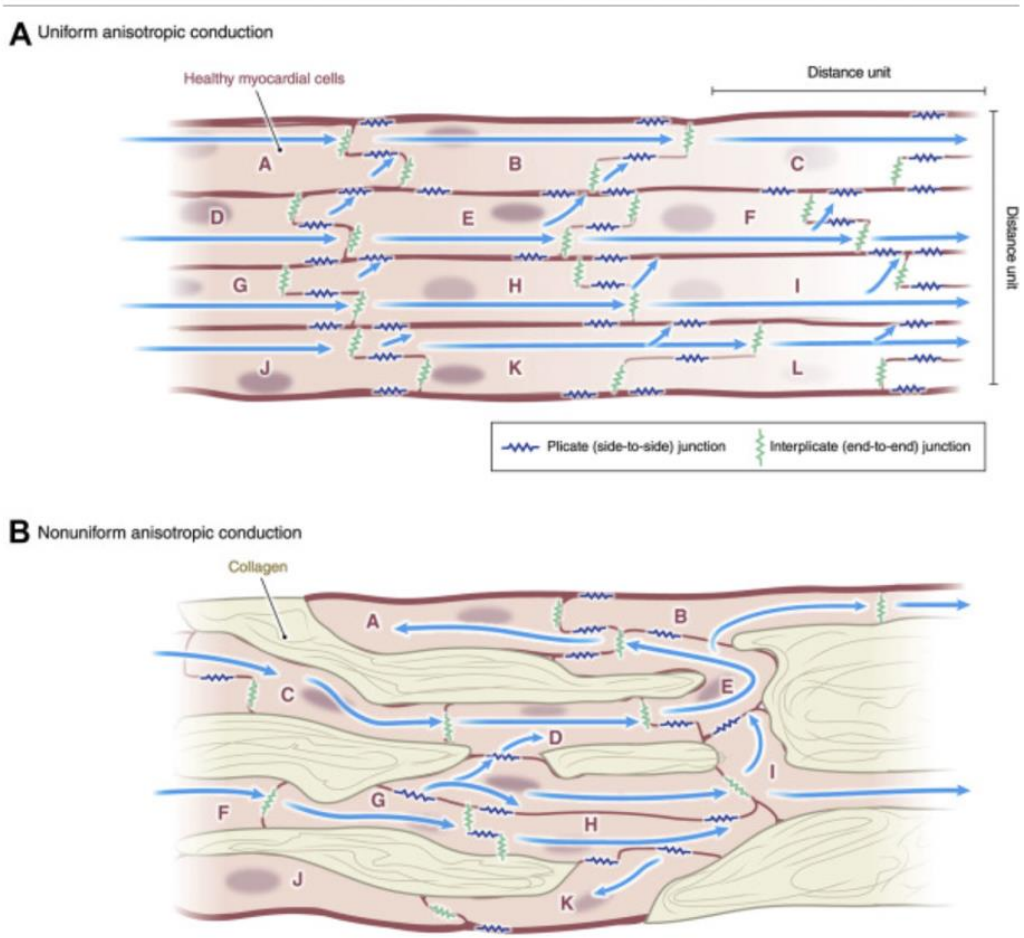

Figure 1.4 Effect of Cardiac Fibrosis on Anisotropic Conduction. A-L labelling represents the 12 depicted cardiomyocytes. Blue arrows represent longitudinal and transverse conduction between cells facilitated by interplicate (green) or plicate (dark blue) gap junctions. A) Uniform anisotropic conduction. B) Nonuniform anisotropic conduction with increased connective tissue disrupting lateral gap junctions, limiting transverse conduction, and slowing overall impulse propagation. Copyright © 2021, Journal of American College of Cardiology: Clinical Electrophysiology [60].

The canonical mechanism of fibrillar fibrosis involves fibroblasts, which are nonhematopoietic, nonepithelial, and nonendothelial cells that are responsible for synthesizing ECM proteins with diverse biochemical and physiological properties [62]. Transforming growth factor-beta 1 (TGF-β1), a cytokine released in response to atrial stretch, binds to its receptor, initiating phosphorylation of transcription factors Small Mothers Against Decapentaplegic two and three (Smad2/3). Subsequently, Smad4 binds to this dimer, translocating into the nucleus, where it regulates the expression of other transcription factors, initiates collagen synthesis, and promotes fibroblast-to-myofibroblast transdifferentiation (FMT) (Figure 1.5).

Nonetheless, many other cardiac-bound cells, including endothelial cells, cardiomyocytes, and macrophages, also aid in maintaining the underlying structure of the ECM by regulating protein production and producing ECM material [50]. All three are not only involved in producing fibrillar and non-fibrillar collagens but also are sources of many proteins, cytokines, chemokines, and proteases which adhere to and interact with the ECM. These include but are not limited to, TGF-β, TNFα, matrix metalloproteinase (MMPs), tissue inhibitor of metalloproteinases (TIMPs), platelet-derived growth factor (PDGF), secreted protein acidic and rich in cysteine (SPARC) thrombospondin (THBS), and lysyl-oxidase (LOX) (Figure 1.5) [54,55,63].

Interestingly, previous research, including studies conducted in our lab, has shown that in models of VO, exercise-induced AF, and aging-induced AF, there is no increase in myofibroblast activity or in the transcription levels of collagen genes [36,64,65]. This research then begs the question of what mechanism promotes fibrosis in such models.

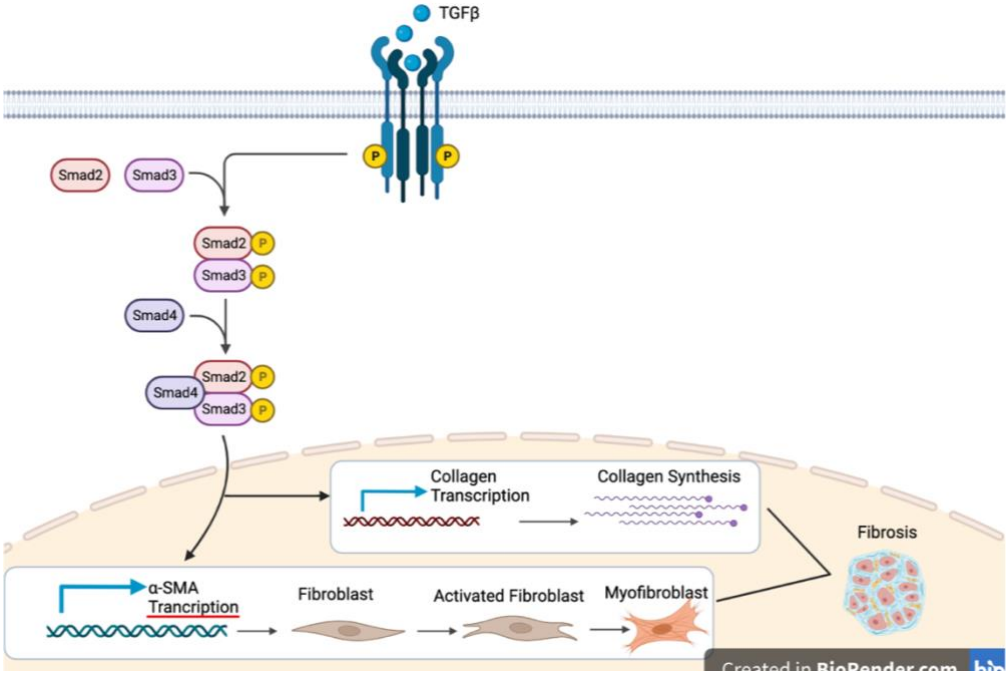

Figure 1.5 Canonical Mechanism of Fibrogenesis. TGF-β1 binds to its receptor, initiating phosphorylation of Smad2/3. Smad4 binds and translocates into the nucleus to regulate the expression of other transcription factors, initiate collagen synthesis, and promote FMT. Adapted from copyrighted material © [66,67]

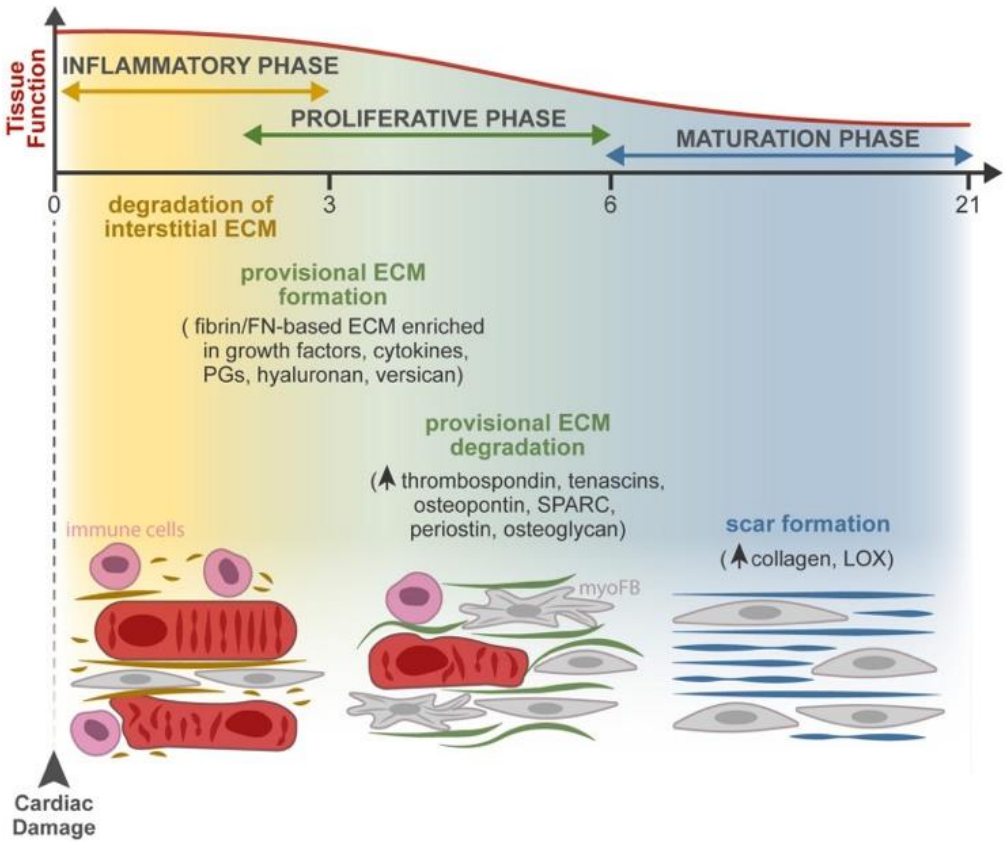

Figure 1.6 Extracellular Matrix Dynamics during Fibrosis. ECM fibrotic remodelling encompasses three main overlapping phases: inflammatory degradation of interstitial matrix, proliferative production and resolution of provisional ECM, and maturation scar forming phases. The inflammatory phase releases inflammatory mediators to recruit immune cells to produce matrikines, which further contribute to the inflammatory cascade. The proliferative phase is comprised of a transient fibrin and fibronectin matrix network formation rich in growth factors and inflammatory cytokines. Larger amounts of ECM structural proteins are deposited during this phase to preserve the integrity of the myocardium. The maturation phase increases collagen content due to the upregulation of LOX collagen cross-linking enzymes, which form rigid scars. Copyright © 2021, Frontiers in Cell and Developmental Biology [54].

1.5 Collagen: Accumulation vs. Degradation

Collagens are dynamic proteins which are constantly being synthesized and degraded. Thus, the degree of collagen present at any one time is due to the balance between these two actions. Excess collagen deposition, leading to fibrosis, can occur in three ways: increased biosynthesis, decreased degradation rates, and improved maturation and stabilization.

As mentioned, previous research that utilized similar models to the ones employed in this study found no increase in the transcription levels of collagen genes [36,64,65]. Hence, the reason for excess collagen deposition is not due to increased biosynthesis.

Degradation of the ECM is controlled by the interaction between MMPs and TIMPs. There are 24 defined MMPs, four of which (1, 8, 13, 18) are defined as 'collagenases' by their ability to cleave interstitial collagens I, II and III [68]. These MMPs cleave at specific glycine-isoleucine bonds three-fourths from the N-terminus in which there is reduced hydroxyproline, causing a relaxed secondary structure [68,69]. If collagen helices are more tightly wound action of these MMPs will be slowed because access to their cleavage points will be diminished. MMP2 and 9 are known as gelatinase A and B and are characterized by three repeats of a type II fibronectin domain within the catalytic domain, helping it bind to and digest gelatins, collagens, and laminin [68]. They function by diffusing laterally along intact collagen fibrils to form a gelatin-like state of unwound helices prior to proteolysis [70]. Collagens initially cleaved by collagenases can be subsequently further digested by gelatinases. However, a key distinction between collagenases and gelatinases is that the former cleaves internally at the ¾-¼ site and the latter at the termini [70]. The function of MMPs is regulated by four TIMPs (1-4), which can inhibit their activation and action [68].

Maturation and stabilization of collagens occur by a crosslinking action, where covalent bonds form inter- and intra-collagen fibrils. Crosslinking matures collagen fibrils creating insoluble helices more difficult to degrade. There are three ways in which collagen molecules are crosslinked: transglutaminase (TG), advanced glycated end products (AGEs) and lysyl oxidase and its like enzyme (LOX / LOXL) [71–73].

TG reinforces the ECM three-dimensional matrix of collagen fibrils by catalyzing reactions between glutamine and the lysine residues within collagen fibrils [73]. AGEs, on the other hand, create highly reactive end products that facilitate crosslinking through interactions involving glucose and oxygen radicals [72]. LOX functions by oxidizing lysine and hydroxylysine

residues on collagen chains, producing highly reactive aldehydes that can spontaneously react with amines or other reactive aldehydes to form inter- and intra-catenary covalent cross-linkages (Figures 1.6) [74,75].

This study will focus specifically on the role of LOX enzymes, as past research from our lab has identified LOX as one of the very few atrial genes differently regulated in a VO model of AF [65]. LOXL2, specifically, has been implicated in cardiac fibrosis in a wide variety of CVDs, including AF, and thus will also be explored [62,76–78]. The following section will present the structural and functional differences among the members of the LOX enzyme family.

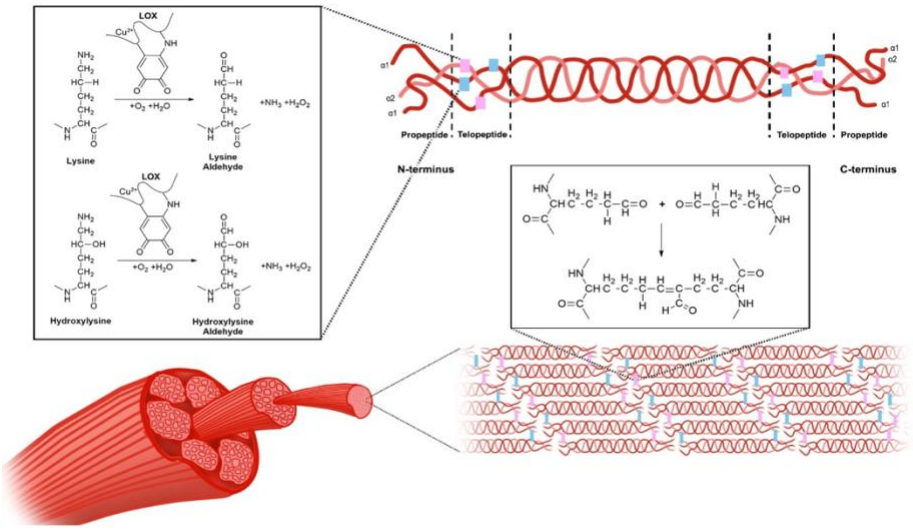

Figure 1.7 Mechanism of Lysyl Oxidase Collagen Crosslinking. LOX catalyzes lysine and hydroxylysine residues into lysine aldehyde and hydroxylysine aldehyde at the telopeptide region of procollagen molecules. These procollagen molecules then truncate to form tropocollagen molecules which self-assemble and crosslink to form collagen fibrils. Copyright © 2020, International Journal of Molecular Sciences [79].

1.6 Lysyl Oxidase Like Enzymes

LOX and it's like isoenzymes (LOXL) are copper-dependent extracellular amine oxidase enzymes [75]. They are a family of enzymes comprised of four isoforms with distinct genes, highly conserved carboxyl-terminal amine oxidase catalytic domains, and unique amino-terminal sequences (Figure 1.8) [75,80]. This means that while all isoenzymes may have similar catalytic properties and substrate requirements, they can have unique biological roles with functional variation. For example, LOXL2 mRNA has been detected in fetal hearts as well as in all four chambers of the adult heart, whereas LOXL3 is undetected in the fetal heart and only found in the adult aorta [80]. Additionally, LOXL3 and LOXL4 have been found to be highly involved in vascular remodelling, with little note of their cardiac involvement, while LOXL2 has already been shown to be positively correlated with left atrial fibrosis in AF patients [78,81].

LOXLs are expressed by four different cell types present in the heart that are also known to be upregulated in AF - fibroblasts [49], endothelial cells [82], cardiomyocytes [75,83], and macrophages [45,84]. However, the expressional pattern of disease progression has yet to be characterized and thus will be explored throughout this study.

LOX has been shown to be upregulated in AF patients and differentially regulated in the endurance exercise model of AF [65,85]. It is known that many of the upstream theorized regulators of LOX enzymes inflammatory mediators produced during the immediate immune inflammatory response seen with stretch [44]. TNFα, a known cytokine driving adverse remodelling, is thought to have a dose-dependent dichotomous effect on LOX expression from fibroblast in vitro [86,87]. Whereby a low dose of TNFα resulted in decreased LOX expression, and a high dose of TNFα resulted in an increased LOX expression. Additionally, TNFα has been found to down-regulate LOX expression and enzymatic activity in endothelial cells [87,88]. Even more, TGFβ-1 through PI3K/Akt and Smad pathways has significantly upregulated LOX mRNA and protein expression in cardiac fibroblasts [89]. Moreover, in a tumour microenvironment, LOX mRNA expression has been shown to be upregulated by interleukin 1 beta (IL-1b) and downregulated by fibroblast growth factor 2 (FGF2) [90]. Little research, however, has been done to study cytokine effects on LOX during a mechanical VO model of AF, as most previous work is done in vitro and with isolated cell types.

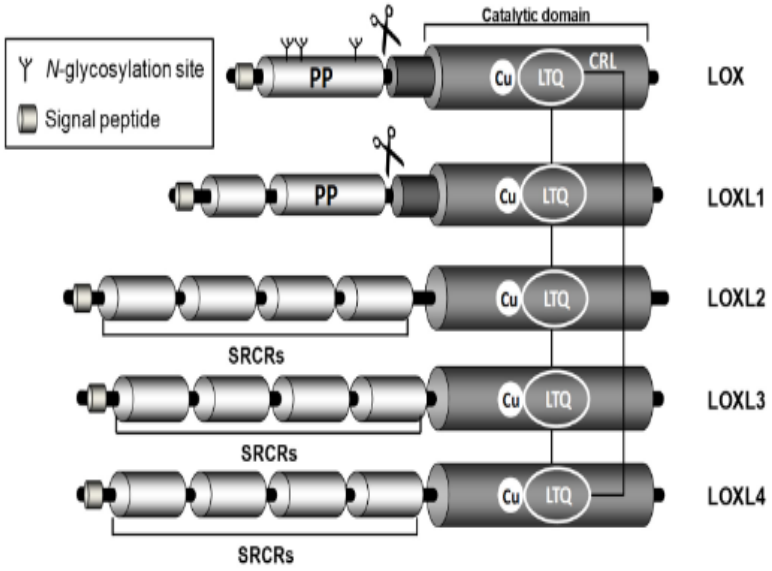

Figure 1.8 Structure of LOX isoenzymes. LOX isoenzymes share highly homologous regions at their C-terminal ends, characterized by a conserved catalytic domain consisting of the copper (Cu) binding site, lysyl tyrosyl quinone (LTQ) cofactor region, and the cytokine receptor-like (CRL) domain. LOX and LOXL1 feature propeptide sequences (PP) which are cleaved by Bone Morphogenic Protein One (BMP-1) protease (at specific sites marked by the scissors) to release the active forms. LOX can also undergo N-glycosylation at the identified locations. In contrast, LOXLs 2-4 contain four scavenger receptor cysteine-rich (SRCR) domains which facilitate protein-protein interactions. Copyright © 2019, Cells [75].

1.7 Atrial Fibrillation and Endurance Exercise

Although exercise is largely a beneficial aspect to include in one's life, there now is a region of research in which the notion of overtraining leading to disease is explored. Specifically, the prevalence of chronic high-level endurance training is now associated with lone AF generation (AF without any other sign of CVD or underlying health concerns). At one time, it was believed that the relationship between exercise and AF was a linear one. Now, however, the relationship is seen as a 'J-shape' in which moderate endurance exercise can initially aid in preventing AF, but frequent endurance exercise dramatically raises the likelihood [91].

The exact cause for AF generation with chronic endurance exercise is not entirely explicable. However, some common themes with pathologically generated AF have emerged. In addition to ventricular hypertrophy, LA hypertrophy is also seen with VO induced by endurance training. In fact, whereas LV hypertrophy has been proven to be a trait that can be detained after time removed from exercise, LA hypertrophy is not [92]. This could largely be due to the composition differences between the chambers, as the LA has a higher percentage of elastin than its inferior counterpart. Akin to over-stretching an elastic band, there is no return to the original form once beyond a threshold. Intern, increasing the size of the LA will extend the electrical pathway encouraging re-entry events and promoting AF. Even more, sinus bradycardia at rest is almost always seen with endurance athletes [93]. This is due to an increase in vagal tone and PNS activity shorting SA firing. $I_{K,ACh}$ channels become activated, shortening ERP and decreasing the impulse wavelength [93]. Altogether, this increases special heterogeneity of the APD and promotes functional re-entry promoting AF.

1.8 Risk Factors for AF

As knowledge and understanding of AF continue to advance, so does the list of risk factors implicated in predisposing individuals to its onset. Primarily, these factors encompass modifiable elements such as lifestyle choices and valvular disease [4]. However, aging – the number one predictor of AF incidence - is not preventable. The association between these determinants and the development of AF will be discussed next.

1.8.1 Non-Modifiable: Age, Sex, Genetics

As age increases, the likelihood of developing AF rises significantly, particularly after age 65. The incidence rate of AF is minimal, less than 0.01%, at 50 years of age but escalates to approximately 9% by age 80 [94]. This progression correlates with natural cardiac remodelling processes, which occur with age, affecting structural and electrical functions and leading to functional decline. Increased arterial compliance imposes greater mechanical stress on the heart. This is exacerbated by age-related changes in cells that typically undergo senescence. Together complicating compensation mechanisms [95]. Since most conditions promoting AF are associated with elevated filling pressures leading to atrial stretch, this uncontrollable increase in mechanical load associated with aging creates the perfect condition for AF creation.

With its high metabolic demand and abundant mitochondria, the heart is susceptible to oxidative damage and subsequent generation of reactive oxygen species (ROS). These ROS can directly affect cardiac fibroblasts or modulate fibrogenic actions through cytokine signalling pathways [95]. Excess fibrosis contributes to stiffness and impaired diastolic function and facilitates anatomical re-entry pathways acting as a unidirectional block, as discussed previously. Notably, there is evidence that de novo synthesis of collagen may not be the leading factor in cardiac fibrogenesis with aging and that collagen degradation may be more important to fibrotic progression. It has been shown that the rate of daily synthesized collagen drops from 20% in 1-month-old rodents to 2% in 24-month-old rodents [96]. Even more, mRNA expression of collagens I and III are significantly reduced in aging rodent myocardium [97]. Crosslinking of collagen molecules, a key post-translational modification, can impede degradation and is a major mechanism of fibrogenesis in the aging heart [95].

Furthermore, aging is associated with impaired reparative response to cardiac injury, promoting adverse dilative remodelling processes [95]. As discussed earlier, cardiac dilation, particularly of the LA, can promote triggered automaticity through mechanisms like EADs, influenced by altered APD and wavelength.

Additional non-modifiable risk factors for AF include one's gender and ancestral genetics. AF is found to be more common in men (1.1%) than women (0.8%), but women present with more severe symptoms [94]. The prevalence of clinically detected AF was greatest in Caucasians (11.3%), followed by Chinese (9.9%), Hispanic (7.8%), and African American

(6.6%) [98]. These differences exist due to inconsistencies between socioeconomic classes leading to variable access to adequate healthcare, surveillance, and recognition of AF.

1.8.2 Modifiable: Lifestyle, Hypertension, Valvular Disorders

Modifiable factors influencing the likelihood of developing AF include lifestyle choices such as inadequate physical activity, poor dietary habits leading to obesity, and excessive smoking or alcohol consumption [4]. These behaviours often contribute to hypertension, the fourth most significant predictor of AF, increasing the risk 2-fold [99]. Chronic hypertension induces structural cardiac remodelling that fosters a profibrotic environment, which in turn supports AF perpetuation [100]. Regular physical activity can mitigate hypertension's negative effects, although caution is warranted regarding excessive intensity, as discussed previously.

Nicotine, prevalent in chronic smokers, triggers a profibrotic response and inhibits cardiac electrophysiology by inhibiting K^+ channels, thereby increasing susceptibility to arrhythmias [101]. Chronic smokers have a 21% chance of developing AF, whereas those who have quit reduce their odds to only 9% [102]. Likewise, excessive alcohol consumption contributes to AF onset, often referred to as "Holiday Heart" [103]. Immoderate alcohol increases oxidative stress and inflammation while inhibiting Ca^{2+} release from the sarcoplasmic reticulum, resulting in cardiomyocyte injury and, subsequently, fibrosis [104]. Even one extra glass per day can increase the risk of AF by 8% compared to those who abstain [105]. For those already suffering from AF, alcohol acts as a trigger, doubling the odds of having a bout of AF within the following four hours after consumption [103].

Valvular diseases, although not directly controllable, are treatable contributors to AF risk. There are three types of valvular diseases in the heart: regurgitations, in which valves between chambers do not close properly, allowing for retrograde flow, stenosis in which the valve opening narrows, restricting blood flow; and atresia, in which the passageway is absent, inhibiting blood flow all together [106]. These can occur at any of the heart's four valves - aortic, pulmonary, tricuspid, or mitral. In this study, the focus remains on aortic regurgitation (AR).

AR imposes a mechanical overload in the form of VO during diastole due to the reflux of blood through the aortic valve. It presents with diastolic wall stress, initial eccentric hypertrophy, chamber dilation at both end-systole and diastole, significant angiogenesis, and eventual fibrosis [107,108]. Two weeks into disease progression, LV free wall thickening associated with pressure

overload concentric hypertrophy is seen due to the need to keep CO constant, increasing stroke volume (SV) and systolic blood pressure [108]. Furthermore, a hallmark of AR is fibrosis composed of non-collagen extracellular matrix elements. It has been proven that proline incorporation, an amino acid composing 10% of collagen, and collagen synthesis are unchanged by AR, but fibronectin was upregulated [64].

AR also exerts hemodynamic stress on the LA, promoting mechanical stretch and remodelling that predisposes to AF. Studies indicate that AR produces substantial conduction delay and block in the superior intercaval area, creating a strong correlation between AP conduction disruption at Bachmann's bundle and AF [109]. Furthermore, AR-induced AF vulnerability involves inflammatory processes, including tumour necrosis factor (TNF), – a proinflammatory cytokine promoting atrial remodelling [35].

1.9 Synopsis and Hypothesis

AR and endurance swim training induce cardiac chamber VO, leading to complex remodelling and heightened susceptibility to AF [16,107]. Notable, this process involves excessive deposition of fibrotic tissue, which can act as a substrate promoting re-entry of electrical impulses and impairing myocardial contractility [25,61]. The accumulation of collagen occurs without alterations in its transcription rates or upregulation of the usual cell types associated with canonical fibrogenesis [66,67]. Thus, the mechanism facilitating fibrosis in AF remains unclear. Previous studies have identified LOX as differently expressed in AF models, suggesting that collagen accumulation may arise from maturation and crosslinking processes [65,85]. Despite links between LOX and LOXL2, and fibrosis in AF, no studies have directly examined its role in AF induced by VO from AR or endurance swim training. Consequently, this study aimed to investigate the impact of LOX family enzymes in AF using two VO models—one pathological and one physiological.

Furthermore, cellular expression patterns of LOXL2 throughout AF disease progression have not been thoroughly characterized. Thus, this study aimed to elucidate these patterns to identify specific cellular targets within the heart.

I hypothesize that LOXL2 inhibition and, even more, broader Pan-LOX inhibition will attenuate fibrosis, impeding structural remodelling and reducing susceptibility to AF.

I hypothesize pathological LOXL2 expression will arise predominantly from macrophage and fibroblast cell type upregulation.

The objectives of this study were to:

1) Assess the structural and electrical effects of pan-LOX and LOXL2 inhibition in the context of AR and endurance swim training.
2) Characterize the temporal changes in cellular LOXL2 expression as AR progresses.
3) Understand the pathophysiological mechanisms underlying fibrosis in AF.

Technical Contributions

I acknowledge the following individuals for contributing to my M.Sc. project:

Dr. Robert Lakin

Performed all aortic regurgitation and sham surgeries, echocardiogram assessments, and in vivo electrophysiological studies (refractory period measurements and AF inducibility data). Provided vast technical consultation and support throughout.

Renée Gorman

Created the swim apparatuses, helped isolate some of the hearts, and assisted with some of the swims. Trained me on many techniques, including the endurance swim training protocol and how to recognize proper swimming techniques in murine species.

Hasti Tajdari

Volunteered to assist with swimming the mice.

I was responsible for organizing endpoint measurements, tracking the consumption of drugged chow and changes in BW, and predominantly swimming the mice. I was also responsible for histological, immunohistochemical, qPCR, and morphological assessments. I also performed all data analysis and generated all figures and tables.

Chapter 2: Materials and Methods

2.1 Experimental Animals and Inhibitors Used

CD1 male mice (Charles River) were randomly assigned to different experimental groups. One cohort underwent AR surgery, while another underwent daily exercise. Additionally, all mice were further randomly divided into three cohorts, each consuming chow incorporated with either PXS-5505 pan-LOX inhibitor (D21012504R, Open-Source Diets), PXS-5382 – LOXL2 inhibitor (Formula 1, Open-Source Diets*)*, or no drug as the control (D20011301, Open-Source Diets). All mice were housed in identical environments, under ambient temperature with 40% humidity, a 12:12 hour light-dark cycle and consumed their assigned diets ad libitum. Experimental procedures adhere to the guidelines set by the Canadian Council on Animal Care Standards.

2.2 Aortic Regurgitation Protocol

Mice were initially anesthetized with a 3% isoflurane-oxygen mixture and then maintained under general anesthesia with a 1.5% isoflurane-oxygen mixture via nose cone throughout the surgery. A depilatory cream was used to remove the chest fur (Nair, Church and Dwight, Princeton, NJ, USA), and iodide soap was used to disinfect the area. Before the initial incision, mice received an intraoperative loading dose of 2mg/kg of Metacam (Meloxicam) for analgesia.

A 5mm incision was made over the trachea to expose the carotid allowing for separation from the vagal nerve. A small incision was made into the right common carotid artery, and under the guidance of ultrasound imaging (Vevo2100 Echocardiography VisualSonics), a plastic catheter with a metal wire was inserted into the carotid through to the aortic orifice. The metal wire was then advanced through the catheter to puncture the aortic valve. This process was repeated until the Doppler imaging presented a diastolic retrograde flow greater than 200mm/s. Once the degree of regurgitation was satisfied, the catheter and metal wire were withdrawn, the right common carotid artery ligated, and the skin sutured closed [35,107,108].

Sham mice were used as controls. These mice underwent an identical procedure for AR production as described above without puncturing the aortic valve.

2.3 Exercise Training Protocol

Exercise training was performed by subjecting the mice to 240 minutes of swimming (two 120-minute sessions separated by a 4-hour rest window) for 5 days a week for 4.5 weeks. This duration was selected following the results of Gorman et al. [110], which proved that this duration significantly increased AF inducibility and fibrosis.

Swimming occurred in buckets filled with thermoneutral water (30-32ºC) to 16cm deep with pumps generating circular currents at 15L/min. CD1 mice naturally swam against the current, inducing resistance training. Before exercising, the mice were acclimatized to the system by performing a 30-minute session that increased by 10 minutes daily until 120 minutes were reached. After 70 minutes, mice swam twice daily to begin acclimating to the full swim schedule (Table 2.1). Following the 8th acclimation day, mice began swimming on their full schedule of two 120-minute sessions daily, separated by a 4-hour rest window.

Sedentary control mice were placed in undisturbed water for 10 minutes twice daily for 6 weeks to match the handling time and environment of the experimental groups.

Table 2.1 Acclimation Period for 240min Swim Duration Protocol. One swimming session per day was held from day one to five and day eight. On day six, seven mice swim twice per day with a four-hour rest window in between. The full training protocol commenced on day 9 and was carried out for 4.5 weeks.

Day 1	Day 2	Day 3	Day 4	Day 5	Day 6	Day 7	Day 8
30min	40min	50min	60min	70min	80min 90min	100min 110min	120min

2.4 Echocardiograms

Mice were initially anesthetized with a 3% isoflurane-oxygen mixture and then placed in the supine position with the anesthetic decreased to 1.5%. Mice were placed on a heating pad to ensure normothermia was maintained, and this core temperature was measured via a rectal probe (THM 150, Indus Instruments, Webster, TX, USA). Respiratory rate and core temperature were monitored and kept between 90-120 per minute and 36.9-37.3ºC respectively. Their heart rate was around 500 bpm. Nair (Church and Dwight, Princeton, NJ, USA) was used for the depilation of the chest fur to allow for the application of acoustic coupling gel (Aquasonic 100, Parker Laboratories Inc., Fairfield, NJ, USA).

Cardiac structure and function were assessed using the high-frequency ultrasound system Vevo2100 (VisualSonics, Toronto, ON, Canada) with Doppler echocardiography in the transthoracic B-mode and M-mode configurations. Left ventricular structural and functional indices (including end-diastolic diameter, end-systolic diameter, posterior wall thickness, ejection fraction and fractional shortening) were assessed using a 30 MHz ultrasonic linear transducer in the long-axis view. Electrocardiograms were simultaneously recorded in the lead II configuration. Data was analyzed using the VisualSonics data analysis suite.

2.5 In vivo Electrophysiology: Intracardiac – Effective Refractory Period and Inducibility

Mice were initially anesthetized with a 3% isoflurane-oxygen mixture and then placed in the supine position with anesthetic decreased to 3% for intracardiac measurements. Core temperature was monitored via rectal probe (THM 150, Indus Instruments, Webster, TX USA), and kept between 36.9-37.3ºC. A small incision on the right side of the chest was made to expose the right jugular vein. Via the superior vena cava, a 2F octopolar recording/stimulating catheter (CI'BER Mouse, Numed, Hopkinton, NY, USA) entered the right atrium and ventricle for bipolar electrogram reading with the use of a Gould ACQ-7700 amplifier with P3 acquisition software (Data Sciences International, New Brighton, MN, USA). For consistency between animals, the largest bundle amplitude would always be found with lead 34.

After 15 minutes of stabilization, assessments began. Stimulations were first repeated at 20ms below the R-R interval to determine the voltage capture threshold. After, all measurements were taken at 1ms pulse duration, at a voltage magnitude of 1.5 times the capture threshold. Due to the small size of the atria compared to the recording rings (0.5mm long, with 0.5mm between each), a short duration of 27 was used. The atrial effective refractory period (AERP) was determined by a driving train (S1) of 7 pulses at 20ms below the R-R interval via leads 78 and 56. This was followed by an S2 coupling interval starting below capture (~15ms) and increasing by 5ms increments until atrial capture. Once here, the S2 interval was then progressively decreased by 1-2ms until capture loss was re-established (Figure 2.1).

Burst pacing with intervals less than the AERP created the AF inducibility protocol [36]. For arrhythmia induction, 27 pulses with a 1ms duration and a 40ms interval were delivered to the right atria. In 2ms decrements, the interval was decreased to 20ms. This was repeated three times. If no arrhythmia events were present, 20 trains were given every 1.5s for 20 pulses with a

20ms interpulse interval. Sustained arrythmias were characterized as episodes of reproducible rapid, chaotic, and continuous activity lasting longer than 10s. (Figure 2.1).

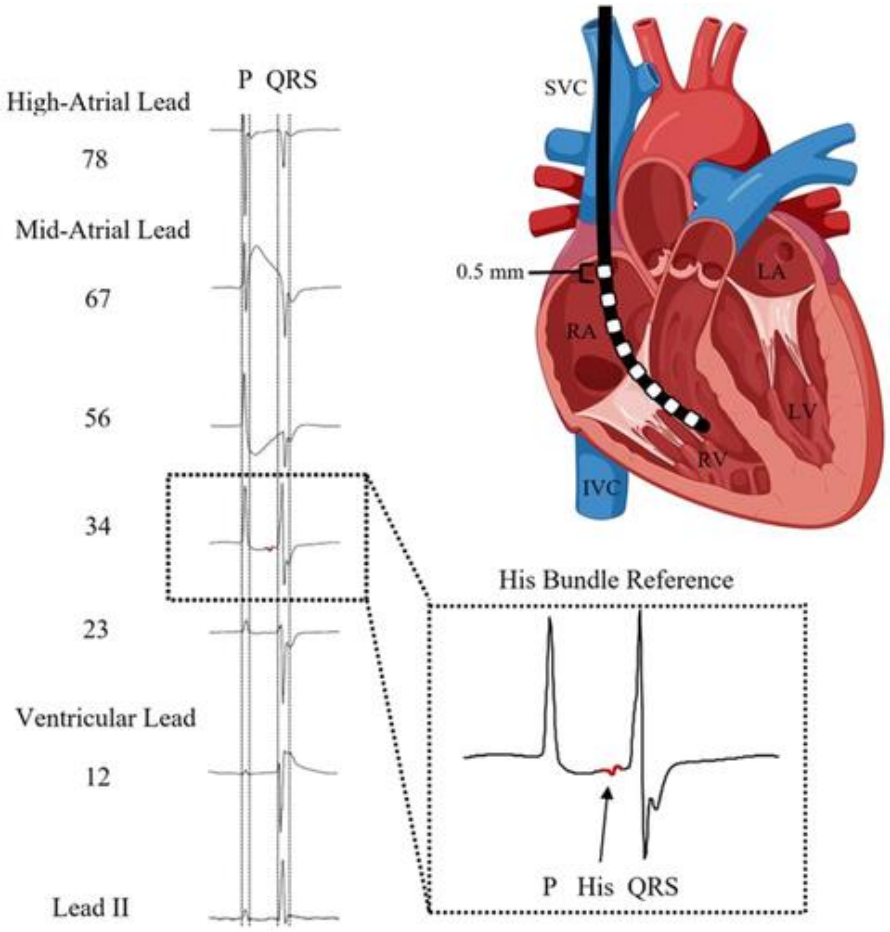

Figure 2.1 Intracardiac 2-Fr electrophysiology catheter placement in the right heart. Through the right jugular vein, a 2F EP catheter was directed through the right atrium and positioned within the ventricle. The atrial P wave progressively increases, while the ventricular QRS complex progressively decreases from the distal (12) to proximal (78) leads. Leads 78 and 56 were used to stimulate the high and mid right atrium. Lead 12 was stimulated in the right ventricle. The bundle of His with Lead 34 (bottom right) confirmed the correct positioning. Concurrent surface ECG recording was represented in Lead II. Each catheter lead is 0.5 mm long and separated by 0.5 mm between each platinum ring. LA, left atrium; RA, right atrium; LV, left ventricle; RV, right ventricle; SVC, superior vena cava; IVC, inferior vena cava. Based on Aschar-Sobbi et al. 36 and illustrated by Gorman et al. [110]. Copyright © 2024, The Journal of Physiology [110].

2.6 Cardiac Morphology

Prior to isolation, mice are heparinized via 0.2ml intraperitoneal injections (1000IU/ml, Leo Pharma, Thornhill, ON, Canada) to prevent blood clots from forming. Following, mice were anesthetized with a 1.5% isoflurane/oxygen mixture, and a toe pinch was performed to ensure an unconscious state was achieved. A ventral incision from the abdomen to the chest along the midsternal line and two perpendicular cuts along the bottom of the sternum laterally to the dorsal side were made to reveal the diaphragm. The diaphragm was cut open to reveal the thoracic cavity and allow for heart extraction. The pericardium, lungs and all other connective tissues were removed. The aorta is cut, and the heart is rinsed in 0.01M phosphate buffer saline (PBS) to remove any residual blood within the chambers. The heart is blotted dry before being weighed. The right hindlimb was also collected and stored in bleach to expose the tibia, and its length was then measured via callipers for normalization of the heart weights.

2.7 Immunohistochemistry and Histology

Hearts were isolated as described above, but instead of direct extraction, once the pericardium and excess tissue were removed, the inferior vena cava was severed, and the heart perfused through the apex using a 25-gauge needle. Perfusion first occurred with 5mL of 1%KCl in 0.01M PBS to arrest the heart in diastole and then with 15mL of 4% paraformaldehyde (PFA) in 0.01M PBS to fix the tissue. Once excised, the tissues were washed in 0.01M PBS, cleaned of any excess connective or adipose tissue and sliced coronally for a 4-chamber view. Half of the heart was denoted for optimal cutting temperature (OCT) embedding, and the other half for paraffin embedding.

2.8 OCT – IHC

After a four-chamber view cut was made, OCT-embedded hearts were placed back in 4%PFA in 0.01M PBS for 1 hour at room temperature for further fixation. Once time had elapsed, the PFA was thoroughly washed out of the hearts and then placed in two solutions of increasing sucrose gradients (15%, 30%) in 0.01MPBS and allowed to become fully saturated (denoted by the tissue sinking), acting as a cryoprotectant before freezing. Individual tissues are embedded and frozen in OCT and then sliced into 10μm thin serial sections via cryostat onto superfrost-charged slides. For immunohistochemical (IHC) staining, tissues were then rinsed in

PBS for 5 minutes to melt off any excess OCT, individually encircled with a hydrophobic barrier pen, and incubated with blocking buffer (1% Bovine Serum Albumin (BSA), 10% Goat Serum with 0.3M glycine in PBS-Tween20 (0.1%)) for 2 hours at room temperature to prevent any non-specific binding. Following this, three washes using PBS-Tween20 for 5 minutes were performed to remove any residual blocking buffer. Two of the three tissues per slide were incubated overnight at 4ºC with a primary antibody buffer solution consisting of PBST, 1% BSA, and the appropriate antibody (Table 2.2). The final tissue was incubated with only the buffer solution and no primary antibody, which acted as the negative control. The following day, three five-minute washes with PBST were performed to remove the primary buffer solution, and all three tissues on the slides were incubated for 1 hour at room temperature with a secondary buffer solution consisting of PBST, 1% BSA, wheat germ agglutinin (WGA) (membrane stain) and the appropriate secondary antibodies (Table 2.2). Followed by another three five-minute washes with PBST, 10-minute incubation with DAPI (nucleus stain), 2 three-minute washes with PBST, and mounting with a homemade antifade aqueous mounting medium (Appendix A.7). 3-4 representative images per chamber were taken with the EVOS AutoFlo 2 for analysis.

Analysis was performed using FIJI software, in which a binary mask was placed on DAPI, LOXL2, and the cellular signal. Only signals overlapping with more than 5 pixels were counted as real and colocalized. Cellular counts were normalized to tissue area by using the WGA channel. This was repeated in 3-4 images per chamber to obtain a complete, accurate representation.

Table 2.2 List of Primary and Secondary Antibodies

** Please note all antibodies listed in italics correspond with section 3.3, which presents and discusses ongoing studies to be completed for future publication. **

Primary Antibodies			
Antibody	**Target**	**Dilution Factor**	**Supplier**
Rat Anti-Mouse Primary F4-80	Macrophages	1:300	BIO-RAD
Rabbit Anti-Mouse CD31	*Endothelial Cells*		*Abcam*
Rat Anti-Mouse Vimentin	*Fibroblasts*	*1:500*	*R&D*
Rabbit Anti-MouseLOXL2	LOXL2		NOVUS
Goat Anti-Human LOXL2	*LOXL2*		*R&D*
Rabbit Anti-Mouse LOXL3	LOXL3		NOVUS

Secondary Antibodies			
Antibody	**Target**	**Dilution Factor**	**Supplier**
Goat Anti-Rabbit TexasRed	*CD31*, LOXL2, LOXL3	1:1000 1:2000	Novus
Goat Anti-Rat 647	F480, *Vimentin*	1:5000	Invitrogen
Donkey Anti-Goat 647	*LOXL2*		*ThermoFisher*

2.9 Paraffin – Histology

After a four-chamber view cut was made, paraffin-embedded hearts were placed back in 4%PFA in 0.01PBS and allowed to incubate overnight at 4ºC. The following day, three 1-hour PBS washes thoroughly rinsed the hearts of residual PFA. Individual samples were then placed in enclosed cassettes to undergo serial washes for dehydration (ethanol at 70%, 80%, 95%, 100%, 100%, respectively), clearing (100% xylene:100% ethanol, xylene, xylene), and acclimation (paraffin at 60ºC x3) of the tissue prior to embedding. Tissues are then sliced into 5µm thin serial sections using a microtome onto super frost-charged slides and allowed to dry overnight. For histological staining, slides were first deparaffinized by a series of 5-minute washes with xylene twice, xylene:ethanol, and then gradually rehydrated through another series of 5-minute washes with ethanol (100%x2, 95%, 70%, 50%) and tap water for 10 minutes. Slides were incubated in Bouin's solution for 2 hours at 56ºC as a mordant to link the dye to the targeted tissue components. Slides were rinsed under tap water for 10 minutes, and tissues were encircled by a hydrophobic barrier pen before Masson Trichrome staining. First, tissues were incubated for 5 minutes with a working Wiegerts Iron Hematoxylin (1:1 ratio of solution A: solution B) to stain nuclei dark brown, then rinsed under running tap water for another 5 minutes. Tissues were incubated for another 5 minutes with Biebrich Scarlet-acid fuchsin, which stained all acidophilic tissue (cytoplasm, muscle, collagen) red and then rinsed in distilled water. Following, tissues were incubated for 15 minutes with phosphomolybdic-phosphotungstic solution, a decolorizer which diffuses the previous acidic stain out of collagen leaving only the muscle tissue with red colouring. This is tapped off, and tissues are finally incubated with Aniline Blue, which stains all collagen blue. Slides are rinsed in distilled water and then incubated in 1% acetic acid for 1 minute to differentiate the tissue colourations by removing excess dye from the tissue creating a sharper and cleaner stain. Tissues are then put through a series of ethanol solutions for dehydration (95% twice, 100% twice), and xylene for clearing (100%) for 15 seconds each, and then mounted with coverslips using Toluene (Fisher Scientific, Waltham, MA, USA). Using the Brightfield EVOS AutoFlo 2, three to four images at 20x magnification were taken in the left atria and ventricle. Data was then analyzed using FIJI-ImageJ software with the colour threshold method, isolating for the blue hue (120-180). These values were presented as a percent of the relative total tissue area.

2.10 Quantitative Polymerase Chain Reaction (qPCR)

Hearts were extracted following the protocol outlined in section 2.6. Once whole hearts were weighed, each chamber was dissected, weighed, and flash-frozen in liquid nitrogen to prevent further RNA degradation. Frozen tissue (either LA or LV) was placed in a 2ml Eppendorf tube containing 500µl of TRIzol, an acid-guanidinium-phenol-based reagent used to extract RNA, for sonication. Once the tissue was fully disrupted, samples were centrifuged for 10 minutes at 12000xg at 4ºC to form a debris pellet for disposal. To the supernatant, 100µl of chloroform was added and left to rest at room temperature for 15 minutes prior to a 15-minute centrifuge cycle. This performs phase separation, leaving RNA in the uppermost aqueous layer. This layer was carefully removed and mixed with 300µl of isopropanol to precipitate the RNA. The sample was then transferred to a silica RNA binding mini spin column (BIORAD - Aurum™ RNA Mini Kit 7326820) and centrifuged for 1 minute. The column was washed twice with 700µl low stringency wash, followed by a 1-minute centrifuge after each wash, to remove any biomolecules (i.e., carbohydrates, fatty acids, proteins) that may have non-specifically bound to the silica membrane. The column was then incubated with diluted DNase1 for 25 minutes to remove any DNA from the sample. This was followed by a 700µl high stringency wash to remove any additional non-specific particles. The column was then spun empty for 2 minutes to ensure it was fully dry and no residual wash buffers were present. At this time, the elution buffer was heated at 75ºC for 3 minutes to ensure a higher yield by releasing more of the RNA from the silica membrane. 20 or 25µl of elution buffer (LA or LV, respectively) was added directly to the bottom of the spin column and centrifuged for 1 minute. This process was repeated twice, producing final volumes of 40µl in LA samples and 50µl in LV samples.

RNA samples were inspected for impurities and their final concentration using the Thermo Scientific™ Nanodrop™ One Microvolume UV-Vis Spectrophotometer. RNA with 260/280nm absorbance of approximately 2.0 and 260/230nm absorbance between 1.0 and 2.0 were considered to have adequate integrity and purity.

Reverse transcription was performed using a high-capacity cDNA Reverse Transcription Kit (Applied Biosystems — 4368814). Briefly, 2.0µl of 10x reverse transcription (RT) buffer, 0.8µl of 25x Deoxynucleotide triphosphate (dNTP), 2.0µl of 10x RT random primers, and 1.0µl of Multiscribe™ reverse transcriptase were combined in a 2ml tube. RNA was added based on

its concentration to create 500ng of cDNA ($\frac{500ng}{[RNA]ng/ul}$). The remaining space in the 20µl was filled by nuclease-free water.

qPCR was performed using PowerUp™ SYBR™ Green Master Mix (Applied Biosystems – A25741) and run on the CFX Opus 96 Real-Time PCR System (BIO-RAD – 12011319). cDNA was loaded at 10ng per well, primers at 500nm, and GAPDH was used as the housekeeping gene. The primers used, and their respective sequences can be found in Table 2.3. PCR results described as a cycle threshold value (CT) were obtained using BR.io online software and compared using relative quantitation of gene expression with the comparative CT method (ΔΔ CT method). The amount of target was normalized to an endogenous reference (GAPDH) and described as relative to the control group by 2-ΔΔCt.

Table 2.3 qPCR Primer Sequences

Gene	Gene Symbol	Sequences
Collagen type I - α1	COLIα1	**Fwd:** CCTCAGGGTATTGCTGGACAAC **Rev:** CGATCTCGTTGGATCCCTGG
Collagen type III - α1	COLIIIα1	**Fwd:** AAGGCTGCAAGATGGATGCT **Rev:** AAGGCTGCAAGATGGATGCT
Collagen type IV - α1	COLIVα1	**Fwd:** ATGGCTTGCCTGGAGAGATAGG **Rev:** TGGTTGCCCTTTGAGTCCTGGA
Lysyl oxidase Like 2	LOXL2	**Fwd:** CGACTTATCCTAGGAGCTCGG **Rev:** CAGGGAAGGCAGCAAGACAA
Fibronectin 1	FN1	**Fwd:** GGGAGGAAGAAGACAGATGAG **Rev:** TACCCAGGGTTGGTGATGAA
Transforming growth factor beta 1	TGF-β1	**Fwd:** GGAATACAGGGCTTTCGATT **Rev:** CTCTGTGGAGCTGAAGCAAT
Secreted protein acidic and cysteine rich	SPARC	**Fwd:** CACCTGGACTACATCGGACCAT **Rev:** CTGCTTCTCAGTGAGGAGGTTG
Thrombospondin 2	THBS2	**Fwd:** TTTCAGTATCAGCAACATCAACCG **Rev:** GAGCCTTTGGCCACGTACATC
Transglutaminase 2	TG2	**Fwd:** GAAGGAACACGGCTGTCAGCAA **Rev:** GATGAGCAGGTTGCTGTTCTGG
Platelet derived growth factor - D	PDGF-D	**Fwd:** TTGTACCGAAGAGATGAGACCA **Rev:** GCTGTATCCGTGTATTCTCCTGA
Glyceraldehyde 3-phosphate dehydrogenase	GAPDH	**Fwd:** TGCACCACCAACTGCTTAG **Rev:** GGATGCAGGGATGATGTTC

2.11 Statistical Analysis

Summary data are presented as Mean ± SEM unless otherwise stated. Statistical assessments primarily included unpaired student's t-test, one-way ANOVA or two-way ANOVAs with Tukey's multiple comparison tests and chi-square Fisher's tests. *$P \leq 0.05$ for significance with analyses performed using Prism.

Chapter 3: Aortic Regurgitation Results

3.1 Aortic Regurgitation: Cardiac Adaptation

In this study, the primary objective was to investigate the relationship between LOX family enzymes and AF. The rationale for the study is due to the knowledge that fibrosis increases in VO models of AF without changes in collagen gene transcription levels [65]. To achieve my objectives, I initially chose to perform my studies with an AR murine model, which was developed in the lab to assess the effect of VO on AF susceptibility and its associated cardiac remodelling. Specifically, I used seven-week-old CD1 male mice which underwent surgery to introduce AR and were fed either normal chow or chow infused with one of two drug conditions (LOXL2 inhibitor or Pan-LOX inhibitor). Controls involved sham surgeries as well as random selection for the three chow conditions. After the surgery, mice were returned to their normal housing for four weeks to allow disease progression.

At four weeks of disease progression (11 weeks old), AR mice exhibited markedly increased ($P<0.0001$) susceptibility to AF with 71% incidence compared to 0% in sham mice (Figure 3.1 Panel A). This AF susceptibility was accompanied by an increase ($P=0.0024$) in atrial arrhythmia duration by 13.8 seconds (Figure 3.1 Panel C) and a decrease ($P=0.0243$) in the atrial effective refractory period (AERP) (Figure 3.1 Panel D). Additionally, AR mice presented with a 5.8% elevation in LA fibrosis (~11.2% versus ~5.4% estimated using Mason's Trichrome, $P<0.0001$) (Figure 3.2). AR mice also presented with increased ($P<0.0001$) total heart (Table 3.1). This was accompanied by increased ($P<0.0001$) left ventricular systolic (LVS) and diastolic (LVD) diameters, as measured by visual inspection and echocardiogram on a live mouse (Table 3.1). AR mice also presented with reduced ($P<0.0001$) ejection fraction and fractional shorting percentage, decreasing from 60.88% ± 3.05 to 55.9% ± 3.03, and 32.26% ± 2.16 to 27.8% ± 0.8 respectively (Table 3.1), consistent with the expected response [107,108]. Additional posterior wall thickness (PWth) was seen to increase ($P<0.0001$), with AR imposing a growth of 0.10mm (Table 3.1).

Left ventricular chambers presented with 0% sustained ventricular arrythmias (VA), no change in VERPs or VA durations, and no increase in the percent of fibrotic tissue ($P=0.0587$) (Appendix A.2/A.3).

Importantly, these alterations in cardiac morphology and function occurred without any change in HR (Table 3.1, P=0.1296) and did not affect chow consumption (Appendix A.1, P=0.8043) nor end body weight (BW) (Table 3.1, P=0.1256).

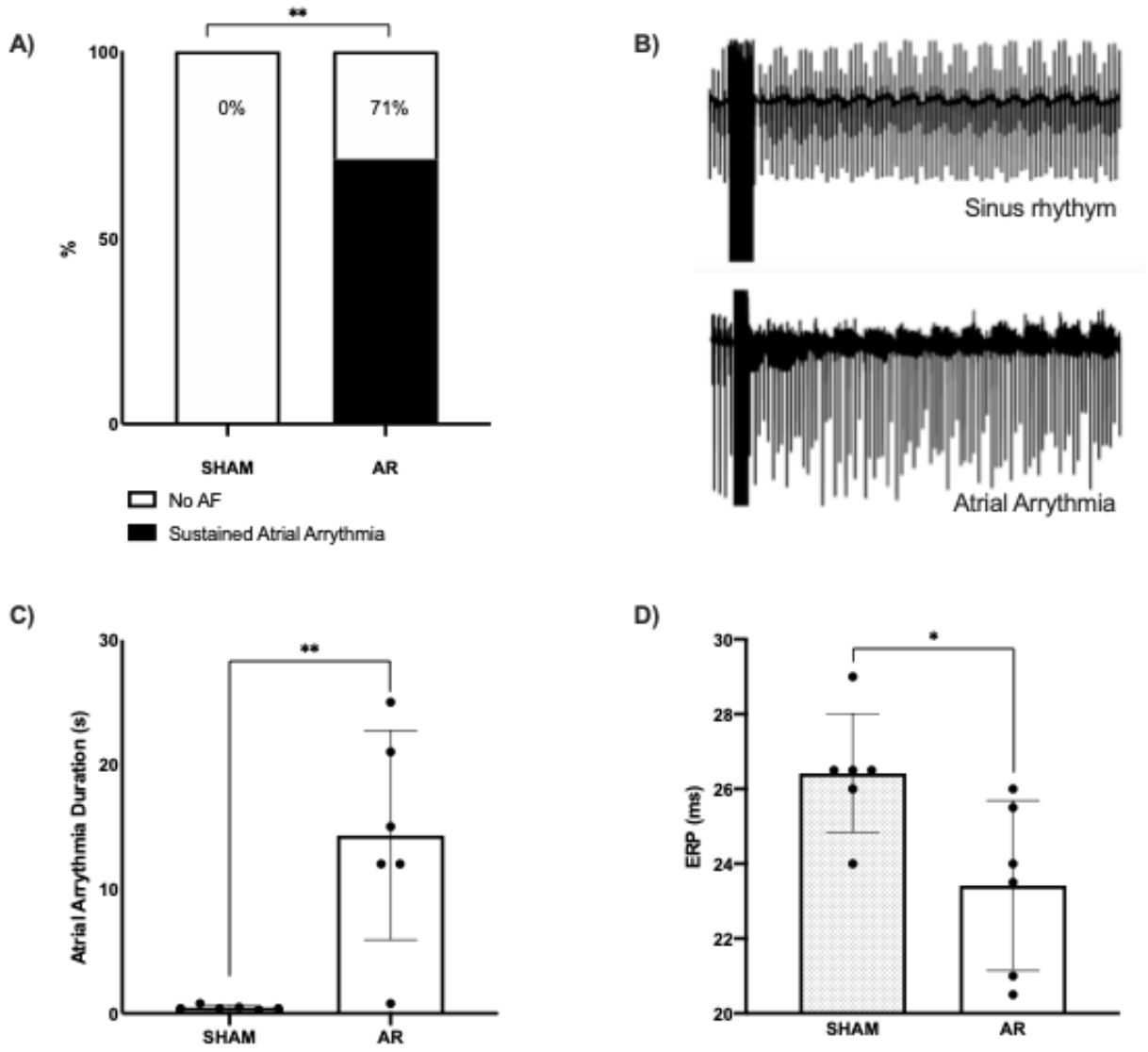

Figure 3.1 Effect of Atrial Refractoriness and AF Susceptibility with AR. The intracardiac analysis assessed differences in electrical remodelling and AF inducibility between sham and AR cohorts. **A/B)** Quantified percent of sustained arrhythmia (longer than 10 seconds) and representative sinus rhythm and arrhythmia tracings. **C)** Changes in atrial arrhythmia duration(s). **D)** Comparison of the atrial effective refractory period (AERP) (P=0.0243). Data presented as mean ± SEM with *P<0.05, **P<0.01 using Chi-Square Fisher's test and unpaired t-tests; *n*=6 sham, *n*=6 AR.

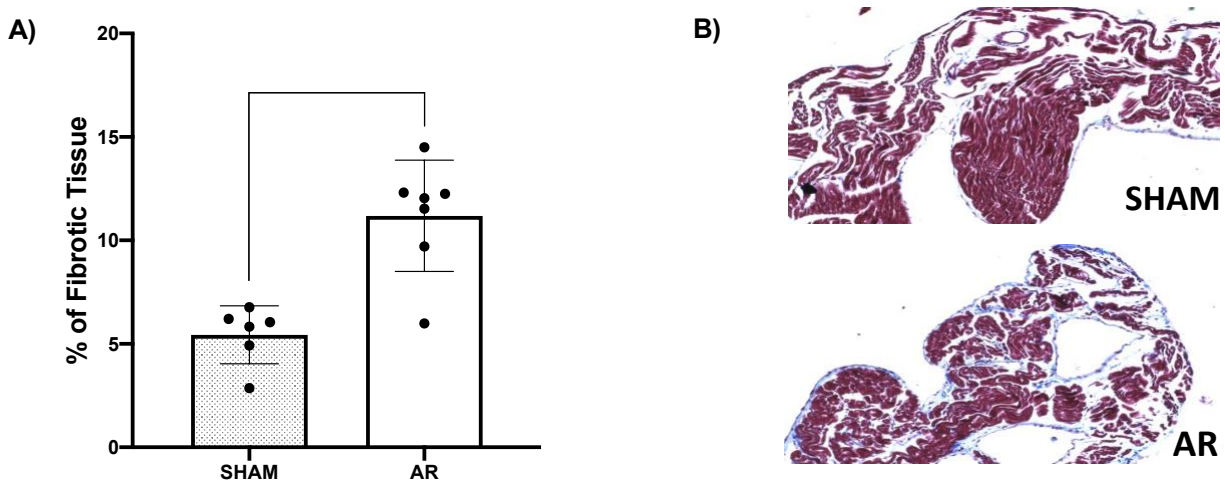

Figure 3.2 Effect of Left Atrial Collagen Deposition with AR. Left atrial collagen percentage estimated with Masson's Trichrome and imaged with EVOS brightfield microscope at 20x magnification. Comparisons between sham and AR cohorts. **A)** Quantification of the percent of left atrial collagen deposition normalized to the tissue area. **B)** Representative images of collagen deposition (blue). Data presented as Mean ± SEM with ****P<0.0001 using unpaired student t-tests; *n*=6 sham, *n*=7 AR.

Table 3.1 Physical Ventricular Parameters of AR and SHAM Mice Under Control, Pan-LOX^{inh}, or LOXL2^{inh} Conditions.

	SHAM Control	AR Control	SHAM LOXL2 ^{inh}	AR LOXL2 ^{inh}	SHAM Pan-LOX ^{inh}	AR Pan-LOX ^{inh}
Body Parameters *n*	7	14	20	16	9	15
BW (g)	36.9 ± 4.4	39.5 ± 4.9	39.0 ± 3.9	40.9 ± 4.4	39.05 ± 3.19	39.71 ± 3.98
TL (mm)	18.5 ± 0.34	18.4 ± 0.61	18.7 ± 0.63	18.9 ± 0.62	18.77 ± 0.53	18.61 ± 0.51
HW (mg) ****	182.3 ± 17.3	236.8 ± 42.9	211.6 ± 37.7	270.3 ± 74.2	206.7 ± 27.8	256.6 ± 31.5
HW / TL (mg/mm) ****	9.8 ± 0.9	12.9 ± 2.3	11.32 ± 1.9	14.3 ± 3.8	11.04 ± 1.64	13.79 ± 1.66
HW/BW (mg/g) ***	5.0 ± 0.76	6.02 ± 0.97	5.46 ± 1.07	6.69 ± 2.05	5.3 ± 0.59	6.5 ± 0.91
Echocardiography *n*	7	14	20	16	9	15
HR (bpm)	459 ± 28.3	522.2 ± 60.9	510.1 ± 50.51	499.7 ± 51.2	464 ± 73.2	484.7 ± 70.7
LVSD (mm) ****	2.93 ± 0.26	3.49 ± 0.29	2.87 ± 0.12	3.45 ± 3.45	2.93 ± 0.29	3.76 ± 0.56
LVDD (mm) ****	4.31 ± 0.33	4.97 ± 0.34	4.27 ± 0.17	4.85 ± 0.267	4.37 ± 0.35	5.10 ± 0.47
EF (%) ****	60.88 ± 3.05	55.9 ± 3.03	61.66 ± 2.31	55.23 ± 4.27	62 ± 3.14	54.2 ± 9.1
FS (%) ****	32.26 ± 2.16	27.8 ± 0.8	33.2 ± 1.65	28.88 ± 2.97	33.67 ± 4.51	32.36 ± 2.16
PWth (mm) ****	0.76 ± 0.02	0.81 ± 0.04	0.76 ± 0.03	0.83 ± 0.02	0.75 ± 0.01	0.81 ± 0.06
VTI $_{Diastolic / Systolic}$	————	44.93 ± 8.5	————	43.49 ± 9.8	————	47.2 ± 8.5

BW, body weight; TL, tibia length; HW, heart weight; HR, heart rate; LVSD, left ventricular systolic diameter; LVDD, left ventricular diastolic diameter; EF, ejection fraction; FS, fractional shortening; PWth, posterior wall thickness; VTI, velocity time integral. Data presented as Mean±SEM. **P<0.01, ****P<0.0001, compared between AR and SHAM within the three drug conditions using two-way ANOVA.

3.1.1 Pan-LOX Inhibition with Aortic Regurgitation

Next, our focus shifted to investigating the impact of total LOX inhibition (pan-LOX) on electrical and structural remodelling associated with AF pathogenesis induced by AR. We wanted to assess the role of the LOX family of enzymes in a pathological VO model of AF due to the knowledge that in a physiological VO model of AF (endurance exercise), these enzymes were differentially regulated and associated with no change in collagen transcription level and yet still presented with increased fibrosis [65]. As well, LOX mRNA and protein levels have been found to be increased in association with fibrosis in the LA of AF patients [85]. Previous studies assessing fibrosis and AF but utilizing alternative models and inhibitor drugs (i.e., beta-aminopropionitrile (BAPN)) have shown pan-LOX inhibition to be beneficial for attenuating fibrosis and AF susceptibility [85]. Thus, we set out to prove the same to be true in our VO AR model.

11-week-old mice were randomly subjected to AR or sham surgeries and either control or pan-lox inhibited chow. Each experimental cohort underwent intracardiac studies to assess changes in arrhythmogenesis and AF inducibility and echocardiogram studies to assess cardiac structure and function. A subset of each cohort was further evaluated for changes in heart weight and fibrotic tissue percentage using Masson's trichrome staining (MTS).

Interestingly, pan-LOX inhibition yielded variable results. AF inducibility with AR and pan-LOX inhibition was reduced to 47% from untreated AR values of 71% (P=0.1778). However, AF inducibility increased by 22% in the pan-LOX-inhibited sham cohort (Figure 3.3 Panel A). These differences were not accompanied by alterations in atrial arrhythmia durations between treated sham and AR cohorts, nor control and treated sham cohorts (P=0.3739) (Figure 3.3 Panel B). Furthermore, while AR cohorts exhibited a decrease in AERP (P=0.0243), no such differences were observed in treated AR cohorts (0.1336) (Figure 3.3 Panel C).

Furthermore, fibrosis in the LA with AR was attenuated (P=0.0064) with pan-LOX inhibition compared to untreated AR mice, decreasing from 11.2% to 7.5% (Figure 3.4). However, fibrosis was elevated (P=0.0029) in pan-LOX-inhibited sham mice, rising from 5.4% in control sham mice to 9.6%. Notably, the degree of fibrosis in pan-LOX-inhibited sham mice was comparable to those in the control AR cohort, with no difference observed (control AR: 11.2%, Pan-LOX-inhibited sham: 9.6%, P=0.3026).

The left ventricular chambers showed an increase ($P<0.0001$) in sustained VAs with pan-LOX inhibition, increasing by 10% in sham and 13% in AR mice. Nonetheless, VERP and ventricular arrhythmia durations showed no difference between untreated or treated sham or AR groups ($P=0.5971$). No change ($P=0.0879$) in the percent of fibrotic tissue was observed with the introduction of AR. However, there was a reduction ($P=0.0310$) within the pan-LOX inhibited AR cohort compared to the untreated AR cohort (Appendix A.2).

Importantly, the response to pan-LOX inhibition in sham and AR mice did not alter HR, LVDD, LVSD, EF, FS, PWth or AR velocity time integral (VTI) (Table 3.1, $P=0.1934$). Pan-LOX inhibition also did not affect chow consumption (Appendix A.2, $P=0.5027$) nor end body weight (BW) (Table 3.1, $P=0.0501$).

These results show that broader inhibition of the entire LOX family with pan-LOX inhibition produces variable effects on fibrosis and AF inducibility, warranting further investigation into its mechanistic implications.

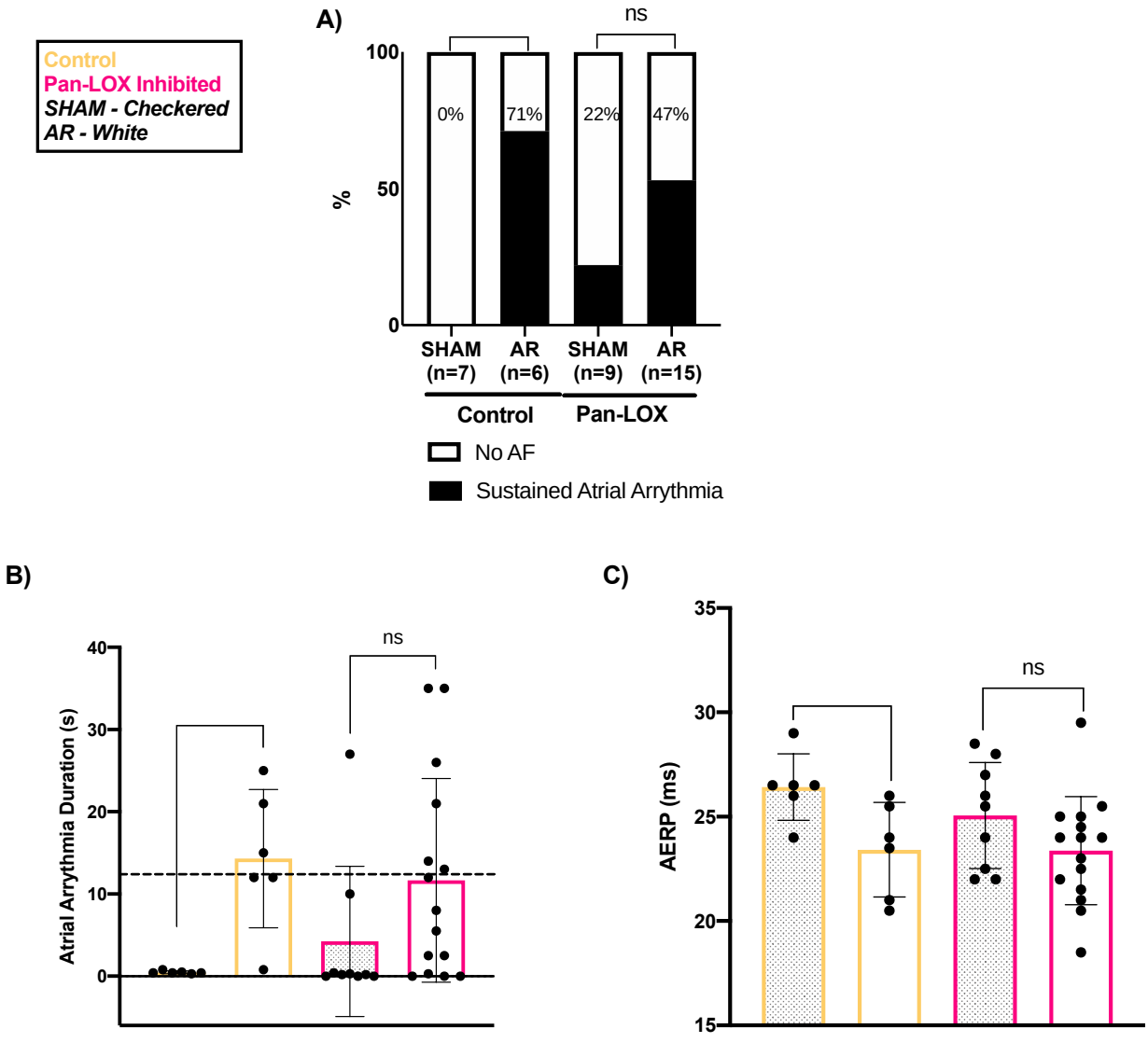

Figure 3.3 Pan-LOX^{inh} Effect on Left Atrial Refractoriness and AF Susceptibility with AR. The intracardiac analysis assessed differences in electrical remodelling and AF inducibility between sham and AR and control untreated (yellow) and pan-LOX^{inh} treated (pink) cohorts. **A)** Quantified percent of sustained arrhythmia (longer than 10 seconds). **B)** Change in atrial arrhythmia duration (s). **C)** Comparison of the atrial effective refractory period (AERP). Data presented as Mean ± SEM with *P<0.05, **P<0.01, using two-way ANOVA with Tukey's multiple comparisons tests; *n*=6 control sham, *n*=7 control AR, *n*=9 pan-LOX^{inh} sham, *n*=15 pan-LOX^{inh} AR.

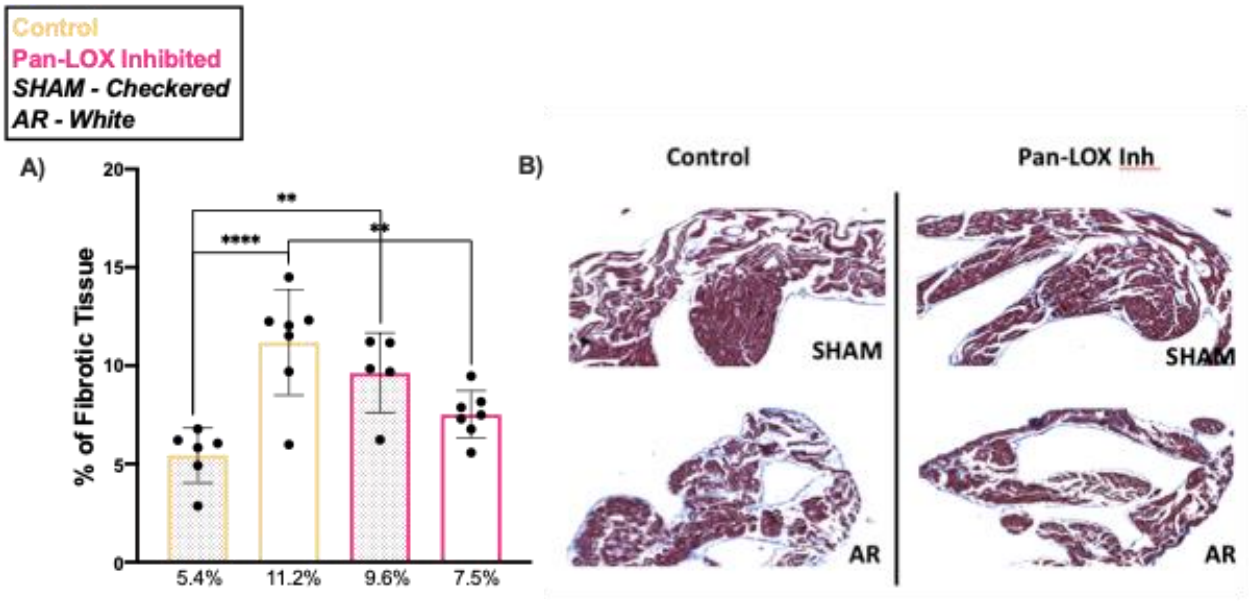

Figure 3.4 Pan-LOX^{inh} Effect on Left Atrial Collagen Deposition. Left atrial collagen percentage estimated with Masson's Trichrome and imaged with EVOS bright field microscope at 20x magnification. Comparisons were made between sham and AR and control untreated (yellow) and Pan-LOX^{inh} treated (pink) cohorts **A)** Quantification of percent of left atrial collagen deposition. **B)** Representative collagen deposition (blue) images in the four cohorts. Data presented as Mean ± SEM with **P<0.01, ***P<0.001 using two-way ANOVA with Tukey's multiple comparisons tests; *n*=6 control sham, *n*=7 control AR, *n*=5 pan- LOX^{inh} sham, *n*=7 pan-LOX^{inh} AR.

3.1.2 LOXL2 Inhibition with AR

After examining the effects of broad LOX inhibition, we next aimed to investigate the impact that LOXL2 inhibition, specifically, had on electrical and structural remodelling associated with AF pathogenesis induced by AR. We chose LOXL2 as it is known to be present in all four chambers of the adult heart and has also been shown to be upregulated in the LA of AF patients [78,80].

Similarly, 11-week-old mice were randomly subjected to AR or sham surgeries and either control or LOXL2-inhibited chow. Each experimental cohort underwent intracardiac studies to assess changes in arrhythmogenesis and AF inducibility, and echocardiogram studies were conducted to assess cardiac structure and function. A subset of each cohort was further evaluated for changes in heart weight, LA weight, fibrotic tissue percentage using MTS, and changes in gene expression through quantitative polymerase chain reactions (qPCR).

Most importantly, AF inducibility was almost completely blunted in the LA when LOXL2 was inhibited. There was a notable 61% decrease ($P<0.0001$) in sustained atrial arrhythmia (arrhythmias lasting longer than 10 seconds) in mice subjected to AR and treated with a LOXL2 inhibitor (Figure 3.5 Panel A). This reduction was accompanied by a decrease ($P=0.0117$) in the average duration of atrial arrhythmia, decreasing from 14.3s to 4.1s (Figure 3.5 Panel B). However, AERP showed no difference ($P=0.4299$) between AR mice treated or untreated, with respective averages of 22.4ms and 23.4ms (Figure 3.5 Panel C).

The data presented in Figure 3.6 presents LOXL2 inhibition as also reducing the percentage of fibrotic tissue. Treating AR mice with LOXL2 inhibition decreased ($P=0.0002$) the percentage of fibrotic tissue to 5.5%, a level comparable and non-significantly different ($P=0.9996$) from that observed in the sham groups.

With LOXL2 inhibition and AR, left ventricular chambers showed an increase ($P<0.0001$) in sustained VA with a 30% rise compared to non-treated AR hearts. This occurred along with a slight reduction ($P=0.0358$) in ventricular ERP (VERP) when LOXL2 was inhibited, which was not present in the untreated AR cohort. The mean VERP in the control group was 29.5ms, whereas it decreased to 26.6ms with LOXL2 inhibition. Despite the shortened VERP, there was no alteration in the average VA duration ($P=0.6212$). Additionally, there was no change in the percent of fibrotic tissue with the introduction of AR or LOXL2 inhibition ($P=0.540$) (Appendix A.3).

Lastly, the response to LOXL2 inhibition in sham and AR mice did not alter HR, LVDD, LVSD, EF, FS, PWth or AR VTI (Table 3.1, P=0.1934). LOXL2 inhibition also did not affect chow consumption (Appendix A.1, P=0.5027) nor end BW (Table 3.1, P=0.0501).

These findings prove the critical role of LOXL2 in mediating both fibrotic tissue accumulation and electrical remodelling associated with promoting and sustaining AF.

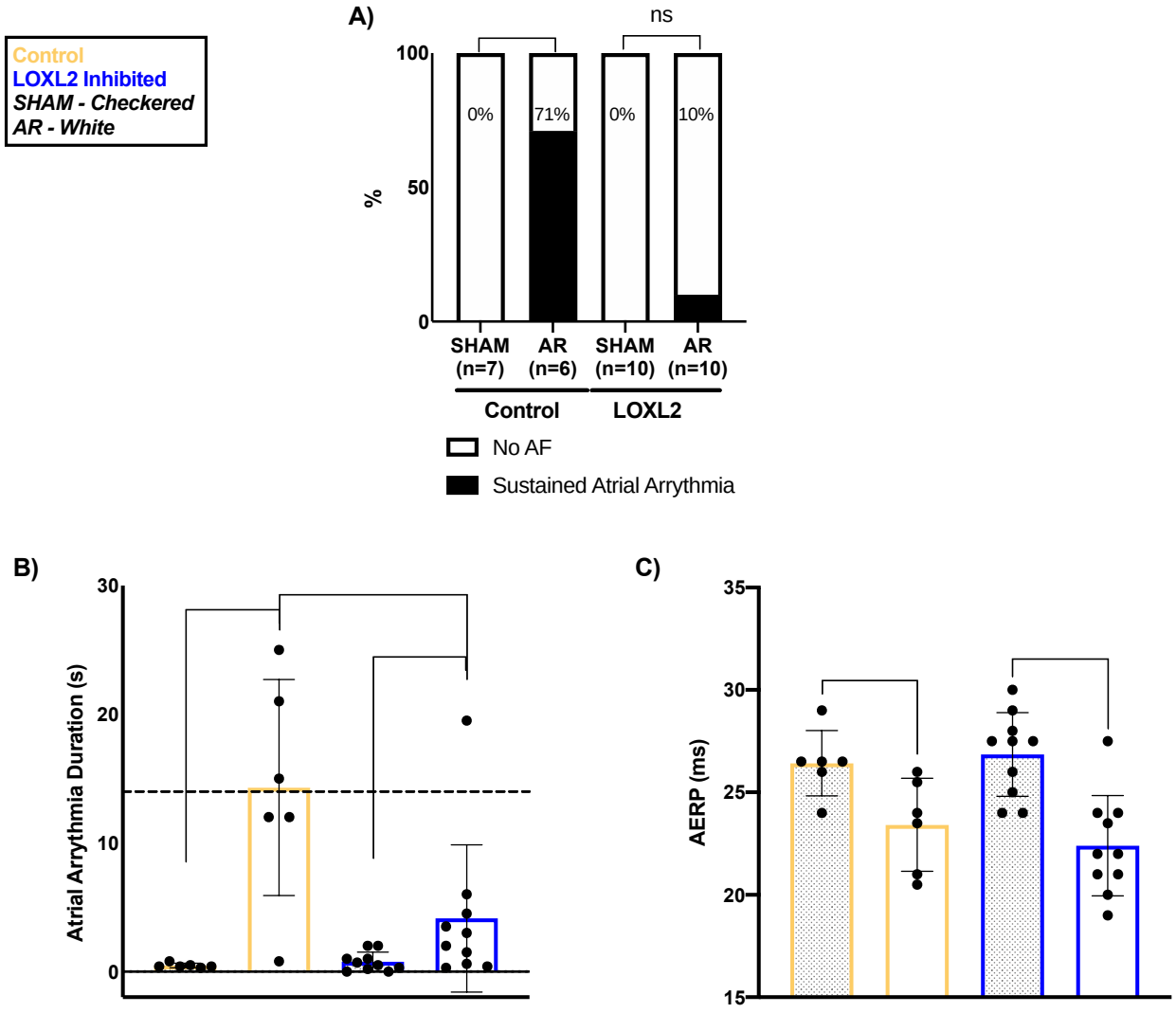

Figure 3.5 LOXL2^{inh} Effect on Atrial Refractoriness and AF Susceptibility with AR. Intracardiac analysis assessed differences in electrical remodelling and AF inducibility between sham and AR and control untreated (yellow) and LOXL2^{inh} treated (blue) cohorts. **A)** Quantified percent of sustained arrhythmia (longer than 10 seconds). **B)** Changes in atrial arrhythmia duration (s). **C)** Comparison of atrial effective refractory period (AERP). Data presented as Mean ± SEM with *P<0.05, **P<0.01, ***P<0.001, using two-way ANOVA with Tukey's multiple comparisons tests; *n*=6 control sham, *n*=6 control AR, *n*=10 LOXL2^{inh} sham, *n*=10 LOXL2^{inh} AR.

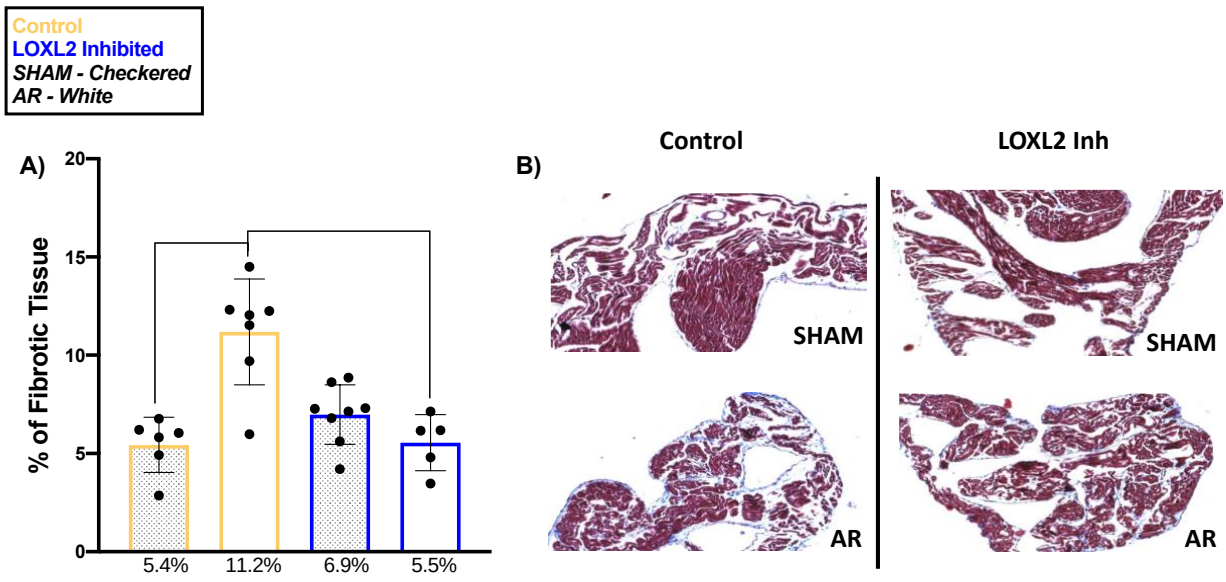

Figure 3.6 LOXL2^{inh} Effect on Left Atrial Collagen Deposition. Left atrial collagen percentage estimated with Masson's Trichrome and imaged with EVOS bright field microscope at 20x magnification. Comparisons were made between sham and AR and control untreated (yellow) and LOXL2^{inh} treated (blue) cohorts **A)** Quantification of percent of left atrial collagen deposition. **B)** Representative images of collagen deposition in the four cohorts. Data presented as Mean ± SEM with ***P<0.001, ****P<0.0001 using two-way ANOVA with Tukey's multiple comparisons tests; *n*=6 control sham, *n*=7 control AR, *n*=8 LOXL2^{inh} sham, *n*=5 LOXL2^{inh} AR.

3.2 Change in Macrophage Expression of LOXL2 with AR

Knowing that LOXL2 inhibition attenuates AF, we then aimed to investigate the cellular source through different time points of disease progression in the AR model. It is known that LOXL2 is expressed by fibroblast [49], endothelial cells [82], macrophages [45,84,] and cardiomyocytes [75,83] - all cell types that are upregulated in AF. However, it is unknown how the cellular sources adapt throughout disease progression.

The change in total cells present in the LA was assessed using immunohistochemistry (IHC) at sham, one-week, and four-week intervals of AR progression. At one week, there was an increase (P=0.0033) in total cells present; denoted by a rise from 3317 DAPI per mm^2 to 4112 DAPI per mm^2 (Figure 3.7 Panel A). To start dissecting the composition of this increase, we assessed the change in LOXL2 presence and macrophages as noted by $F480^+$ cells. At one week of AR progression, LOXL2 increased (P=0.0201) by 20%, and macrophages (P=0.0008) more than 2-fold (Figure 3.7 Panel B/C). However, at four weeks, the total number of cells present in the LA decreased (P=0.0083) to 3478 DAPI per mm^2, comparable to sham levels (P=0.7311). LOXL2 and $F480^+$ cells were also reduced (P=0.4857) to sham levels. Interestingly, $LOXL2^+$ signals accounted for approximately 20% of total cells present at all time points (P=0.1955) (Figure 3.7 Panel D). Whereas $F480^+$ signals increased (P=0.0010) from 3.6% of the total cells present in sham animals to 6% at 1-week of AR progression (Figure 3.7 Panel E).

We then assessed the change in LOXL2 expression from macrophages across the same time frame using colocalization techniques with IHC. Macrophages showed a 6% increase (P=0.0609) in the expression of LOXL2 at one week, which was then maintained through four weeks of AR progression (Figure 3.8 Panel A). The percent of LOXL2, which was expressed by macrophage cells, increased (P<0.0001) at one week of AR progression, showing an elevation from 8.9% to 15%. However, at four weeks, only 9.8% of LOXL2 was found to be colocalized with macrophage cells, similar to sham levels (P=0.7721) (Figure 3.8 Panel B).

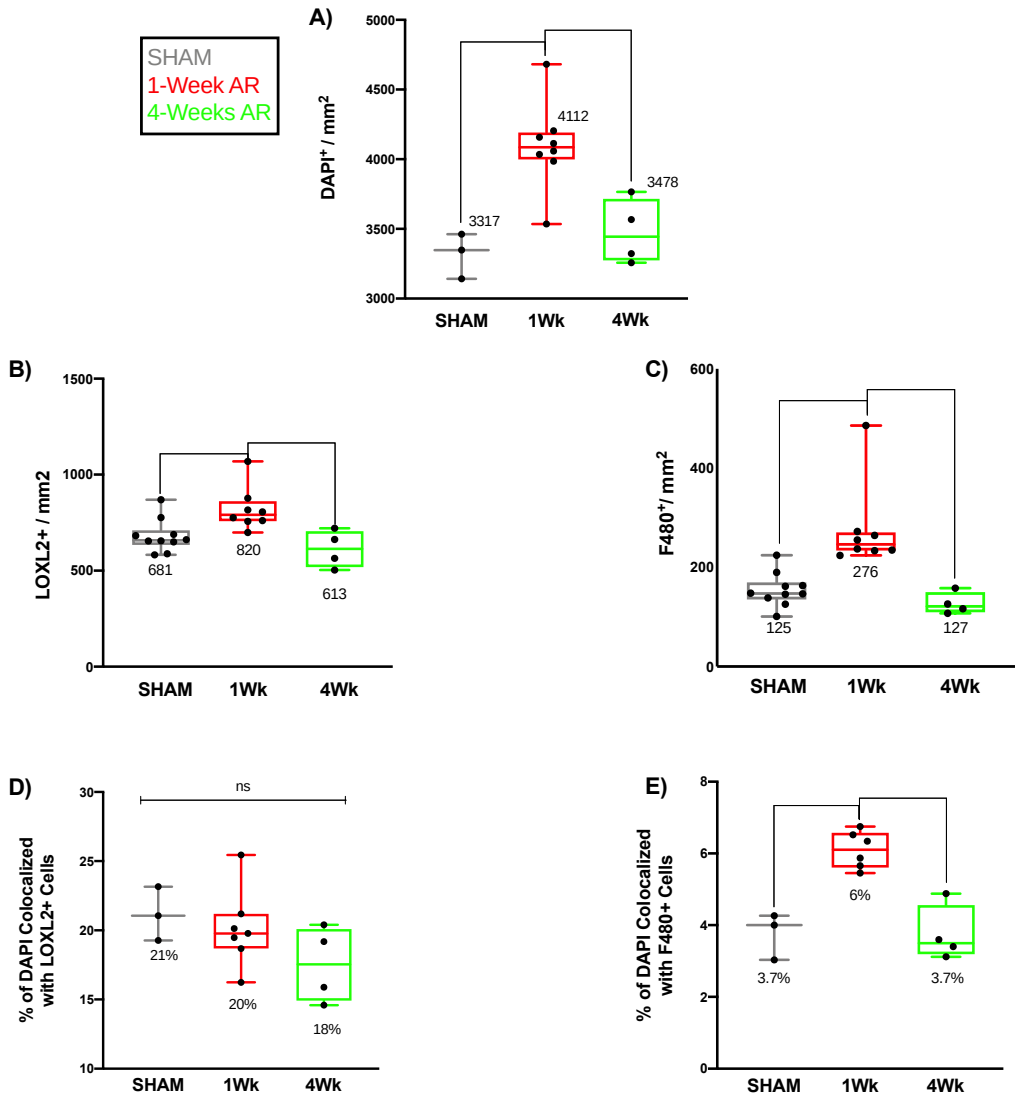

Figure 3.7 Macrophage and LOXL2 Response to AR. Left atrial macrophage ($F480^+$) and LOXL2 response to AR were evaluated with IHC and imaged with an EVOS microscope at 20x magnification. Analysis was performed using FIJI software to assess changes across three-time points – sham (grey), 1-week (red) and 4-weeks (green) of AR progression. **A)** Total cell count, represented by nuclei $DAPI^+$ signals, normalized to tissue. **B)** Total LOXL2 count normalized to the tissue area. **C)** Total macrophage count, represented by $F480^+$ signals, normalized to the tissue area. **D)** Percent of total cells (nuclei) colocalized with LOXL2. **E)** Percent of total cells (nuclei) which present as $F480^+$. Data presented as Mean ± SEM with *P<0.05, **P<0.001, ***P<0.001 using one-way ANOVA with Tukey's multiple comparisons tests; *n*=3 sham, *n*=7 1-week AR, *n*=4 4-weeks AR.

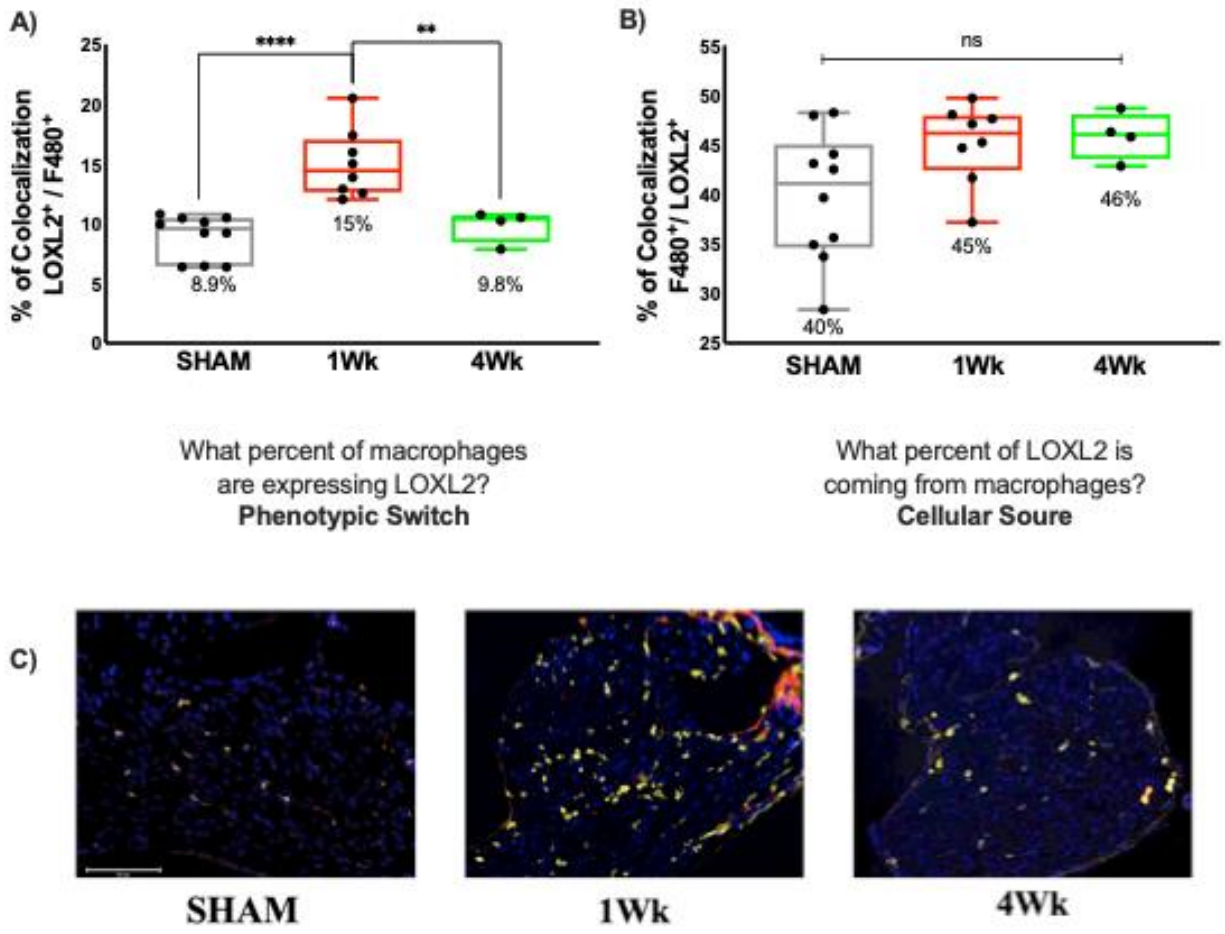

Figure 3.8 Interaction Between LOXL2 and Macrophages. Left atrial colocalization of macrophages ($F480^+$) and LOXL2 in response to AR evaluated with IHC and imaged with EVOS microscope at 20x magnification. Analysis was performed using FIJI software to assess changes across three-time points – sham (grey), 1-week (red) and 4-weeks (green) of AR progression. **A)** Percent of macrophages expressing LOXL2 (phenotype) **B)** Percent of LOXL2 being expressed by macrophages (cell source). **C)** Representative images of macrophage (yellow) and LOXL2 (red) colocalization with DAPI (blue). Data presented as Mean ± SEM with **P<0.001, ****P<0.0001 using one-way ANOVA with Tukey's multiple comparisons tests; *n*=10 sham, *n*=8 1-week AR, *n*=4 4-weeks AR.

3.3 Preliminary Data and Future Studies

Two ongoing studies will be completed for future publication. These will aid in elucidating the origin and mechanism of LOXL2 action to identify specific therapeutic targets to mitigate its role in AF-inducing and sustaining fibrogenesis. These experiments include IHC

assessment of LOXL2 cellular source and qPCR analysis of key fibrotic markers that influence or can be influenced by LOXL2.

As seen in section 3.2, the contribution of LOXL2 enzymes in AR tissue expressed by macrophages was already assessed. However, the relationship between the remaining cell types which express LOXL2 in the heart, including fibroblasts, endothelial cells, and cardiomyocytes, has yet to be analyzed. The presence and behaviour of these cell types in the response to LOXL2 inhibition with AR will also be explored.

It has been shown that many of the upstream and downstream regulators of LOX are released in response to stretch [86,87]. Thus, we will be exploring the change in such markers in response to AR and LOXL2 inhibition. As well, in the endurance swim training model collagen transcription rates were presented to remain unchanged [65]. Therefore, we have set out to confirm this fact in the AR model, a pathological version of VO. Preliminary work has been done by running a qPCR panel assessing all the primers listed in Table 2.3 on LOXL2 inhibited AR and sham LA tissue. These results have been compared to pooled atrial (LA and RA) samples from alternative studies ongoing within our lab for initial evaluation while control untreated AR and sham mice are generated. Once direct one-to-one samples have been isolated, results will be updated, and LA enlargement will be specifically measured as we isolate and weigh the LA chamber from the RA.

With the data currently available, there presents no change between untreated AR and LOXL2 inhibited AR, and between LOXL2 inhibited sham and AR when assessing transcription rates of COLIIIα1 (P=0.2285), COLIVα1 (P=0.1092), TG2 (P=0.0903), SPARC (P=0.7514), and FN1 (P=0.4777). There is also no change between untreated sham and AR when evaluating SPARC (P=0.8797), FN1 (P=0.2704), and PDGF-D (P=0.1651).

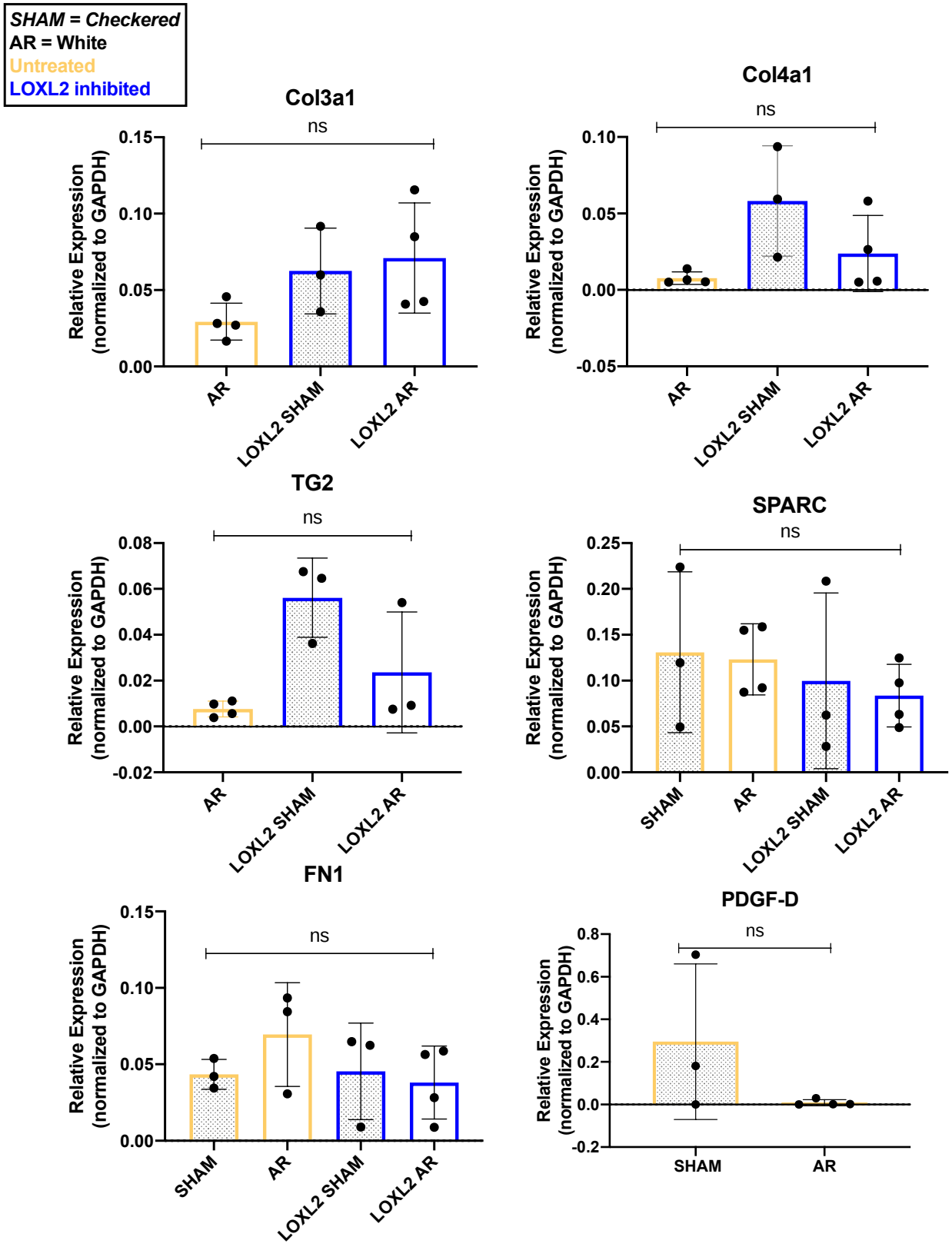
SHAM = Checkered
AR = White
Untreated
LOXL2 inhibited
Col3a1
ns
Relative Expression (normalized to GAPDH)
0.15
0.10
0.05
0.00
AR
LOXL2 SHAM
LOXL2 AR
Col4a1
ns
Relative Expression (normalized to GAPDH)
0.10
0.05
0.00
-0.05
AR
LOXL2 SHAM
LOXL2 AR
TG2
ns
Relative Expression (normalized to GAPDH)
0.08
0.06
0.04
0.02
0.00
-0.02
AR
LOXL2 SHAM
LOXL2 AR
SPARC
ns
Relative Expression (normalized to GAPDH)
0.25
0.20
0.15
0.10
0.05
0.00
SHAM
AR
LOXL2 SHAM
LOXL2 AR
FN1
ns
Relative Expression (normalized to GAPDH)
0.15
0.10
0.05
0.00
SHAM
AR
LOXL2 SHAM
LOXL2 AR
PDGF-D
ns
Relative Expression (normalized to GAPDH)
0.8
0.6
0.4
0.2
0.0
-0.2
SHAM
AR

Figure 3.9 Aortic Regurgitation and LOXL2 inhibition induced transcriptional changes COL3*α*1, COL4*α*1, TG2, SPARC, FN1 and PDGF-D. Left atrial changes in gene transcription levels were assessed with qPCR SYBR green. Analysis was performed using BR.io and compared using relative quantitation of gene expression with ΔΔ CT method normalized to GAPDH and described as relative to the control group by 2-ΔΔCT. COL3a1, Collagen 3-α1; COL4a1, collagen 4-α1; TG2, transglutaminase 2; SPARC, secreted protein acidic and cysteine-rich; FN1, fibronectin 1; PDGF-D, platelet-derived growth factor subunit D. Data presented as Mean ± SEM with *P<0.05, using two-way ANOVA with Tukey's multiple comparisons tests; *n*=3 sham, *n*=3 AR, *n*=4 LOXL2 inhibited SHAM, *n*=4 LOXL2 inhibited AR.

Chapter 4: Endurance Swim Training Model Results

4.1 Endurance Exercise

Following the assessment of pan-LOX and LOXL2 inhibition in a pathological, AR, VO model of AF, we then wanted to determine the effect such inhibition would have on a physiological, endurance swim training VO model of AF. Past studies from within our lab have shown an increase in fibrosis and AF susceptibility along with changes in LOX expression in an endurance swim training model in the absence of increased collagen transcription [65,110]. To achieve these objectives, we first aimed to characterize the physiological response to endurance swim training in mice irrespective of any drug treatment.

Eight-week-old CD1 male mice swam against a 15L/min current for 4.5 weeks for two hours each morning and evening to receive a chronic VO stimulus. Controls consisted of sedentary age-matched mice placed in the water without any current for 10 minutes each morning and evening. All mice were allowed to rest for 48 hours before end-point assessments to evaluate chronic adaptation independently of acute exercise stress [110].

Contrary to previous results seen using the same model and apparatus [110], after 4.5 weeks of endurance swim training, mice exhibited no increase ($P>0.999$) in susceptibility to AF, with 0% presenting with sustained atrial arrythmias (Figure 4.1, Panel A). This was accompanied by no change in atrial arrhythmia duration ($P=0.0613$) nor AERP ($P=0.4471$), with an average duration of 26.4ms and 24.9ms in sedentary and swim-trained mice, respectively (Figure 4.1 Panel C/D). However, swim-trained mice did present with a 3.6% elevation ($P=0.0046$) in LA fibrosis estimated using Mason's Trichrome (Figure 4.2). Swim-trained mice also were observed to have increased ($P=0.0091$) total heart weights (Table 4.1). These alterations were accompanied by increased ($P=0.0021$, $P=0.0014$) LVSD and LVDD and decreased ($P=0.0059$, $P=0.0078$) EF and FS when at rest as measured by an echocardiogram on a live mouse (Table 4.1). EF was reduced by 4.4% and FS by 2.7%. Additional PWth showed no difference ($P=0.8906$) between sedentary and swim-trained mice, with an average of 0.76mm in the former and 0.76mm in the latter (Table 4.1).

In alignment with past swim studies from our lab [110], we observed no difference ($P=0.5420$) in end BW between sedentary and swim-trained mice, with the average mouse weighing approximately 38g. Swim-trained mice did, however, consume more ($P=0.0176$) chow than sedentary mice (Appendix A.4) and presented with sinus bradycardia post-swim training, with the

average HR decreasing ($P<0.0001$) from 507 bpm in sedentary mice to 442 bpm in trained mice (Table 4.1).

Left ventricular chambers presented with 0% sustained ventricular arrythmias (VA), no change in VERPs or VA durations, and no increase in the percent of fibrotic tissue ($P=0.1447$) (Appendix A5 and A6).

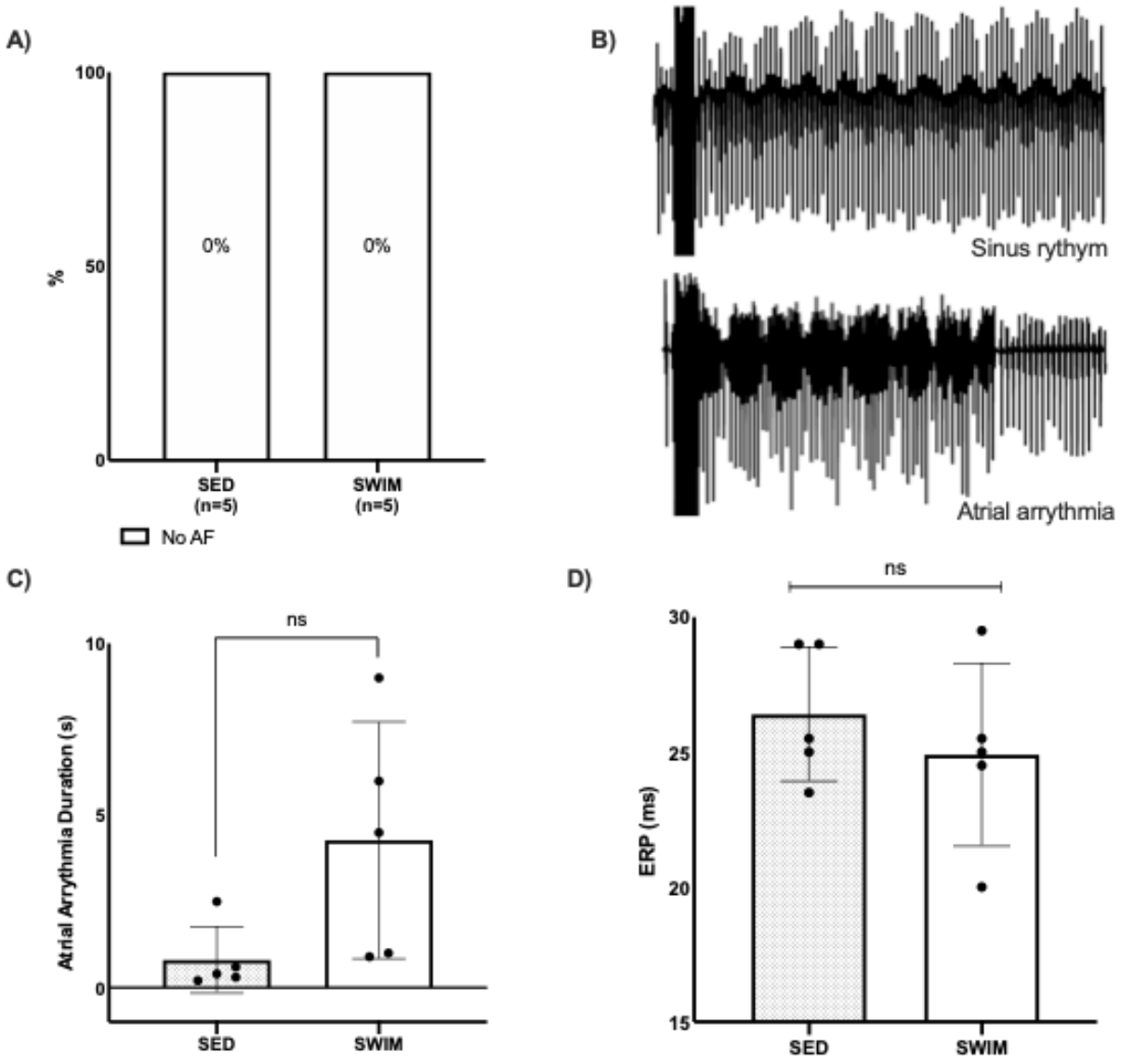

Figure 4.1 Effect on Atrial Refractoriness and AF Susceptibility with Endurance Swim Training. Intracardiac analysis assessed differences in electrical remodelling and AF inducibility between sedentary and swim cohorts**. A/B)** Percent of sustained arrhythmia (longer than 10 seconds) and representative sinus rhythm and arrhythmia tracings. **C)** Change in atrial arrhythmia duration (s). **D)** Comparison of atrial effective refractory period (AERP). Data presented as Mean ± SEM with *P<0.05 using Chi-Squared Fisher test and students t-tests; *n*=5 sedentary, *n*=5 swim.

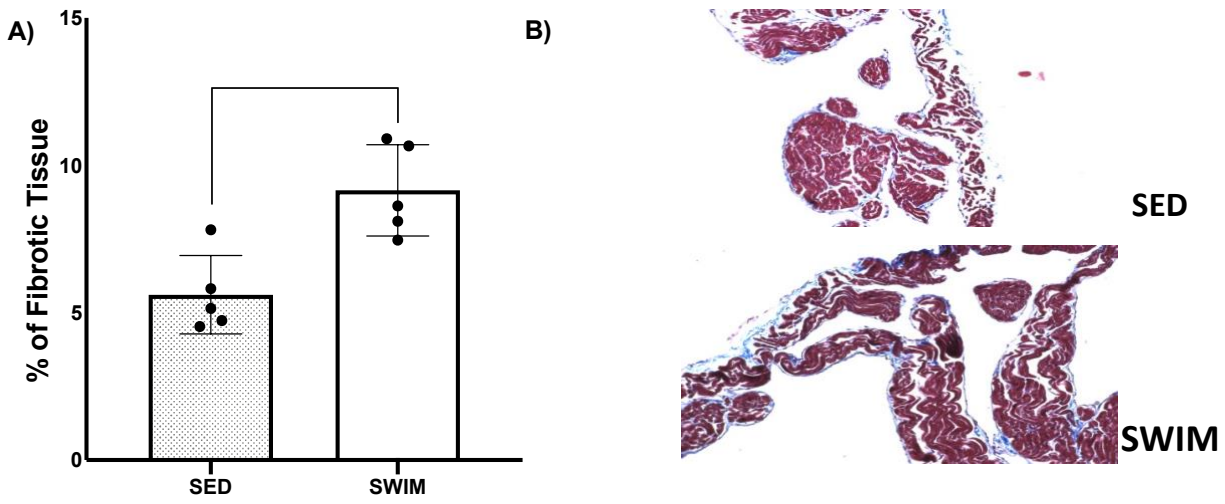

Figure 4.2 Effect on Left Atrial Collagen Deposition. Left atrial collagen was estimated using Masson's Trichrome and imaged with an EVOS bright field microscope at 20x. Comparisons presented between sedentary and swim cohorts **A)** Quantification of the percent of left atrial collagen deposition. **B)** Representative collagen deposition (blue) images in the four cohorts. Data presented as Mean ± SEM with *P<0.05, **P<0.001 using students t-tests; *n*=5 sedentary, *n*=5 swim.

Table 4.1 Physical Ventricular Parameters of Swim and Sedentary Mice Under Control, Pan-LOX^{inh}, or LOXL2^{inh} Conditions.

	SED Control	**SWIM Control**	**SED LOXL2 ^{inh}**	**SWIM LOXL2 ^{inh}**	**SED Pan-LOX ^{inh}**	**SWIM Pan-LOX ^{inh}**
Body Parameters *n*	5	5	10	10	10	9
BW (g)	37.67 ± 6.24	39.58 ± 2.43	38.48 ± 3.57	34.01 ± 1.87	40.72 ± 2.26	39.04 ± 2.43
TL (mm)	18.71 ± 0.49	18.61 ± 0.42	18.59 ± 0.49	18.55 ± 0.39	19.16 ± 0.47	19.06 ± 0.57
HW (mg)	213.6 ± 39.38	247.6 ± 34.15	195.7 ± 16.27	220.9 ± 35.16	210.9 ± 26.71	220.4 ± 32.44
HW / TL (mg/mm) **	11.39 ± 1.88	13.31 ± 1.86	10.54 ± 0.95	11.89 ± 1.74	11.01 ± 1.36	11.57 ± 1.72
HW/BW (mg/g) **	5.67 ± 0.47	6.23 ± 0.49	5.12 ± 0.61	6.49 ± 0.96	5.18 ± 0.57	5.66 ± 0.89
Echocardiography *n*	5	5	10	10	10	9
HR (bpm) ****	515.6 ± 44.03	449.8 ± 80.83	517.3 ± 31.67	424.6 ± 30.93	488 ± 39.6	451 ± 66.62
LVSD (mm) ****	2.68 ± 0.23	3.11 ± 0.17	2.89 ± 0.25	3.18 ± 0.32	2.89 ± 0.2	3.23 ± 0.19
LVDD (mm) ****	4.02 ± 0.33	4.67 ± 0.24	4.33 ± 0.25	4.56 ± 0.27	4.3 ± 0.25	4.67 ± 0.17
EF (%) ***	62.85 ± 2.99	60.87 ± 0.97	62.72 ± 2.62	58.09 ± 4.8	62.49 ± 2.9	58.18 ± 3.07
FS (%) **	33.35 ± 2.6	32.49 ± 0.73	33.59 ± 2.07	30.52 ± 3.17	33.2 ± 1.71	30.59 ± 2.03
PWth (mm)	0.75 ± 0.02	0.77 ± 0.03	0.76 ± 0.02	0.76 ± 0.04	0.76 ± 0.02	0.76 ± 0.03

BW, body weight; TL, tibia length; HW, heart weight; HR, heart rate; LVSD, left ventricular systolic diameter; LVDD, left ventricular diastolic diameter; EF, ejection fraction; FS, fractional shortening; PWth, posterior wall thickness; VTI, velocity time integral. Data presented as Mean±SEM. **P<0.01, ***, P<0.001, ****P<0.0001, compared between swim and sedentary and the three drug conditions using two-way ANOVA.

4.1.1 Pan-LOX Inhibition with Endurance Swim Training

Following the AR model's assessment pattern, we first investigated the effects of pan-LOX inhibition on the electrical and structural remodelling induced by endurance swim training, following the same methods outlined in the prior section. The rationale is that LOX was named as a differentially regulated gene in a past study on endurance exercise training in association with elevated fibrosis and reduced collagen synthesis [65].

We evaluated all 12-week-old CD1 male mice for changes in arrhythmogenesis and AF inducibility via intracardiac studies, cardiac function and structure by echocardiograms, fibrotic tissue percentage using MTS, and total heart weight.

Pan-LOX inhibition and endurance swim training showed a 10% increase (P=0.6178) in susceptibility to AF; however, there was no change (P=0.1065) in atrial arrhythmia duration nor AERP (Figure 4.3). Additionally, fibrosis was not attenuated (P=0.6426) in swim-trained pan-LOX inhibited mice, with a negligible 0.5% difference between treated and untreated cohorts (Figure 4.4). Unexpectedly, sedentary mice treated with pan-lox inhibition exhibited increased (P=0.0084) fibrosis, rising from 5.2% in untreated sedentary mice to 8.9%. The degree of fibrosis in the sedentary treated cohort reached levels comparable to untreated swim-trained mice (8.9% vs. 9.2%, P=0.8744) (Figure 4.4).

The left ventricular chamber of sedentary pan-LOX-inhibited mice showed a 22% increase (P=0.1891) in sustained VAs but no change (P=0.1044) in VERP or VA durations. Additionally, no difference (P=0.4512) in the percent of deposited collagen with the swim-training or pan-LOX inhibition was observed (Appendix A.5).

The response to pan-LOX inhibition in sedentary and swim-trained mice did not alter HR, LVDD, LVSD, EF, FS, or PWth trends that were already present by swim-training alone (Table 4.1, P=0.2117). Pan-LOX inhibition also did, however, reduce chow consumption (Appendix A.4, P<0.0001) but not end BW or HW (Table 4.1, P=0.5091).

These findings provide evidence against pan-LOX inhibition being beneficial toward preventing AF susceptibility and fibrosis progression in an endurance swimming VO model of AF.

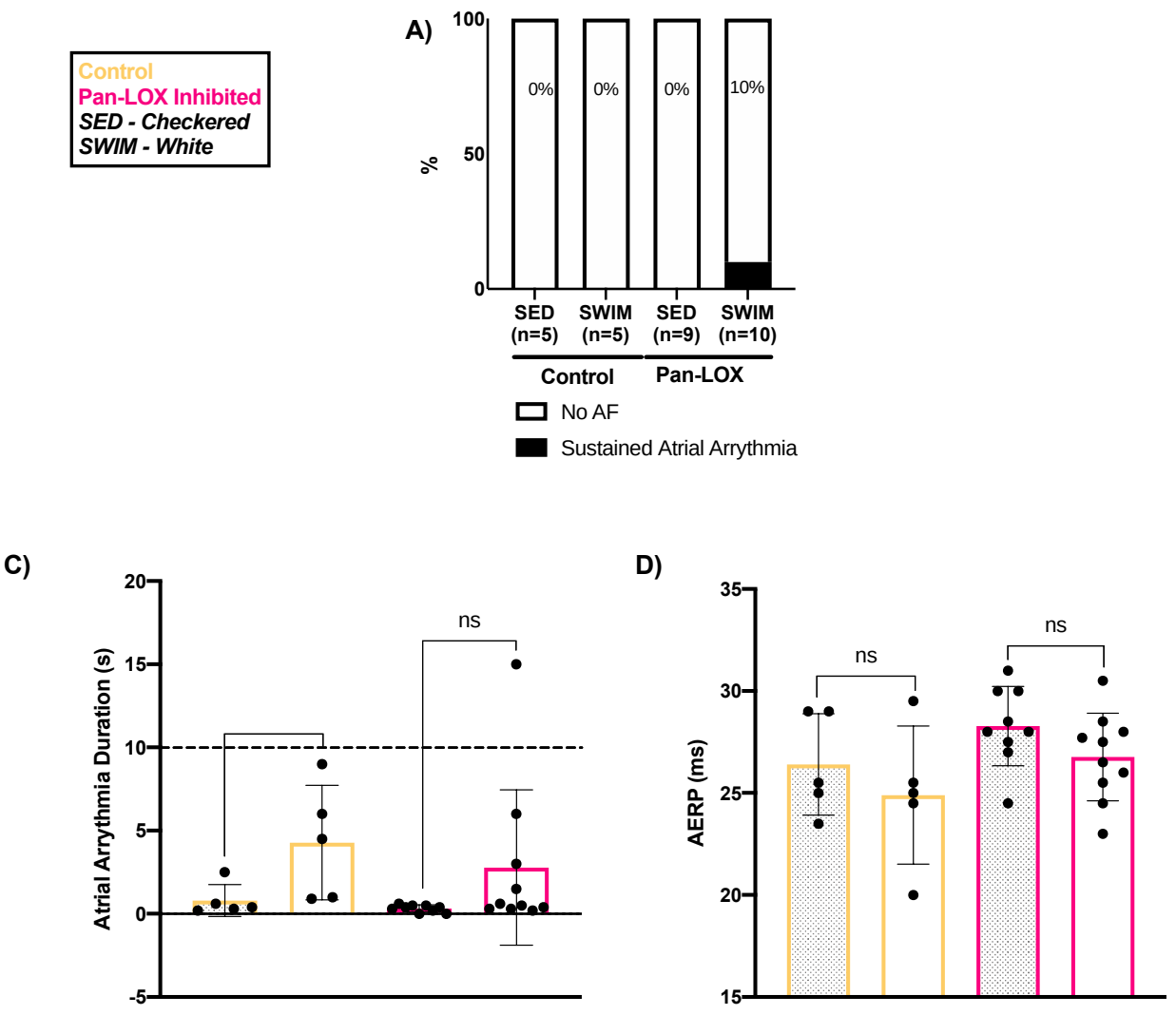

Figure 4.3 Pan-LOX^{inh} Effect on Atrial Refractoriness and AF Susceptibility with Endurance Swim Training. Intracardiac analysis assessed differences in electrical remodelling and AF inducibility between sedentary and swim and control untreated (yellow) and pan-LOX^{inh} treated (pink) cohorts. **A)** Percent of sustained arrhythmia (longer than 10 seconds). **B)** Comparison of atrial effective refractory period (AERP). **C)** Change in atrial arrhythmia duration(s). Data presented as Mean ± SEM with *P<0.05 using two-way ANOVA with Tukey's multiple comparisons tests; *n*=5 control sed and swim, *n*=9 Pan-LOX^{inh} sed, *n*=10 Pan-LOX^{inh} swim-trained.

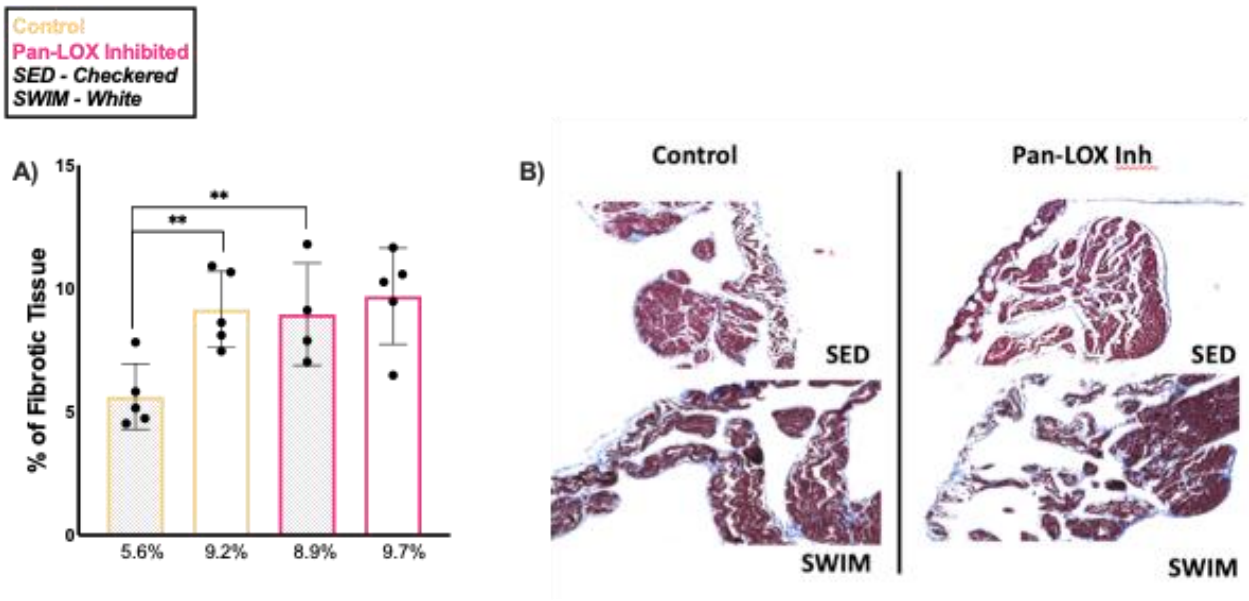

Figure 4.4 Pan-LOX^{inh} Effect on Left Atrial Collagen Deposition. Left atrial appendage collagen was identified using Masson's Trichrome and imaged using an EVOS bright field microscope at 20x. Comparisons present are between sedentary and swim and control untreated (yellow) and Pan-LOX^{inh} treated (pink) cohorts **A)** Quantification of percent of left atrial collagen deposition. **B)** Representative collagen deposition (blue) images in the four cohorts. Data presented as Mean ± SEM with **P<0.01 using two-way ANOVA with Tukey's multiple comparisons tests; *n*=5 for all cohorts.

4.1.2 LOXL2 Inhibition with Endurance Swim Training

Following the AR model pattern of assessment, after examining the effects of broad LOX inhibition, we next analyzed the impact of LOXL2 inhibition, specifically on electrical and structural remodelling associated with AF induced by endurance swim training. Again, LOXL2 was chosen as has been proven to be present in all chambers of the adult heart and has been shown to be upregulated in the LA of AF patients [78,80].

Once more, we evaluated all 12-week-old CD1 male mice for differences in AF inducibility, ERP, and arrhythmia durations via intracardiac studies, cardiac function and structure by echocardiograms, fibrotic tissue percentage using MTS, and total heart weight.

Swim-trained LOXL2-inhibited mice had a 30% increase in AF susceptibility, coinciding with a 10% increase in sedentary LOXL2-inhibited mice (P=0.2573) (Figure 4.5 Panel A). Although the incidence of sustained atrial arrhythmia rose, there was no change (P=0.4932) in atrial arrhythmia duration nor AERP (Figure 4.5 Panel B/C). LOXL2 inhibition also did not alter collagen content in either sedentary (P=0.1828) or swim-trained mice (P=0.7190). Collagen percentages were as follows: 5.6% in sedentary control mice, 7.4% in sedentary treated mice, 9.2% in swimming control mice, and 8.2% in swimming treated mice (Figure 4.6).

The left ventricular chamber exhibited a 10% increase (P=0.3799) in sustained ventricular arrhythmia in the sedentary LOXL2-inhibited cohort, along with no differences (P=0.2085) in VERP or ventricular arrhythmia durations. Furthermore, there was no change (P=0.5061) in the percent of deposited collagen in sedentary swim-trained mice treated with LOXL2 inhibition (Appendix A.6).

Lastly, the response to LOXL2 inhibition in sedentary and endurance swim-trained mice did not alter HR, LVDD, LVSD, EF, FS, or PWth trends that were already present by swim-training alone (Table 4.1, P=0.2117) LOXL2 inhibition also did not affect chow consumption (Appendix A.4) or HW, but did present with a lower (P=0.0257) end BW in the swim-trained cohort (Table 4.1).

Thus, inhibition of LOXL2 in swim-trained mice shows limited effectiveness in attenuating structural and electrical remodelling associated with AF.

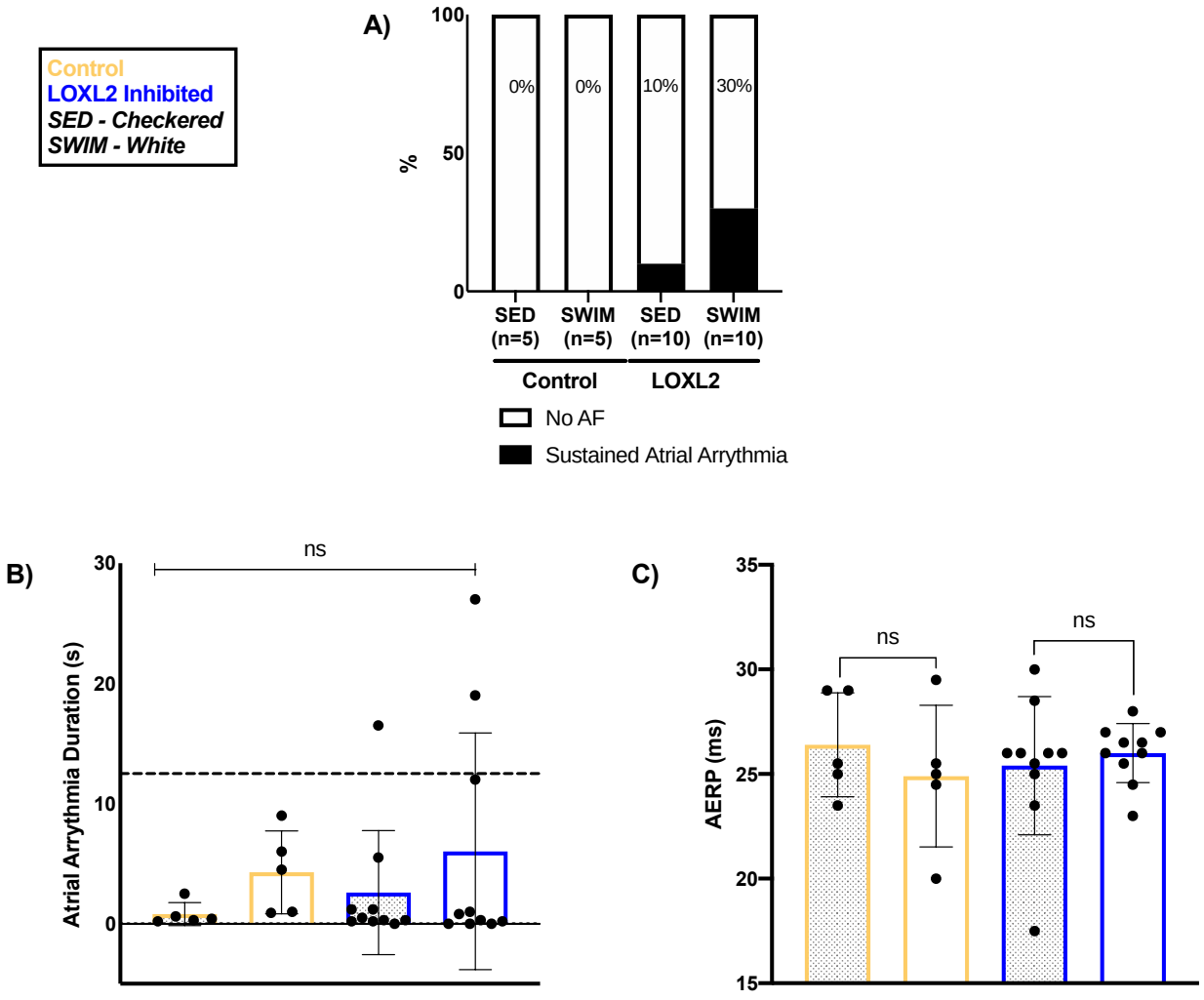

Figure 4.5 LOXL2^{inh} Effect on Atrial Refractoriness and AF Susceptibility with Endurance Swim Training. Intracardiac analysis assessed differences in electrical remodelling and AF inducibility between sedentary and swim and control untreated (yellow) and LOXL2^{inh} treated (blue) cohorts **A)** Percent of sustained arrhythmia (longer than 10 seconds). **B)** Comparison of atrial effective refractory period (AERP). **C)** Change in atrial arrhythmia duration (s). Data presented as mean ± SEM with *P<0.05 using TWO-way ANOVA with Tukey's multiple comparisons tests; *n*=5 control SED and swim, *n*=10 LOXL2^{inh} SED and swim.

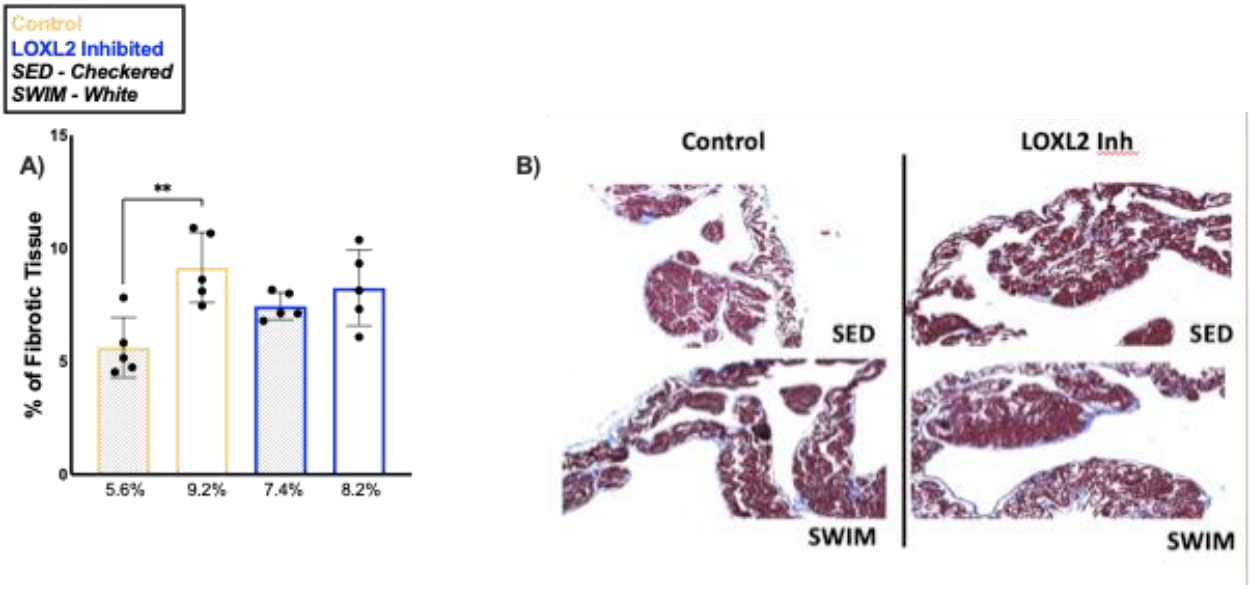

Figure 4.6 LOXL2^{inh} Effect on Left Atrial Collagen Deposition. Left atrial collagen was estimated using Masson's Trichrome and imaged with an EVOS bright field microscope at 20x. Comparisons presented between sedentary and swim and control untreated (yellow) and LOXL2^{inh} treated (blue) cohorts **A)** Quantification of percent of left atrial collagen deposition. **B)** Representative collagen deposition (blue) images in the four cohorts. Data presented as Mean ± SEM with **P<0.01 using two-way ANOVA with Tukey's multiple comparisons tests; *n*=5 for all cohorts.

Chapter 5: Discussion

In this study, we investigated the roles of LOX family enzymes, particularly LOXL2, in atrial fibrillation (AF) pathogenesis using experimental models of VO in the form of AR and endurance swim training. VO causes compensatory remodelling driven by increased wall stress, which promotes a progressive increase in susceptibility to and perpetration of AF. AF utilizes a combination of electrical and structural remodelling to develop and sustain itself. What combination of remodelling characteristics creates the perfect conditions to induce AF is an ongoing study. However, fibrotic remodelling remains a hallmark of AF regardless of the population or triggering event. Nonetheless, previous findings have shown that in an endurance exercise VO model of AF and with age-induced AF, transcription rates of collagen biosynthesis are unchanged, yet their respective degrees of fibrotic tissue in the heart are elevated [65,85].In conjunction with increased fibrosis, these models of AF also possessed increased LOX and LOXL2, as reported through RNAseq data [65]. Together, these results suggest collagen accumulation in VO-induced AF could be due to LOX enzymes' crosslinking and stabilization action on collagen fibrils. This study thus set out to directly assess the effects of the LOX family of enzymes in such an AF-inducing model and went a step further to assess their role in a pathological model of VO, AR. Our findings provide valuable insights into the molecular mechanisms underlying fibrosis in AF and the effects of specific LOX inhibitors on cardiac remodelling and arrhythmogenesis.

5.1.1 Pan-LOX Inhibition with AR

Our results demonstrate that broad inhibition of the entire LOX family of enzymes, with pan-LOX inhibitors, yielded variably and less favourable outcomes. Contrary to the hypothesis, pan-LOX inhibition reduced fibrosis in AR mice by 3.7% but led to unexpected increases (4.2%) in fibrotic deposition in sham mice. Moreover, pan-LOX inhibition was associated with a higher incidence of sustained AF in sham mice, 22% in treated compared to 0% in untreated. Interestingly, atrial arrhythmia duration and AERP were unchanged by treatment with a pan-LOX inhibitor. A potential explanation for these results follows the notion that fibrosis functions as a double-edged sword. When too much fibrosis exists, the mechanical function of the myocardium is diminished due to stiffening, and anisotropic conduction is disrupted and delayed due to the presence of anatomical blockades forcing transverse propagation [25,60,61]. However,

when too little fibrosis exists, the structure of the ECM and, thus, the myocardium is weakened, becoming more susceptible to dilation and potential rupture [111,112]. Hence, the divergent effects of pan-LOX inhibition may stem from its broad impact on multiple LOX enzymes that are involved in diverse physiological processes. If all LOX isoenzymes, responsible for cross-linking and stabilizing collagen fibrils, are inhibited, then the process of collagen maturation and ECM construction will be impeded. This disorganization of ECM composition will result in not only structural complications in the mechanical function of the myocardium but also communication breakdown between cells since the ECM acts as a central regulatory signalling sub-network used for cellular decision-making [53,113]. This highlights the delicate balance required for ECM homeostasis in maintaining cardiac structure and function. It is thus important to have feedback loops with regulatory backup functions to ensure such destruction does not occur.

Our findings raise questions about compensatory mechanisms or alternative cross-linking pathways that may be disrupted or overcompensated when broader LOX inhibition occurs. The compensatory mechanisms could include upregulating alternative crosslinking mechanisms like TG [73] or AGES [72] or increased expression of additional non-fibrillar ECM structural proteins like fibulin[111] or fibronectin [114]. Future studies should explore these mechanisms and proteins to dissect further the response to pan-LOX inhibition in AR-induced AF and cardiac health.

Furthermore, although the results of our pan-LOX inhibition in sham mice contradicted the hypothesis, the outcome in AR mice does follow the expected pattern, as seen in other models of AF with broad LOX inhibition. A model of VO induced by aortocaval fistula in Sprague–Dawley rats, treated with BAPN, a broad amine oxidase inhibitor, resulted in attenuated interstitial myocardial collagen, reduced protein levels of collagen I and III, and improved LV function as assessed through ventricular pressure-volume loops, fractional shortening, and LV stiffness [115]. In this model, fibrosis was decreased back to sham levels in VO BAPN-treated mice, unlike our model in which fibrosis in AR pan-LOX treated mice was still significantly elevated by 2.1% from sham mice. Notably, sham rats also presented with no change in cardiovascular fibrosis when treated with BAPN, whereas treatment with PXS-5505 pan-LOX inhibitor resulted in a 4.2% increase in sham mice. BAPN and PXS-5505 are both small molecule inhibitors, functioning by covalently and irreversibly binding to the active site of LOX, inhibiting its activity and ability to cross-link collagen [115]. BAPN, however, will inhibit all amine oxidases, including semicarbazide-sensitive amine oxidase (SSAO), whereas PXS-5505 was

uniquely designed to inhibit just those enzymes in the LOX family [116]. SSAO has been shown to deaminate methylamine and aminoacetone, forming formaldehyde and methylglyoxal, which promote protein crosslinking through oxidative stress and AGEs [117,118]. Hence, BAPN may act as a stronger inhibitor of collagen crosslinking and fibrosis formation by acting on two methods of crosslinking (LOX and AGEs), whereas PXS-5505 only acts on one (LOX). Thus, potentially AGEs act as the compensatory mechanism in sham mice when the entire LOX family is inhibited. Therefore, it must also be inhibited to combat the counterbalance, as BAPN does. It would thus be beneficial to assess the presence of SSAO and its downstream effectors, including measuring AGEs, to aid in explaining the unexpected results observed with PXS-5505 pan-LOX inhibition.

Pan-LOX inhibition may cast too wide of a net regarding collagen inhibition, forcing compensatory mechanisms to be upregulated, ceasing any potential benefit it may generate in with AR model.

5.1.2 LOXL2 Inhibition with AR

Conversely, specific inhibition of LOXL2 effectively attenuated AF susceptibility by 61% in the AR model. LOXL2 inhibition also reduced atrial fibrosis by half, bringing it to levels comparable to sham-untreated mice (5.5% vs. 5.4%), and decreased the duration of atrial arrhythmias by ~10 seconds. However, this reduction in AF vulnerability was also not attributed to changes in the AERP, indicating that the mechanism of action likely involves structural alterations rather than purely electrical. By modulating ECM dynamics, LOXL2 inhibition mitigates the presence of anatomical substrates necessary for re-entry circuits, thereby reducing the likelihood of sustained AF. Reduced fibrotic tissue also entails less disruption of cardiomyocyte orientation, allowing for proper and quick anisotropic conduction. Impulse propagation would more frequently occur in a longitudinal linear fashion rather than a transverse slow-moving zig-zag pattern (Figure 1.4) [60,61]. In such conditions, the wavefront would not be as prolonged, and the excitable gap conducive to re-entry promoting AF would be shortened and thus harder to penetrate.

The ECM structure would also remain intact since the fibrotic percentage was only reduced to sham levels and not completely lost. Thus, there is still myocardium compensation, avoiding excessive dilation, hypertrophy, and potential rupture and allowing for appropriate

diastolic function. This is most likely due to the function and action of the other non-inhibited LOXL isoenzymes. Together with avoiding ECM dysregulation, prevention of hypertrophy would also reduce susceptibility to AF. This is because as the length of the myocardium increases (either through stretch or hypertrophy), the extrinsic biophysical conduction velocity will increase, extending the wavelength and allowing for easier opportunity for re-entry [22,119]. LA-specific enlargement will soon be assessed, as explained in section 3.3.

Furthermore, the results in Figures 3.7 and 3.8 presented macrophages as significantly increasing at 1 week of AR but decreasing at 4 weeks, yet the percentage of LOXL2 expressed from macrophages remains at 45% through both time points (Figure 3.8 Panel B). This leads to the idea of a phenotypic switch in the macrophage population between infiltrating and resident cells. It is known that cardiac macrophages represent a heterogeneous cell population with distinct origins, dynamics, and functions. They can express various proteins and cytokines involved with ECM synthesis and degradation. Specifically, C-C Chemokine receptor 2 positive ($CCR2^{+}$) macrophages, derived from infiltrating monocytes, are involved in the regulation of myocardial inflammation [120]. Knowing macrophages are the primary cell accumulated throughout the atria with AF [121], it would thus be beneficial to explore this potential phenotypic switch, especially as it relates to mechanical stress, inflammation, and AF.

In conclusion, LOXL2 inhibition attenuates fibrosis and maintains anisotropic conduction while preserving ECM structure and potentially inhibiting excessive hypertrophy. This underscores the potential therapeutic value of targeting LOXL2 to manage AF by preserving atrial structure and reducing arrhythmogenicity.

5.1.3 Endurance Swim-Training

The endurance swim training model results pose slight difficulty to interpret in terms of AF susceptibility. This is because in this study, none of the untreated exercised mice presented with arrythmias lasting longer than 10 seconds (distinguished as sustained) (Figure 4.1). Therefore, when interpreting the inducibility data (Figures 4.3 & 4.5), treatment with pan-LOX and LOXL2 inhibitors presents as either causing no change or an increase in sustained AF. However, in a recent study published by another member of our lab in which the same model and equipment were used, untreated mice swimming 240 minutes twice daily were 36.7% inducible [110]. A key reason for the difference in results between the two studies was simply the sample

size, whereby her study utilized a sample size four times that of this study. Therefore, if the results seen from this study (Figures 4.3 & 4.5) were compared to the aforementioned study, pan-LOX inhibition would attenuate AF inducibility by 26.7% and LOXL2 inhibition by 6.7%. LOXL2 inhibition would also increase AF inducibility by 10% in sedentary mice. Future studies should aim for a sample size of at least 10 when performing intracardiac inducibility studies to represent the stimulus effect on susceptibility to arrhythmia accurately.

Neither mice from this study nor Gorman et al. [110] presented with changes in AERP when exercise was introduced. This suggests that AF vulnerability with endurance exercise is more likely to be based on tissue structural factors like hypertrophy and fibrosis. Hypertrophy permits increased capacity by amplifying ejection fraction to accommodate the elevated workload required in endurance exercise [122]. Fibrosis preserves the structural integrity of the thin atrial walls following hemodynamic stress observed with endurance exercises[123,124].

In contrast to the beneficial effects of pan-LOX and LOXL2 inhibition on fibrosis seen in AR, no change was observed with endurance exercise training and the respective drug treatments. There are two divergent streams of thought in the literature when discussing LOXL inhibition with endurance exercise. One belief is that LOXL2 is already reduced in endurance exercise models. Inhibition of LOXL2 may not have affected collagen accumulation because nitric oxide (NO) has been shown to decrease LOXL2 expression and activity [62,125]. In exercise, NO levels are notably elevated, particularly in the heart, a highly metabolic organ requiring increased blood flow and oxygen delivery during physical activity [126]. This heightened NO production during exercise suggests that LOXL2 expression and activity may already be reduced under these conditions. Therefore, when LOXL2 is already suppressed by NO, the addition of a pharmacological inhibitor may not lead to any further changes. Following a similar notion, it has been shown that an increase in inflammatory markers, as seen with endurance swimming and AF, also decreases LOXL2 expression [127,128]. This further supports the theory that LOXL2 inhibition would result in no change due to levels of LOXL2 already being relatively low. The other belief is that exercise significantly increases LOX via osteopontin [125] and ROS [129,130] regulatory mechanisms; thus, treatment with a pan-LOX inhibitor would only bring LOX abundance down to physiological sedentary levels [131,132]. With the added knowledge that collagen biosynthesis rates remain unchanged with endurance exercise, then physiological baseline levels of LOX should be sufficient to catalyze collagen residues at the present rate of

appearance [65,131]. Thus, inhibition of LOX would again not cause any effect of collagen accumulation and fibrosis. These interactions underscore the complex regulatory networks involved in cardiovascular physiology and highlight the need for nuanced approaches when targeting LOX and LOXL2 for therapeutic purposes in conditions such as atrial fibrillation induced by endurance exercise. Further research would need to be conducted to elucidate whether NO and inflammation or osteopontin and ROS play a larger role in endurance exercise training and their respective influences on LOXL enzymes.

Our results conclude that both pan-LOX and LOXL2 inhibition is not beneficial for attenuating endurance exercise-induced AF. Further research would need to be performed to understand better what is facilitating fibrogenesis if not for the LOX family of enzymes or increased collagen transcription.

5.3 Limitations

One limitation of the study was our access to and choice of inhibitors. Multiple forms of pan-LOX inhibitors exist; however, there are very few LOXL2 inhibitors and even fewer available LOXL1, 3 and 4 inhibitors. This meant that once we knew pan-LOX inhibition was not beneficial for reducing AF inducibility in our models, our next step was to assess individual LOXLs. Although LOXL2 was a favourable target due to its connection with fibrotic development in other organs and diseases [133] interest still existed in the remaining LOXL isoenzymes. The question remains whether LOXL2 specifically is a beneficial target for attenuating AF susceptibility and fibrosis or whether another LOXL isoenzyme inhibited alone can also act in a similar fashion. Even more, if LOXL2 inhibition only attenuated AF inducibility by 61%, could inhibition of LOXL2 and LOXL3 together, for example, be even more advantageous. Ideally, inhibitors of each LOXL isoform alone would be available to assess and characterize their individual roles in AF promotion and fibrogenesis.

Additionally, this study only assessed one side of the mechanism of managing collagen accumulation. Collagen turnover occurs based on the interplay between synthesis and degradation. If biosynthesis rates of collagen proteins are increased and more fibrils are maturing and stabilizing in the ECM, then collagen accumulation is observed. However, if MMP activity is increased at the same time, the net accumulation of collagen remains unchanged. Thus, even if crosslinking activity is increased in AF, it may not be acting alone – MMPs could also be

downregulated, aiding it in progressive AF and CVD development. Assessing mechanisms involved in the degradation of collagen and ECM turnover (i.e. MMPs and TIMPs) should be performed to fully understand collagen-based fibrogenesis in AF.

5.4 Conclusion

Our study underscores the complex interplay between LOX family enzymes and AF pathogenesis. While LOXL2 inhibition in AR shows promise in attenuating AR-induced AF by reducing atrial fibrosis and arrhythmogenicity, pan-LOX inhibition in AR exhibits more variable effects requiring further mechanistic exploration. As well we can also conclude that both pan-LOX and LOXL2 inhibition do not have any beneficial effects on attenuating fibrosis and AF susceptibility in endurance swim-trained mice. This highlights the diverse mechanisms of AF fibrosis development and LOX function between pathological and physiological stimuli and aids in directing the development of therapeutics to help combat AF.

5.5 Future Directions

Additional future studies outside of the ongoing experiments laid out in section 3.3 should include attention towards post-translational modifications of LOXL2. Unlike LOX and LOXL1, which require activation via cleavage by bone morphogenic protein one (BMP1), proteolytic processing of LOXL2 is not essential for activation and function [80,134]. This makes LOXL2 more readily available to interact with its substrates. Nonetheless, studies have begun to emerge elucidating the effects of LOXL2 proteolytic processing by various proteases. For example, factor Xa (FXa) processes LOXL2 at Arg-338, decreasing cross-linking activity in the ECM and shifting the substrate preference from type IV collagen to type I collagen [135]. Cleavage by FXa also showed increased LOX recruitment to regions of cleaved LOXL2, potentially acting as a compensatory mechanism to preserve LOX activity. Ensuring there is some degree of collagen crosslinking and preserved ECM structure is important to prevent excessive chamber dilation and potential rupture brought on by chronic volume overload [111]. Dilation, or stretch, has been shown to trigger ectopic beats, shorten the refractory period and induce heterogeneity in the APD, key factors involved in initiating and maintaining AF [41]. Even more, cleavage of LOXL2 by proprotein convertase PACE4 proved to enhance collagen cross-linking of basement membrane collagen type IV ~2-fold [134]. This is an important discovery as it has been shown in AF patients

that mRNA and collagen type IV protein levels are significantly elevated in the LA, contributing to AF-associated non-fibrillar fibrosis [136]. As such, future studies should investigate post-translational modifications of LOXL2 further, assessing its mechanistic role in promoting AF. Such knowledge would greatly inform the development of potential therapies.

Chapter 6: References

1. Calkins, H. *et al.* 2017 HRS/EHRA/ECAS/APHRS/SOLAECE expert consensus statement on catheter and surgical ablation of atrial fibrillation. *Heart Rhythm* **14**, e275–e444 (2017).
2. Kornej, J., Börschel, C. S., Benjamin, E. J. & Schnabel, R. B. Epidemiology of Atrial Fibrillation in the 21st Century: Novel Methods and New Insights. *Circulation Research* vol. 127 4–20 Preprint at https://doi.org/10.1161/CIRCRESAHA.120.316340 (2020).
3. Li, C., Zhang, J., Hu, W. & Li, S. Atrial fibrosis underlying atrial fibrillation (Review). *Int J Mol Med* **47**, 9 (2020).
4. Joglar, J. A. *et al.* 2023 ACC/AHA/ACCP/HRS Guideline for the Diagnosis and Management of Atrial Fibrillation: A Report of the American College of Cardiology/American Heart Association Joint Committee on Clinical Practice Guidelines. *Circulation* **149**, (2024).
5. Enderle, J. D. *et al. Understanding Atrial Fibrillation: The Signal Processing Contribution Part I SYNTHESIS LECTURES ON BIOMEDICAL ENGINEERING Editor Understanding Atrial Fibrillation: The Signal Processing Contribution, Part I Lung Sounds: An Advanced Signal Processing Perspective An Outline of Information Genetics Neural Interfacing: Forging the Human-Machine Connection Quantitative Neurophysiology Tremor: From Pathogenesis to Treatment Introduction to Continuum Biomechanics*. (2008).
6. Kamel, H., Okin, P. M., Elkind, M. S. V. & Iadecola, C. Atrial Fibrillation and Mechanisms of Stroke. *Stroke* **47**, 895–900 (2016).
7. National Institute of Health. Atrial Fibrillation: Types, Symptoms, Diagnosis, Causes, Risk Factors, Treatment. *NIH: National Heart, Lung and Blood Institute* https://www.nhlbi.nih.gov/health/atrial-fibrillation (2022).
8. Schnabel, R. B. *et al.* 50 year trends in atrial fibrillation prevalence, incidence, risk factors, and mortality in the Framingham Heart Study: a cohort study. *The Lancet* **386**, 154–162 (2015).
9. Rob Oberman, Karlie R. Shumway & Abhishek Bhardwaj. Physiology, Cardiac. *National Institute of Health* https://www.ncbi.nlm.nih.gov/books/NBK526089/ (2023).
10. Bers, D. M. Cardiac excitation–contraction coupling. *Nature* **415**, 198–205 (2002).
11. Grant, A. O. Cardiac Ion Channels. *Circ Arrhythm Electrophysiol* **2**, 185–194 (2009).
12. Ravens, U. & Cerbai, E. Role of potassium currents in cardiac arrhythmias. *Europace* **10**, 1133–1137 (2008).
13. Nystoriak, M. A. & Bhatnagar, A. Cardiovascular Effects and Benefits of Exercise. *Front Cardiovasc Med* **5**, (2018).
14. Caspersen, C. J., Powell, K. E. & Christenson, G. M. Physical activity, exercise, and physical fitness: definitions and distinctions for health-related research. *Public Health Rep* **100**, 126–31 (1985).
15. Fagard, R., Van Den Broeke, C. & Amery, A. Left ventricular dynamics during exercise in elite marathon runners. *J Am Coll Cardiol* **14**, 112–118 (1989).
16. Weeks, K. L. & McMullen, J. R. The Athlete's Heart vs. the Failing Heart: Can Signaling Explain the Two Distinct Outcomes? *Physiology* **26**, 97–105 (2011).

17. Wasfy, M. M. & Baggish, A. L. Endurance Exercise and the Right Ventricle. *Circulation* **133**, 1913–1915 (2016).
18. Claessen, G. *et al.* Reduced Ejection Fraction in Elite Endurance Athletes: Clinical and Genetic Overlap With Dilated Cardiomyopathy. *Circulation* **149**, 1405–1415 (2024).
19. Houston, C. *et al.* Characterisation of re-entrant circuit (or rotational activity) in vitro using the HL1-6 myocyte cell line. *J Mol Cell Cardiol* **119**, 155–164 (2018).
20. Nattel, S., Burstein, B. & Dobrev, D. Atrial remodeling and atrial fibrillation: mechanisms and implications. *Circulation. Arrhythmia and electrophysiology* vol. 1 62–73 Preprint at https://doi.org/10.1161/CIRCEP.107.754564 (2008).
21. Veenhuyzen, G. D., Simpson, C. S. & Abdollah, H. Atrial fibrillation. *CMAJ. Canadian Medical Association Journal* vol. 171 755–760 Preprint at https://doi.org/10.1503/cmaj.1031364 (2004).
22. Shiroshita-Takeshita, A., Brundel, B. J. J. M. & Nattel, S. Atrial Fibrillation: Basic Mechanisms, Remodeling and Triggers. *Journal of Interventional Cardiac Electrophysiology* **13**, 181–193 (2005).
23. Allessie, M. A., Bonke, F. I. M. & Schopman, F. J. G. *Circus Movement in Rabbit Atrial Muscle as a Mechanism of Tachycardia III. The 'Leading Circle' Concept: A New Model of Circus Movement in Cardiac Tissue without the Involvement of an Anatomical Obstacle*. http://ahajournals.org.
24. Waks, J. W. & Josephson, M. E. Mechanisms of Atrial Fibrillation – Reentry, Rotors and Reality. *Arrhythm Electrophysiol Rev* **3**, 90 (2014).
25. Varró, A. *et al.* Cardiac transmembrane ion channels and action potentials: cellular physiology and arrhythmogenic behavior. *Physiol Rev* **101**, 1083–1176 (2021).
26. Elliott, J., Mainardi, L. & Rodriguez Matas, J. F. Cellular heterogeneity and repolarisation across the atria: an in silico study. *Med Biol Eng Comput* **60**, 3153–3168 (2022).
27. Lee, S., Khrestian, C. M., Sahadevan, J. & Waldo, A. L. Reconsidering the multiple wavelet hypothesis of atrial fibrillation. *Heart Rhythm* **17**, 1976–1983 (2020).
28. Klabunde, R. E. *Cardiovascular Physiology Concepts*. (Wolters Kluwer, 2021).
29. Marban, E., Robinson, S. W. & Wier, W. G. Mechanisms of arrhythmogenic delayed and early afterdepolarizations in ferret ventricular muscle. *Journal of Clinical Investigation* **78**, 1185–1192 (1986).
30. Antzelevitch, C. & Burashnikov, A. Overview of Basic Mechanisms of Cardiac Arrhythmia. *Card Electrophysiol Clin* **3**, 23–45 (2011).
31. Christ, T. *et al.* Arrhythmias, elicited by catecholamines and serotonin, vanish in human chronic atrial fibrillation. *Proceedings of the National Academy of Sciences* **111**, 11193–11198 (2014).
32. Kawashima, T. The autonomic nervous system of the human heart with special reference to its origin, course, and peripheral distribution. *Anat Embryol (Berl)* **209**, 425–438 (2005).
33. Kharbanda, R. K. *et al.* Vagus Nerve Stimulation and Atrial Fibrillation: Revealing the Paradox. *Neuromodulation: Technology at the Neural Interface* **25**, 356–365 (2022).
34. Fedele, L. & Brand, T. The Intrinsic Cardiac Nervous System and Its Role in Cardiac Pacemaking and Conduction. *J Cardiovasc Dev Dis* **7**, 54 (2020).

35. Lakin, R. *et al.* Atrial Stretch-Dependent Tumor Necrosis Factor-Mediated Adverse Atrial Remodeling and Atrial Arrhythmia Inducibility in a Mouse Model of Aortic Regurgitation. *Canadian Journal of Cardiology* **37**, S3 (2021).
36. Aschar-Sobbi, R. *et al.* Increased atrial arrhythmia susceptibility induced by intense endurance exercise in mice requires TNFα. *Nat Commun* **6**, (2015).
37. Thanigaimani, S. *et al.* Progression and reversibility of stretch induced atrial remodeling: Characterization and clinical implications. *Prog Biophys Mol Biol* **130**, 376–386 (2017).
38. Ravelli, F. & Allessie, M. Effects of Atrial Dilatation on Refractory Period and Vulnerability to Atrial Fibrillation in the Isolated Langendorff-Perfused Rabbit Heart. *Circulation* **96**, 1686–1695 (1997).
39. Henry, W. L. *et al.* Relation between echocardiographically determined left atrial size and atrial fibrillation. *Circulation* **53**, 273–279 (1976).
40. Sardana, M. *et al.* Association of Left Atrial Function Index with Atrial Fibrillation and Cardiovascular Disease: The Framingham Offspring Study. *J Am Heart Assoc* **7**, (2018).
41. Ninio, D. M. & Saint, D. A. The role of stretch-activated channels in atrial fibrillation and the impact of intracellular acidosis. *Prog Biophys Mol Biol* **97**, 401–416 (2008).
42. Eckstein, J., Verheule, S., de Groot, N., Allessie, M. & Schotten, U. Mechanisms of perpetuation of atrial fibrillation in chronically dilated atria. *Prog Biophys Mol Biol* **97**, 435–451 (2008).
43. Chen, M.-C. *et al.* Increased Inflammatory Cell Infiltration in the Atrial Myocardium of Patients With Atrial Fibrillation. *Am J Cardiol* **102**, 861–865 (2008).
44. Zhou, X. & Dudley, S. C. Evidence for Inflammation as a Driver of Atrial Fibrillation. *Frontiers in Cardiovascular Medicine* vol. 7 Preprint at https://doi.org/10.3389/fcvm.2020.00062 (2020).
45. Barnes, J., Dell'Italia, L. J. & Weber, K. T. The Multiple Mechanistic Faces of a Pure Volume Overload: Implications for Therapy. *Am J Med Sci* **348**, 337–346 (2014).
46. Marott, S. C. W. *et al.* Does Elevated C-Reactive Protein Increase Atrial Fibrillation Risk? *J Am Coll Cardiol* **56**, 789–795 (2010).
47. Chung, M. K. *et al.* C-Reactive Protein Elevation in Patients With Atrial Arrhythmias. *Circulation* **104**, 2886–2891 (2001).
48. Yao, Y., Yang, M., Liu, D. & Zhao, Q. Immune remodeling and atrial fibrillation. *Front Physiol* **13**, (2022).
49. Hartupee, J. & Mann, D. L. Role of inflammatory cells in fibroblast activation. *Journal of Molecular and Cellular Cardiology* vol. 93 143–148 Preprint at https://doi.org/10.1016/j.yjmcc.2015.11.016 (2016).
50. Pelouch, V., Dixon, I. M. C., Golfman, L., Beamish, R. E. & Dhalla, N. S. Role of extracellular matrix proteins in heart function. *Mol Cell Biochem* **129**, 101–120 (1993).
51. Ferreira, J. & Santos, M. Heart Failure and Atrial Fibrillation: From Basic Science to Clinical Practice. *Int J Mol Sci* **16**, 3133–3147 (2015).
52. van den Berg, N. W. E. *et al.* Extracellular matrix remodeling precedes atrial fibrillation: Results of the PREDICT-AF trial. *Heart Rhythm* **18**, 2115–2125 (2021).
53. Chute, M., Aujla, P., Jana, S. & Kassiri, Z. The Non-Fibrillar Side of Fibrosis: Contribution of the Basement Membrane, Proteoglycans, and Glycoproteins to Myocardial Fibrosis. *J Cardiovasc Dev Dis* **6**, 35 (2019).

54. Silva, A. C., Pereira, C., Fonseca, A. C. R. G., Pinto-do-Ó, P. & Nascimento, D. S. Bearing My Heart: The Role of Extracellular Matrix on Cardiac Development, Homeostasis, and Injury Response. *Front Cell Dev Biol* **8**, (2021).
55. Weber, K. T. Cardiac interstitium in health and disease: The fibrillar collagen network. *J Am Coll Cardiol* **13**, 1637–1652 (1989).
56. Travers, J. G., Kamal, F. A., Robbins, J., Yutzey, K. E. & Blaxall, B. C. Cardiac fibrosis: The fibroblast awakens. *Circulation Research* vol. 118 1021–1040 Preprint at https://doi.org/10.1161/CIRCRESAHA.115.306565 (2016).
57. Mewton, N., Liu, C. Y., Croisille, P., Bluemke, D. & Lima, J. A. C. Assessment of Myocardial Fibrosis With Cardiovascular Magnetic Resonance. *J Am Coll Cardiol* **57**, 891–903 (2011).
58. Liu, T. *et al.* Current Understanding of the Pathophysiology of Myocardial Fibrosis and Its Quantitative Assessment in Heart Failure. *Front Physiol* **8**, (2017).
59. Schimmel, K., Ichimura, K., Reddy, S., Haddad, F. & Spiekerkoetter, E. Cardiac Fibrosis in the Pressure Overloaded Left and Right Ventricle as a Therapeutic Target. *Front Cardiovasc Med* **9**, (2022).
60. Anter, E. Limitations and Pitfalls of Substrate Mapping for Ventricular Tachycardia. *JACC Clin Electrophysiol* **7**, 542–560 (2021).
61. de Bakker, J. M. *et al.* Slow conduction in the infarcted human heart. 'Zigzag' course of activation. *Circulation* **88**, 915–926 (1993).
62. Poe, A., Martinez Yus, M., Wang, H. & Santhanam, L. Lysyl oxidase like-2 in fibrosis and cardiovascular disease. *American Journal of Physiology-Cell Physiology* **325**, C694–C707 (2023).
63. Anderson, D. E. J. & Hinds, M. T. Extracellular matrix production and regulation in micropatterned endothelial cells. *Biochem Biophys Res Commun* **427**, 159–164 (2012).
64. Borer, J. S. *et al.* Myocardial fibrosis in chronic aortic regurgitation molecular and cellular responses to volume overload. *Circulation* **105**, 1837–1842 (2002).
65. Oh, Y. *et al.* Transcriptomic Bioinformatic Analyses of Atria Uncover Involvement of Pathways Related to Strain and Post-translational Modification of Collagen in Increased Atrial Fibrillation Vulnerability in Intensely Exercised Mice. *Front Physiol* **11**, (2020).
66. Schiller, M., Javelaud, D. & Mauviel, A. TGF-β-induced SMAD signaling and gene regulation: Consequences for extracellular matrix remodeling and wound healing. *Journal of Dermatological Science* vol. 35 83–92 Preprint at https://doi.org/10.1016/j.jdermsci.2003.12.006 (2004).
67. Bujak, M. & Frangogiannis, N. G. The role of TGF-β signaling in myocardial infarction and cardiac remodeling. *Cardiovascular Research* vol. 74 184–195 Preprint at https://doi.org/10.1016/j.cardiores.2006.10.002 (2007).
68. Visse, R. & Nagase, H. Matrix Metalloproteinases and Tissue Inhibitors of Metalloproteinases. *Circ Res* **92**, 827–839 (2003).
69. Williams, K. E. & Olsen, D. R. Matrix metalloproteinase-1 cleavage site recognition and binding in full-length human type III collagen. *Matrix Biology* **28**, 373–379 (2009).
70. Van Doren, S. R. Matrix metalloproteinase interactions with collagen and elastin. *Matrix Biology* **44–46**, 224–231 (2015).
71. Cox, T. R. *et al.* LOX-Mediated Collagen Crosslinking Is Responsible for Fibrosis-Enhanced Metastasis. *Cancer Res* **73**, 1721–1732 (2013).

72. Sajithlal, G. B., Chithra, P. & Chandrakasan, G. Advanced glycation end products induce crosslinking of collagen in vitro. *Biochimica et Biophysica Acta (BBA) - Molecular Basis of Disease* **1407**, 215–224 (1998).
73. Fortunati, D., Chau, D. Y. S., Wang, Z., Collighan, R. J. & Griffin, M. Cross-linking of collagen I by tissue transglutaminase provides a promising biomaterial for promoting bone healing. *Amino Acids* **46**, 1751–1761 (2014).
74. González-Santamaría, J. *et al.* Matrix cross-linking lysyl oxidases are induced in response to myocardial infarction and promote cardiac dysfunction. *Cardiovasc Res* **109**, 67–78 (2016).
75. Rodríguez, C. & Martínez-González, J. The Role of Lysyl Oxidase Enzymes in Cardiac Function and Remodeling. *Cells* **8**, 1483 (2019).
76. Zhong, H. *et al.* Expression of Lysyl OXidase-Like2 (LOXL2) Correlates with Left Atrial Size and Fibrotic Gene Expression in Human Atrial Fibrillation. *J Am Coll Cardiol* **63**, A285 (2014).
77. Yang, J. *et al.* Targeting LOXL2 for cardiac interstitial fibrosis and heart failure treatment. *Nat Commun* **7**, 13710 (2016).
78. Zhao, Y. *et al.* Increased serum lysyl oxidase-like 2 levels correlate with the degree of left atrial fibrosis in patients with atrial fibrillation. *Biosci Rep* **37**, (2017).
79. Erasmus, M. *et al.* Linking LOXL2 to cardiac interstitial fibrosis. *International Journal of Molecular Sciences* vol. 21 1–18 Preprint at https://doi.org/10.3390/ijms21165913 (2020).
80. Molnar, J. *et al.* Structural and functional diversity of lysyl oxidase and the LOX-like proteins. *Biochimica et Biophysica Acta (BBA) - Proteins and Proteomics* **1647**, 220–224 (2003).
81. Busnadiego, O. *et al.* LOXL4 Is Induced by Transforming Growth Factor β1 through Smad and JunB/Fra2 and Contributes to Vascular Matrix Remodeling. *Mol Cell Biol* **33**, 2388–2401 (2013).
82. van den Berg, N. W. E. *et al.* Epicardial and endothelial cell activation concurs with extracellular matrix remodeling in atrial fibrillation. *Clin Transl Med* **11**, (2021).
83. Ohmura, H. *et al.* Cardiomyocyte-specific transgenic expression of lysyl oxidase-like protein-1 induces cardiac hypertrophy in mice. *Hypertension Research* **35**, 1063–1068 (2012).
84. Li, L., Sawamura, T. & Renier, G. Glucose Enhances Human Macrophage LOX-1 Expression: Role for LOX-1 in Glucose-Induced Macrophage Foam Cell Formation. *Circ Res* **94**, 892–901 (2004).
85. Adam, O. *et al.* Increased lysyl oxidase expression and collagen cross-linking during atrial fibrillation. *J Mol Cell Cardiol* **50**, 678–685 (2011).
86. Voloshenyuk, T. G., Hart, A. D., Khoutorova, E. & Gardner, J. D. TNF-α increases cardiac fibroblast lysyl oxidase expression through TGF-β and PI3Kinase signaling pathways. *Biochem Biophys Res Commun* **413**, 370–375 (2011).
87. Rodríguez, C. *et al.* Lysyl oxidase (LOX) down-regulation by TNFα: A new mechanism underlying TNFα-induced endothelial dysfunction. *Atherosclerosis* **196**, 558–564 (2008).
88. Alcudia, J. F. *et al. Lysyl Oxidase and Endothelial Dysfunction: Mechanisms of Lysyl Oxidase down-Regulation by pro-Inflammatory Cytokines*. *Frontiers in Bioscience* vol. 13 (2008).

89. Voloshenyuk, T. G., Landesman, E. S., Khoutorova, E., Hart, A. D. & Gardner, J. D. Induction of cardiac fibroblast lysyl oxidase by TGF-β1 requires PI3K/Akt, Smad3, and MAPK signaling. *Cytokine* **55**, 90–97 (2011).
90. Wang, T. H., Hsia, S. M. & Shieh, T. M. Lysyl oxidase and the tumor microenvironment. *International Journal of Molecular Sciences* vol. 18 Preprint at https://doi.org/10.3390/ijms18010062 (2017).
91. Buckley, B. J. R., Lip, G. Y. H. & Thijssen, D. H. J. The counterintuitive role of exercise in the prevention and cause of atrial fibrillation. *American Journal of Physiology-Heart and Circulatory Physiology* **319**, H1051–H1058 (2020).
92. Elliott, A. D., Ariyaratnam, J., Howden, E. J., La Gerche, A. & Sanders, P. Influence of exercise training on the left atrium: implications for atrial fibrillation, heart failure, and stroke. *American Journal of Physiology-Heart and Circulatory Physiology* **325**, H822–H836 (2023).
93. D'Souza, A., Sharma, S. & Boyett, M. R. CrossTalk opposing view: Bradycardia in the trained athlete is attributable to a downregulation of a pacemaker channel in the sinus node. *J Physiol* **593**, 1749–1751 (2015).
94. Go, A. S. *et al.* Prevalence of Diagnosed Atrial Fibrillation in Adults. *JAMA* **285**, 2370 (2001).
95. Biernacka, A. & Frangogiannis, N. G. *Aging and Cardiac Fibrosis*. *Aging and Disease* • vol. 2 (2011).
96. Mays, P. K., McAnulty, R. J., Campa, J. S. & Laurent, G. J. Age-related changes in collagen synthesis and degradation in rat tissues. Importance of degradation of newly synthesized collagen in regulating collagen production. *Biochemical Journal* **276**, 307–313 (1991).
97. Annoni, G. *et al.* Age-dependent expression of fibrosis-related genes and collagen deposition in the rat myocardium1This study was presented in part at the 49th Annual Meeting of the `Gerontological Society of America', Washington, November 17–21, 1996.1. *Mech Ageing Dev* **101**, 57–72 (1998).
98. Heckbert, S. R. *et al.* Differences by Race/Ethnicity in the Prevalence of Clinically Detected and Monitor-Detected Atrial Fibrillation. *Circ Arrhythm Electrophysiol* **13**, (2020).
99. Aune, D. *et al.* Blood pressure, hypertension and the risk of atrial fibrillation: a systematic review and meta-analysis of cohort studies. *Eur J Epidemiol* **38**, 145–178 (2023).
100. Dzeshka, M. S., Lip, G. Y. H., Snezhitskiy, V. & Shantsila, E. Cardiac Fibrosis in Patients With Atrial Fibrillation. *J Am Coll Cardiol* **66**, 943–959 (2015).
101. Goette, A. Nicotine, atrial fibrosis, and atrial fibrillation: do microRNAs help to clear the smoke? *Cardiovasc Res* **83**, 421–422 (2009).
102. Aune, D., Schlesinger, S., Norat, T. & Riboli, E. Tobacco smoking and the risk of atrial fibrillation: A systematic review and meta-analysis of prospective studies. *Eur J Prev Cardiol* **25**, 1437–1451 (2018).
103. Ettinger, P. O. *et al.* Arrhythmias and the "Holiday Heart": Alcoholassociated cardiac rhythm disorders. *Am Heart J* **95**, 555–562 (1978).
104. Voskoboinik, A., Prabhu, S., Ling, L., Kalman, J. M. & Kistler, P. M. Alcohol and Atrial Fibrillation. *J Am Coll Cardiol* **68**, 2567–2576 (2016).

105. Samokhvalov, A. V., Irving, H. M. & Rehm, J. Alcohol consumption as a risk factor for atrial fibrillation: a systematic review and meta-analysis. *European Journal of Cardiovascular Prevention & Rehabilitation* **17**, 706–712 (2010).
106. Aluru, J. S., Barsouk, A., Saginala, K., Rawla, P. & Barsouk, A. Valvular Heart Disease Epidemiology. *Medical Sciences* **10**, 32 (2022).
107. You, J. *et al.* Differential cardiac hypertrophy and signaling pathways in pressure versus volume overload. *American Journal of Physiology-Heart and Circulatory Physiology* ajpheart.00212. (2017) doi:10.1152/ajpheart.00212.2017.
108. Wu, J. *et al.* Left ventricular response in the transition from hypertrophy to failure recapitulates distinct roles of Akt, β-arrestin-2, and CaMKII in mice with aortic regurgitation. *Ann Transl Med* **8**, 219–219 (2020).
109. van der Does, L. J. M. E. *et al.* The Effects of Valvular Heart Disease on Atrial Conduction During Sinus Rhythm. *J Cardiovasc Transl Res* **13**, 632–639 (2020).
110. Gorman, R. A. *et al.* The effects of daily dose of intense exercise on cardiac responses and atrial fibrillation. *J Physiol* **602**, 569–596 (2024).
111. Murtha, L. A. *et al.* Fibulin-3 is necessary to prevent cardiac rupture following myocardial infarction. *Sci Rep* **13**, 14995 (2023).
112. Scalise, R. F. M. *et al.* Fibrosis after Myocardial Infarction: An Overview on Cellular Processes, Molecular Pathways, Clinical Evaluation and Prognostic Value. *Medical Sciences* **9**, 16 (2021).
113. Hastings, J. F., Skhinas, J. N., Fey, D., Croucher, D. R. & Cox, T. R. The extracellular matrix as a key regulator of intracellular signalling networks. *Br J Pharmacol* **176**, 82–92 (2019).
114. Valiente-Alandi, I. *et al.* Inhibiting Fibronectin Attenuates Fibrosis and Improves Cardiac Function in a Model of Heart Failure. *Circulation* **138**, 1236–1252 (2018).
115. El Hajj, E. C., El Hajj, M. C., Ninh, V. K. & Gardner, J. D. Featured Article: Cardioprotective effects of lysyl oxidase inhibition against volume overload-induced extracellular matrix remodeling. *Exp Biol Med* **241**, 539–549 (2016).
116. Yao, Y. *et al.* Pan-Lysyl Oxidase Inhibitor PXS-5505 Ameliorates Multiple-Organ Fibrosis by Inhibiting Collagen Crosslinks in Rodent Models of Systemic Sclerosis. *Int J Mol Sci* **23**, 5533 (2022).
117. Deng, Y. & Yu, P. H. Simultaneous Determination of Formaldehyde and Methylglyoxal in Urine: Involvement of Semicarbazide-Sensitive Amine Oxidase-Mediated Deamination in Diabetic Complications. *J Chromatogr Sci* **37**, 317–322 (1999).
118. Wong, M. Y. W., Saad, S., Pollock, C. & Wong, M. G. Semicarbazide-sensitive amine oxidase and kidney disease. *American Journal of Physiology-Renal Physiology* **305**, F1637–F1644 (2013).
119. Han, B., Trew, M. L. & Zgierski-Johnston, C. M. Cardiac Conduction Velocity, Remodeling and Arrhythmogenesis. *Cells* **10**, 2923 (2021).
120. Wong, N. R. *et al.* Resident cardiac macrophages mediate adaptive myocardial remodeling. *Immunity* **54**, 2072-2088.e7 (2021).
121. Yamashita, T. *et al.* Recruitment of Immune Cells Across Atrial Endocardium in Human Atrial Fibrillation. *Circulation Journal* **74**, 262–270 (2010).
122. Pelliccia, A. *et al.* Prevalence and Clinical Significance of Left Atrial Remodeling in Competitive Athletes. *J Am Coll Cardiol* **46**, 690–696 (2005).

123. Henry, W. L. *et al.* Relation between echocardiographically determined left atrial size and atrial fibrillation. *Circulation* **53**, 273–279 (1976).
124. De Jong, A. M. *et al.* Mechanisms of atrial structural changes caused by stretch occurring before and during early atrial fibrillation. *Cardiovasc Res* **89**, 754–765 (2011).
125. Steppan, J. *et al.* Lysyl oxidase-like 2 depletion is protective in age-associated vascular stiffening. *American Journal of Physiology-Heart and Circulatory Physiology* **317**, H49–H59 (2019).
126. Dyakova, E. Y., Kapilevich, L. V., Shylko, V. G., Popov, S. V. & Anfinogenova, Y. Physical exercise associated with NO production: signaling pathways and significance in health and disease. *Front Cell Dev Biol* **3**, (2015).
127. Cerqueira, É., Marinho, D. A., Neiva, H. P. & Lourenço, O. Inflammatory Effects of High and Moderate Intensity Exercise—A Systematic Review. *Front Physiol* **10**, (2020).
128. Alshenibr, W. *et al.* Anabolic role of lysyl oxidase like-2 in cartilage of knee and temporomandibular joints with osteoarthritis. *Arthritis Res Ther* **19**, 179 (2017).
129. He, F. *et al.* Redox Mechanism of Reactive Oxygen Species in Exercise. *Front Physiol* **7**, (2016).
130. Thirupathi, A. *et al.* Effect of Running Exercise on Oxidative Stress Biomarkers: A Systematic Review. *Front Physiol* **11**, (2021).
131. Hammond, M. A. & Wallace, J. M. Exercise prevents β-aminopropionitrile-induced morphological changes to type I collagen in murine bone. *Bonekey Rep* **4**, (2015).
132. Schreckenberg, R. *et al.* Effects of 6-months' Exercise on Cardiac Function, Structure and Metabolism in Female Hypertensive Rats–The Decisive Role of Lysyl Oxidase and Collagen III. *Front Physiol* **8**, (2017).
133. Findlay, A. *et al.* An activity-based bioprobe differentiates a novel small molecule inhibitor from a LOXL2 antibody and provides renewed promise for anti-fibrotic therapeutic strategies. *Clin Transl Med* **11**, (2021).
134. Okada, K., Moon, H.-J., Finney, J., Meier, A. & Mure, M. Extracellular Processing of Lysyl Oxidase-like 2 and Its Effect on Amine Oxidase Activity. *Biochemistry* **57**, 6973–6983 (2018).
135. Wang, H. *et al.* Lysyl oxidase-like 2 processing by factor Xa modulates its activity and substrate preference. *Commun Biol* **6**, 375 (2023).
136. Jiang, Y., Yang, Q., Liu, X. & He, G. Mechanism of Atrial Fibrillation is Related to Changes of Type IV Collagen in Rheumatic Heart Valvular Disease. *The FASEB Journal* **30**, (2016).

Chapter 7: Appendix

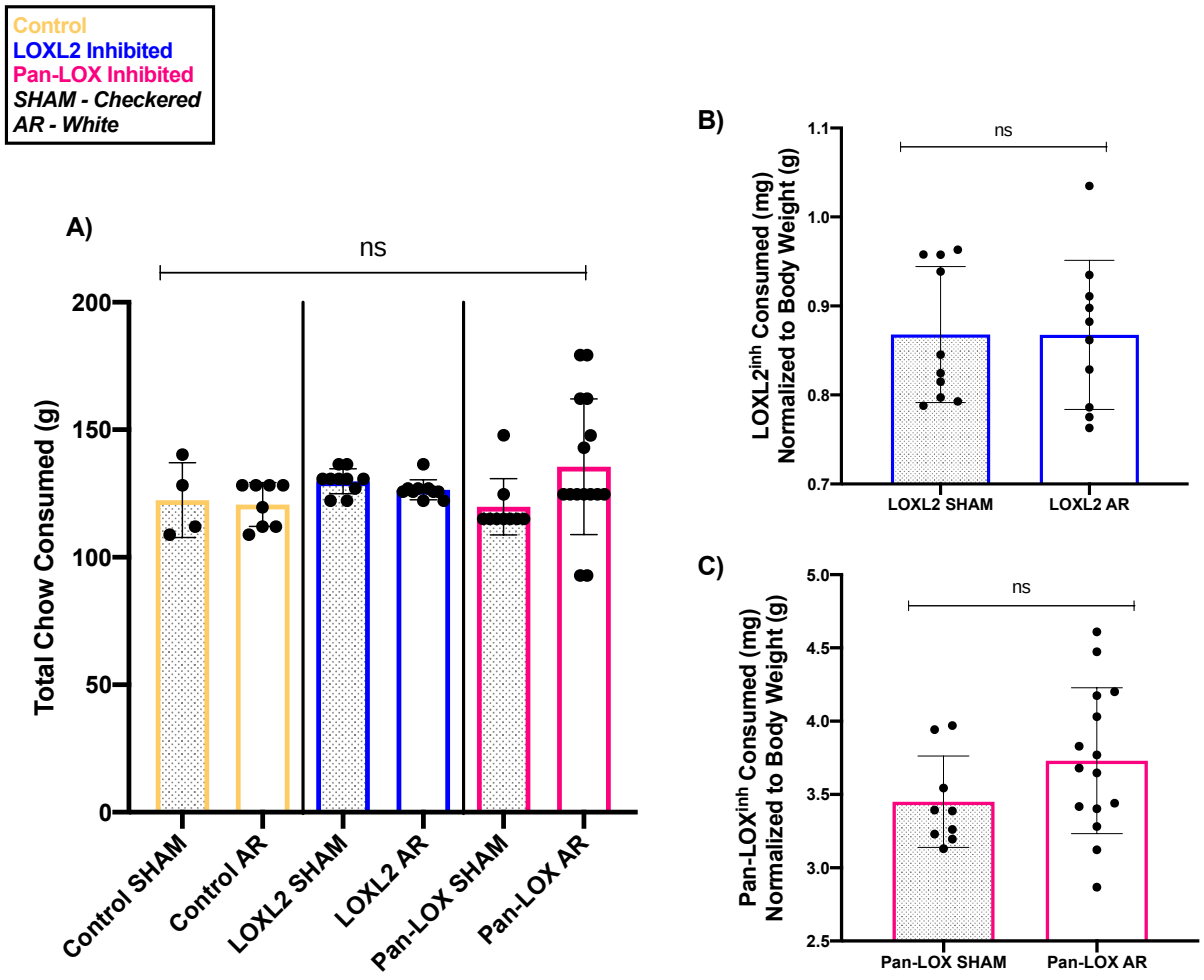

Appendix Figure A.1 Chow and Drug Consumption in AR and SHAM Cohorts. A) Total chow consumed (g) in control (yellow), LOXL2 inhibited (blue), and Pan-LOX inhibited (pink) cohorts (P=0.1674). B) Total LOXL2 inhibitor consumed (mg) normalized to body weight in AR and SHAM cohorts (P=0.9904). C) Total Pan-LOX inhibitor consumed (mg) normalized to body weight in AR and SHAM cohorts (P=0.1450). Data presented as Mean ± SEM with *P<0.05 using two-way ANOVA with Tukey's multiple comparisons tests and student's t-tests; *n*=4 control sham, *n*=8 control AR, *n*=10 LOXL2^{inh} sham and AR, *n*=9 pan-LOX^{inh} sham, *n*=15 pan-LOX^{inh} AR.

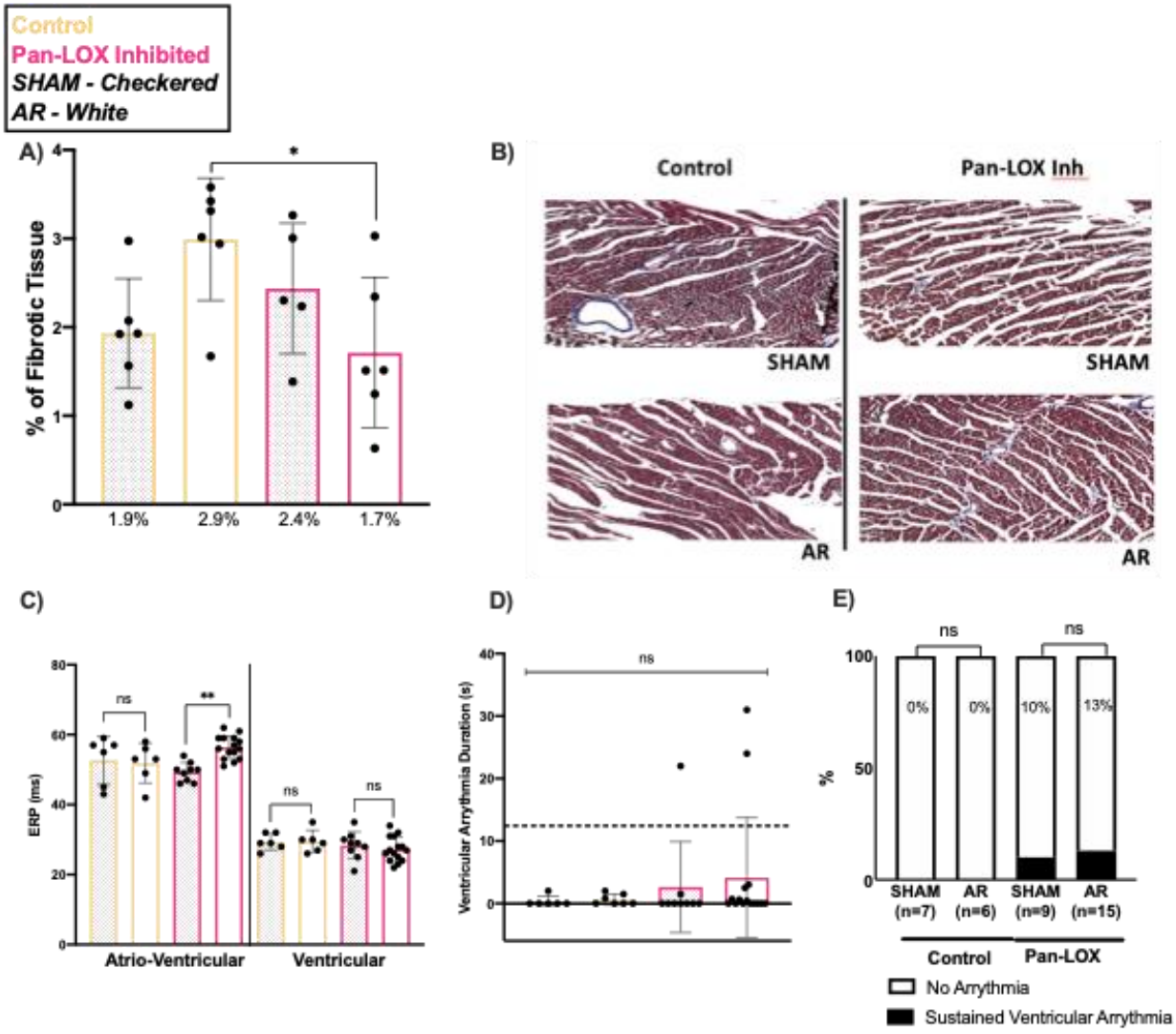

Appendix Figure A.2. Left Ventricle Electrical and Structural Remodelling with AR and Pan-LOX Inhibition. A) Total percent of fibrotic tissue normalized to tissue area (P=0.0308). B) Representative images of fibrotic tissue using MTS. C) AVERP (P=0.0029) and VERP (P=0.4291). D) Ventricular arrhythmia duration (P=0.6212). E) Sustained ventricular arrhythmias (longer than 10 seconds) (P=0.2402). Data presented as Mean ± SEM with *P<0.05, **P<0.01 using two-way ANOVA with Tukey's multiple comparisons tests; *n*=4 control sham, *n*=8 control AR, *n*=15 pan-LOX^{inh} AR.

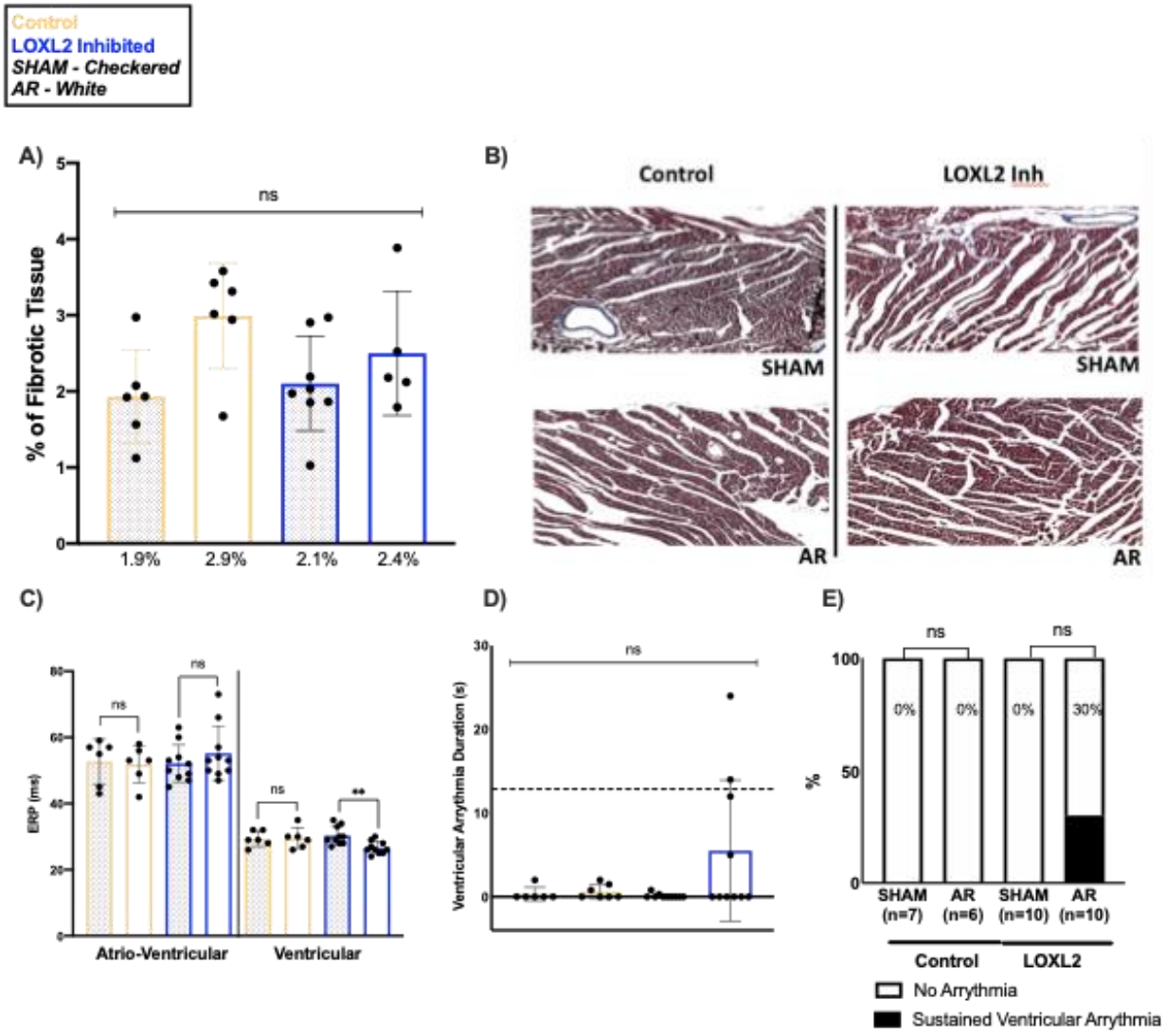

Appendix Figure A.3. Left Ventricle Electrical and Structural Remodelling with AR and LOXL2 Inhibition. A) Total percent of fibrotic tissue normalized to tissue area (P=0.2995). B) Representative images of fibrotic tissue using MTS. C) AVERP (P=0.7084) and VERP (P=0.0177). D) Ventricular arrhythmia duration (P=0.0570). E) Sustained ventricular arrhythmias (longer than 10 seconds) (P=0.0210). Data presented as Mean ± SEM with **P<0.01 using two-way ANOVA with Tukey's multiple comparisons tests; *n*=4 control sham, *n*=10 LOXL2^{inh} sham and AR.

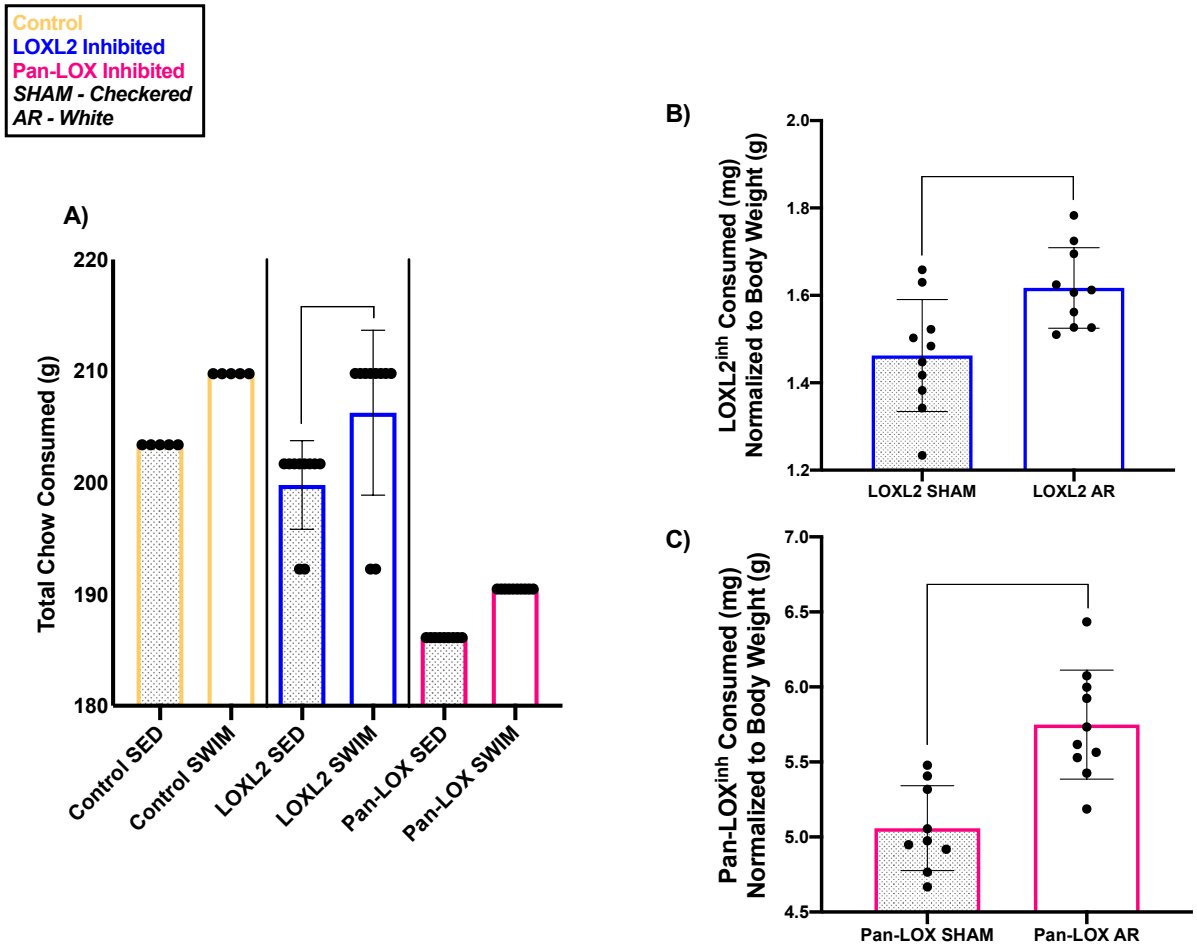

Appendix Figure A.4 Chow and Drug Consumption in Swim- and Sedentary Cohorts. A) Total chow consumed (g) in control (yellow), LOXL2 inhibited (blue) and Pan-LOX inhibited (Pink) cohorts (P<0.0001). B) Total LOXL2 inhibitor consumed (mg) normalized to body weight in swim-trained and sedentary cohorts (P=0.0061). C) Total Pan-LOX inhibitor consumed (mg) normalized to body weight in swim-trained and sedentary cohorts (P=0.0003). Data presented as Mean ± SEM with **P<0.01, ***P<0.001 using two-way ANOVA with Tukey's multiple comparisons tests; *n*=5 control SED and swim, *n*=8 control AR, *n*=10 LOXL2^{inh} SED and swim, *n*=9 pan-LOX^{inh} SED, *n*=10 pan-LOX^{inh} swim.

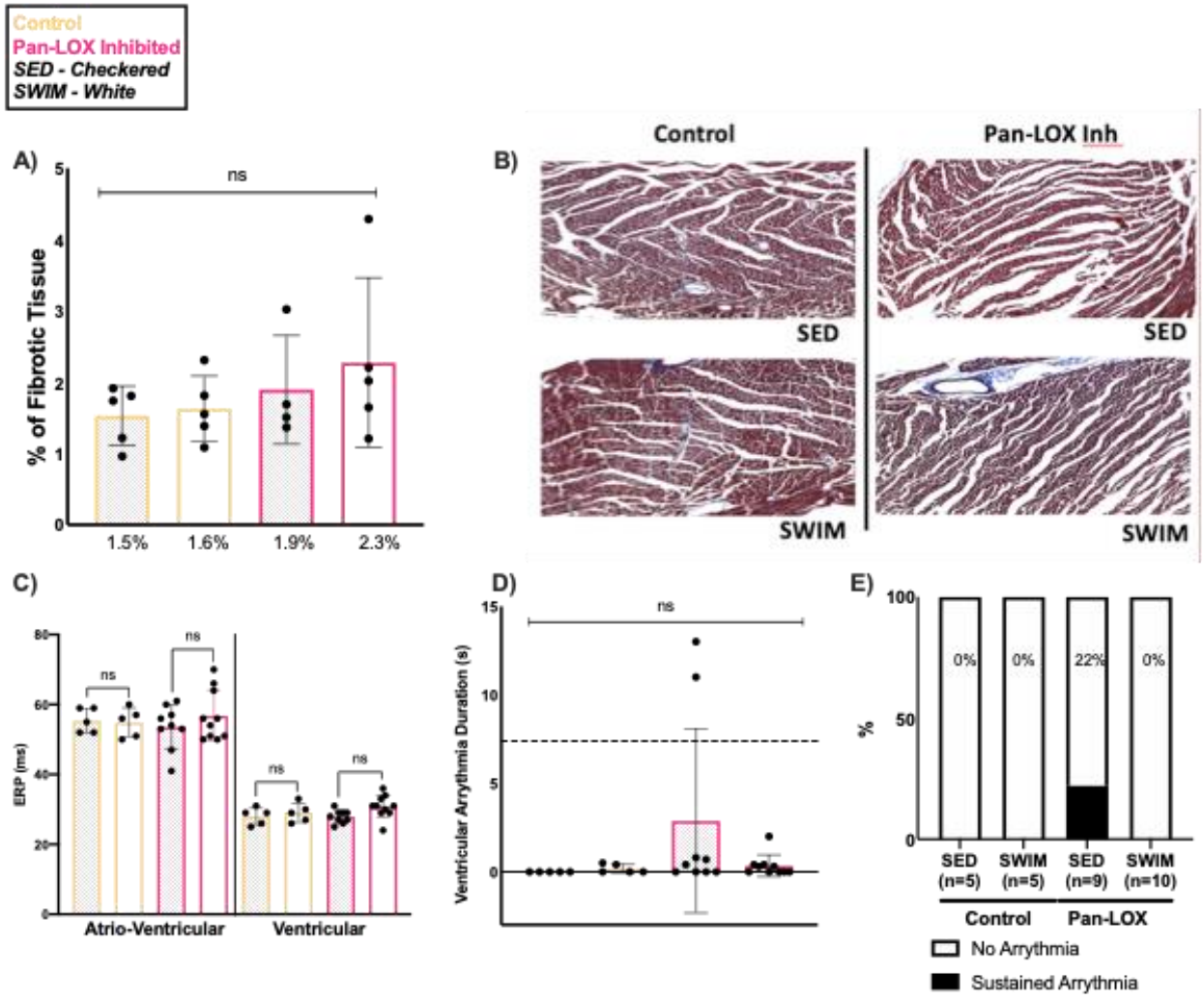

Appendix Figure A.5. Left Ventricle Electrical and Structural Remodelling with Endurance Swim Training and Pan-LOX Inhibition. A) Total percent of fibrotic tissue normalized to tissue area (P=0.4512). B) Representative images of fibrotic tissue using MTS. C) AVERP (P=0.7103) and VERP (P=0.1044). D) Ventricular arrhythmia duration (P=0.1969). E) Sustained ventricular arrhythmias (longer than 10 seconds) (P=0.1891). Data presented as Mean ± SEM with **P<0.01, ***P<0.001 using two-way ANOVA with Tukey's multiple comparisons tests; *n*=5 control SED and swim, *n*=8 control AR, *n*=9 pan-LOX^{inh} SED, *n*=10 pan-LOX^{inh} swim.

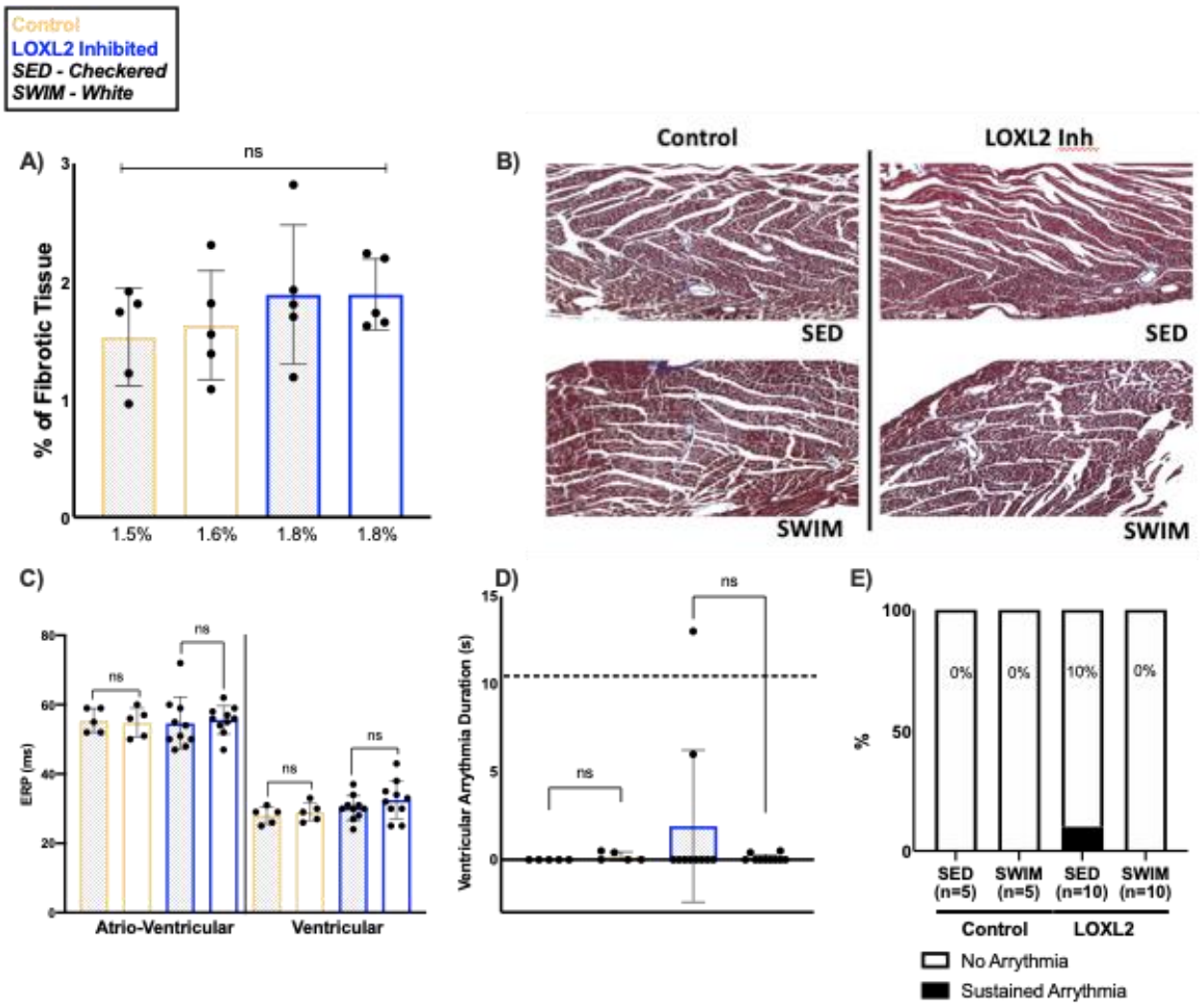

Appendix Figure A.6. Left Ventricle Electrical and Structural Remodelling with Endurance Swim Training and LOXL2 Inhibition. A) Total percent of fibrotic tissue normalized to tissue area (P=0.5061). B) Representative images of fibrotic tissue using MTS. C) AVERP (P=0.0029) and VERP (P=0.4291). D) Ventricular arrhythmia duration (P=0.6212). E) Sustained ventricular arrhythmias (longer than 10 seconds) (P=0.2402). Data presented as mean ± SEM with **P<0.01, ***P<0.001 using two-way ANOVA with Tukey's multiple comparisons tests; *n*=5 control SED and swim, *n*=8 control AR, *n*=10 LOXL2^{inh} SED and swim.

A.7 Homemade Mounting Medium for IHC

500mg N-Propyl Gallate (NPG) dissolved in 10mL of 0.1M Tris buffer (pH 8-9) with 90mL (9:1) of glycerol. NPG was chosen as the anti-fade constituent due to its lack of acute toxicities. Tris buffer at pH 8-9 was used to avoid the quenching effect seen in acidic solutions and increase the fluorescent intensity by its basic properties. Glycerol was chosen as the aqueous base due to its refractive index (RI) of 1.47 being closest to the RI created by the coverslip and objective (1.52). Stored at -20ºC for 3-4 months.

A.8 Chow Ingredients from Research Diets in Collaboration with Syntara

D20011301 and Modified Formulas

Formulated by:
Sridhar Radhakrishnan
Research Diets, Inc
4/20/2021

Rodent Diets With 10 kcal% Fat with Compounds/Peanut Flavor

Product #		**D20011301**		**D21012504R**		**Formula 1**	
	%	gm	*kcal*	gm	*kcal*	gm	*kcal*
Protein		19.0	*20*	19.0	*20*	19.0	*20*
Carbohydrate		66.6	*70*	66.5	*70*	66.6	*70*
Fat		4.2	*10*	4.2	*10*	4.2	*10*
Total			*100*		*100*		*100*
kcal/gm		3.81		3.80		3.81	
Ingredient		**gm**	***kcal***	**gm**	***kcal***	**gm**	***kcal***
Casein		200	*800*	200	*800*	200	*800*
L-Cystine		3	*12*	3	*12*	3	*12*
Corn Starch		315	*1260*	315	*1260*	315	*1260*
Maltodextrin 10		35	*140*	35	*140*	35	*140*
Sucrose		350	*1400*	350	*1400*	350	*1400*
Cellulose, BW200		50	*0*	50	*0*	50	*0*
Soybean Oil		25	*225*	25	*225*	25	*225*
Lard		20	*180*	20	*180*	20	*180*
Mineral Mix S10026		10	*0*	10	*0*	10	*0*
DiCalcium Phosphate		13	*0*	13	*0*	13	*0*
Calcium Carbonate		5.5	*0*	5.5	*0*	5.5	*0*
Potassium Citrate, 1 H2O		16.5	*0*	16.5	*0*	16.5	*0*
Vitamin Mix V10001		10	*40*	10	*40*	10	*40*
Choline Bitartrate		2	*0*	2	*0*	2	*0*
PXS-5505		0	*0*	**1.195**	*0*	**0**	*0*
PXS-5382		0	*0*	0	*0*	**0.282**	*0*
Flavor, Peanut Powder		**10.7**	*0*	**10.7**	*0*	**10.7**	*0*
FD&C Yellow Dye #5		0.05	*0*	0	*0*	0	*0*
FD&C Red Dye #40		0	*0*	0.05	*0*	0	*0*
FD&C Blue Dye #1		0	*0*	0	*0*	0.05	*0*
Total		**1065.75**	***4057***	**1066.95**	***4057***	**1066.03**	***4057***
Compound, mg/kg diet		**0**		**1120**		**265**	
% Flavor		**1.0**		**1.0**		**1.00372**	

Research Diets, Inc.
20 Jules Lane
New Brunswick, NJ 08901 USA
info@researchdiets.com

JarolimekW01.for